A Dissertation

entitled

In vitro and *In vivo* Study using Chitosan Microparticles with Growth Factors and
Antibiotics for Bone Tissue Regeneration

by

Venkata Prasanna R Mantripragada

Submitted to the Graduate Faculty as partial fulfillment of the requirements for the
Doctor of Philosophy Degree in Biomedical Engineering

_____
Dr. Ambalangodage C. Jayasuriya, Committee Chair

_____
Dr. Beata Lecka-Czernik, Committee Member

_____
Dr. Mark Wooten, Committee Member

_____
Dr. Patricia A. Relue, Committee Member

_____
Dr. Stephen K. Callaway, Committee Members

_____
Dr. Patricia R. Komuniecki, Dean
College of Graduate Studies

The University of Toledo
August, 2014

An Abstract of

In vitro and *In vivo* Study using Chitosan Microparticles with Growth Factors and
Antibiotics for Bone Tissue Regeneration

by

Venkata Prasanna R Mantripragada

Submitted to the Graduate Faculty as partial fulfillment of the requirements for the
Doctor of Philosophy Degree in Biomedical Engineering

The University of Toledo

August, 2014

The objective of this study is to fabricate chitosan microparticles under mild
environmental conditions. These microparticles will serve as a better carrier for relevant
growth factors and facilitate the repair and regeneration of critical-sized defects in bones.
Chitosan is structurally similar with glucosaminoglycans, and this makes it particularly
attractive as a biomaterial for bone defects, as glucosaminoglycans are usually the
interacting molecules with osteoblasts. Chitosan and tri-ppolyphosphate (TPP)
microparticles were employed because this system can be engineered quantitatively to
obtain a scaffold with desired physical and biological properties. Coacervation technique
was employed to cross-link amine groups in chitosan with phosphate groups in TPP.
Temperatures below room temperature were maintained during the cross-linking process
to ensure maximum encapsulation efficiency of the growth factors. Physical and
morphological characteristics of the microparticles were determined using scanning
electron microscopy; the microparticles have a diameter in the range of 400-700 μm, and

the surface was found to be groovy and rough. Degradation study conducted *in vitro* indicated that the microparticles remained unaltered for 30 weeks when suspended in phosphate buffered saline (PBS) of pH 7.4 containing lysozyme (10 mg/L), but when the microparticles were suspended in PBS solution of pH 5.1 containing lysozyme enzyme, the microparticles degraded within 15 weeks. In order to evaluate the harms of organic solvents like hexane and acetone on growth factor encapsulation, cumulative release profiles of insulin-like growth factor 1 (IGF-1) was compared between particles prepared using the emulsification and coacervation techniques. These results indicated a significant decrease ($p < 0.05$) in the encapsulation efficiency, which in turn also decreased the cumulative release from the emulsification microparticles in comparison with coacervation technique during the two-week period. In order to optimize various parameters that control the release kinetics of growth factor from microparticles, IGF-1 was used and it was found that microparticles with IGF-1 encapsulated in it and prepared at below room temperatures using 50% TPP, exhibited a better controlled release profile. With these optimized parameters, microparticles were fabricated incorporating bone morphogenetic protein 7 (BMP-7), which is the protein of interest in this study and *in vitro* experiments were conducted. BMP-7 was incorporated in two ways: encapsulation and coating. The release study results suggest that BMP-7 encapsulated microparticles exhibited a controlled release profile, while a burst release was observed in BMP-7 coated microparticles. Cell proliferation study conducted using DNA assay indicated a statistical significant increase ($p < 0.05$) in the amount of DNA obtained from BMP-7 encapsulated and coated microparticles in comparison with microparticles without any growth factors. Cell differentiation study conducted by real time RT-PCR demonstrated a

significant up-regulation in the expression of transcription factors – runx 2 and osx as well as late osteoblast markers – OCN, OPN and BSP, which lead to increased mineralization. These results indicate that chitosan microparticles obtained by coacervation method are biocompatible and help in improving the encapsulation efficiency of BMP-7.

The local application and controlled release of growth factors and antibiotics is beneficial to stimulate bone healing and prevent infection at the same time. Therefore, dual release of growth factor bone morphogenetic protein-7 (BMP-7) along with antibiotics-vancomycin and cefazolin respectively was also studied. In both the release study experiments, only about 50% of the total encapsulated drug is released and it was observed that cefazolin could inhibit bacterial growth to a greater extent (~85%) in comparison with vancomycin (~80%). BMP-7 release profile in the presence of antibiotics remained unaltered, indicating that the drugs do not affect the stability of the protein. It is also important to consider the amount of drugs incorporated into the microparticles, as it is cytotoxic for osteoblasts. 50 µg/ml and 100 µg/ml of cefazolin were found to positively influence osteoblasts cell proliferation. In the complete duration of our release study, the concentration of cefazolin remained <70 µg/ml. Interestingly, in cefazolin and BMP-7 group, a significant increase in osteoblasts cell proliferation was observed in comparison with BMP-7 only, indicating that cefazolin also may play a role in osteoblast proliferation. On the other hand, 1000 µg/ml of vancomycin was found to significantly reduce cell proliferation, indicating it is toxic for osteoblasts. Therefore, the amount of vancomycin to be incorporated was chosen accordingly.

Microparticles with and without BMP-7 were finally tested *in vivo* to determine the biological response in bone tissue in rats. Healthy bone growth was observed adhered to the microparticles. Histology images indicated minor inflammatory response observed around the microparticles at 6 weeks, which reduced by 12 weeks. Bone volume fraction was found to be significantly less in comparison with controls, which can be explained by the presence of microparticles occupying the defect site. μ-CT analysis of bone surface density and porosity was found to be significantly more ($p<0.05$) for microparticles containing groups, which include microparticles without growth factors, microparticles with BMP-7 encapsulated and BMP-7 coated microparticles in comparison with controls, which suggests that the new bone formed in the presence of microparticles is more interconnected and porous. Collagen fibrils analysis conducted using multiphoton microscopy indicated a significant improvement in the formation of bundled collagen area (%) in microparticles containing groups in comparison with controls, from which we understand that the collagen fibril diameter is higher and therefore the cross-linking between the fibrils is higher. The effect of BMP-7 was not effectively observed and this can be hypothesized to be due to (i) insufficient concentration of BMP-7 incorporated (ii) formation of fibrous capsule by macrophages around the microparticles, which inhibit growth factor release and (iii) highly acidic conditions created by macrophages at the surface of the microparticles may degrade the growth factor being released. This study therefore proves that even though the microparticles with growth factors significantly improved proliferation and differentiation of osteoblasts *in vitro*, *in vivo* conditions are completely different, and all the observations from this study should be considered for fabricating chitosan microparticles in future for bone tissue engineering applications.

This research endeavor is dedicated to the memory of my beloved brother Anil, who taught me that every day, hour, minute, second is a time to be treasured. He taught me not to dwell on the sorrow but on the happiness and good that comes out of things. I didn't get a chance to tell you how much you mean to me and how much I love you.

Acknowledgements

Table of Contents

List of Tables

List of Figures

Chapter 1

Introduction

Bone is a remarkable organ playing critical functions in many physiological processes in humans, which include movement, protection of critical organs, blood production, mineral storage and homeostasis, blood pH regulation, multiple progenitor cells production (mesenchymal, hemopoietic), and others. It is known that bone is one of the few tissues that can heal without forming a fibrous scar. It is a dynamic organ in the body, which is constantly being resorbed and formed, through very meticulous processes. Bone remodeling requires coordination of cellular, hormonal, and systemic components in response to chemical and mechanical stimuli. This ability of bone to remodel with its high degree of vascularity gives it the high regeneration potential.

However, despite the excellent regenerative capacity of skeletal tissue, the biological process fails sometimes and fractures healing in unfavorable anatomical position show a delay in healing or even develop pseudo-arthrosis or non-union. These situations may arise either due to diseases such as osteogenesis imperfect, osteoarthritis, osteomyelitis,

and osteoporosis in which bone does not function properly or due to traumatic injury or total joint replacements.

Bone graft is a huge business, generating sales of more than $2.5 billion a year [1]. Of nearly 3 million musculoskeletal procedures done annually in the United States, about half involve bone grafting with either an autograft or an allograft [2]. Although autografts are considered the gold standard for healing bone defects, their usage is limited by donor site morbidity and supply [1]. Limitations of using allograft include immunogenic response and potential disease transmission [3]. Due to these limitations, the development of new orthobiologic materials to aid in the management of bony defects is increasing. Demineralized bone matrix (DBM) is produced by acid extraction of allograft cortical bone and possesses both osteoconductive and osteoinductive properties [3,4]. However, the potency of different DBM preparations depends on the manufacturing process [4]. BMP-2 and BMP-7 have been found to possess independent osteoinductive activity and have been approved for clinical use [1,4]. Contraindications for the use of BMP include pregnancy, history of cancer, skeletal immaturity and history of bone tumors [1]. Cost is a major limitation of BMP products: one 5-ml vial costs around $5000 [1]. Further research lead to the usage of osteoconductive bone graft substitutes like coralline hydroxyapatite, collagen based matrices, calcium phosphate and bioglass. These products however lack osteoinductivity unless an osteoinductive product is added [5]. But due to either their mechanical or degradation properties, they are not considered ideal.

1.1 Problem

The lack of ideal bone tissue engineering scaffolds necessitates continuous research for new biomaterials and novel fabrication techniques to improve the repair of load bearing bone defects. A number of biocompatible natural and synthetic biomaterials including polymers and ceramics have been explored for critical-sized bone repair and regeneration in the past [6]. Natural polymer chitosan has been investigated for a variety of tissue engineering applications, but the fabrication techniques used were not favorable for serving as a carrier for therapeutically relevant factors [7] and the scaffolds thus obtained generally suffered from inferior biomechanical properties [8,9].

1.2 Objective

In thus study, we intend to fabricate chitosan microparticles/scaffold for bone tissue regeneration, which will act as a favorable carrier for the growth factors and antibiotics; is biocompatible so that the scaffold can be well-integrated into the host tissue without much immune response; is mechanically competent to withstand local stress and very importantly, is biodegradable, and the degradation products are not toxic.

1.3 Approach

In order to achieve the above-mentioned objective, we divided our experimentation into five segments:

Aim 1. To fabricate and characterize chitosan-tri polyphosphate (TPP) microparticles using mild environmental conditions. *Hypothesis: The microparticles formed using mild environmental conditions will have biocompatible surface morphology and composition to support active growth factor encapsulation and cell attachment, proliferation and differentiation.*

I. Optimize the parameters of fabrication method of chitosan-TPP microparticles to obtain spherical shape microparticles with desired surface morphology and composition.

II. Compare insulin like growth factors (IGF-1) incorporation into the microparticles prepared using ionic-crosslinking and emulsification method to determine the effect of organic solvents on the proteins.

III. Study the degradation of optimized coacervation microparticles.

Aim 2. To design an efficient method of growth factor encapsulation for improved encapsulation efficiency and sustained release of protein over time and test its bioactivity. *Hypothesis: The sustained release of growth factors encapsulated into the microparticles is dependent of several parameters like the degree of cross-linking of the microparticles, amount of growth factor being encapsulated, method of incorporation of the growth factor and pH of the release medium.*

I. Quantify the growth factors being released to optimize the amount of growth factor that needs to be encapsulated, degree of cross-linking and method of growth factor encapsulation for sustained release.

II. In order to determine the effect of temperature on stability of the growth factors, microparticles were prepared at room temperature and below room temperature and compared.

Aim 3. To perform *in vitro* cell studies to demonstrate the biocompatibility of the chitosan microparticles and bioactivity of the growth factors released from the microparticle. *Hypothesis: Pre-osteoblasts will show improved cell attachment, proliferation and differentiation in the presence of the chitosan microparticles with and without growth factors over controls.*

I. Determine whether the surface of the microparticle can initiate attachment and adhesion of the undifferentiated cells, which play an important role how they react to the material.

II. Determine whether the surface of the microparticles supports survival of the attached cells and promotes their proliferation over its three dimensional structure, which is known to be directly governed by the surface morphology.

III. Determine the effect of the interaction of the microparticles with the cells to dictate their differentiation into mature osteoblasts that later produce calcified matrix, which are necessary to bone remodeling.

Aim 4: To design efficient encapsulation of antibiotic for their sustained release from chitosan microparticles and determine the activity of the released drug. *Hypothesis: The concentration of antibiotics released from the microparticles should be optimized in order to prevent microbial contamination as well as improve bone healing at the same time.*

I.   Define the influence of a range of antibiotic concentrations on pre-osteoblasts to determine which concentrations will not affect their proliferation and can be incorporated into the microparticles.

II.   Optimize the release of antibiotics from the chitosan microparticles.

III.   Determine the effect of the released antibiotics on the growth of *Staphylococcus epidermidis* to demonstrate the bioactivity of the released antibiotic and determine the time period until which the encapsulated antibiotic can be released in a sustained manner to inhibit bacterial growth.

Aim 5: To perform *in vivo* studies to determine bone healing after implanting chitosan microparticles with and without growth factors in rat femur. *Hypothesis: Rats will show improved and faster healing in the presence of microparticles with and without growth factors in comparison with controls which do not have any scaffold material inserted in the defect site.*

I.   Examine the formation of new bone in the presence and absence of chitosan microparticles over a period of time and compare it with control to determine the effect of chitosan microparticles

1.4 Outline

Chapter 1 presents a brief introduction stating the significance of conducting the research and the objectives that will be addressed in this study. Chapter 2 includes a detailed review on the structure and physiology of bone, understanding the process of fracture healing, the role of chitosan as a biomaterial, various fabrication techniques used and the

disadvantages associated with them and the importance of controlled growth factors and antibiotics delivery.

In Chapter 3, microparticles are fabricated using two approaches - emulsification and coacervation and were compared to determine encapsulation efficiency of the growth factor. Section 3.2 describes the methodology followed to obtain the two types of microparticles and their characterization by scanning electron microscopy (SEM). Enzyme linked immunosorbent assay (ELISA) was used to quantify the growth factors. Section 3.3 compares the results obtained and section 3.4 discusses the reasons for the obtained results and compares it with the existing literature.

From Chapter 4 onwards, we consider only the microparticles obtained by coacervation method (as concluded from Chapter 3). In Chapter 4, we optimize various parameters considered necessary for the controlled release of growth factor. For the purpose of optimization, insulin-like growth factor 1 (IGF-1) was used. Section 4.1 and 4.2 describe the various parameters considered, ELISA was used to quantify the growth factor and the bioactivity of the released growth factor was tested by live/dead cell assay, vonkossa and real time RT-PCR. Section 4.3 describes the results obtained and section 4.4 discusses the reasons for the observations and compares it with the literature.

One of the aims in this study was to observe the influence of BMP-7 incorporated chitosan microparticles *in vitro* and *in vivo*. Therefore, in Chapter 5, we conducted *in vitro* studies to demonstrate the effect of BMP-7 incorporated chitosan microparticles on pre-osteoblasts. Section 5.2, 5.3 and 5.4 describe the various methods used to determine

the influence, the results obtained and the discussion regarding the observations respectively.

In Chapter 6, since infections are also a major concern after bone surgeries, therefore we intended to incorporate antibiotics also along with growth factors, to determine their release kinetics, determine the influence of antibiotics on osteoblasts and also determine the bioactivity of the released antibiotics by microbial tests. Section 6.2, 6.3 and 6.4 describe the various methods used to determine the influence, the results obtained and the discussion regarding the observations respectively.

In vitro and *in vivo* conditions are completely different, and therefore to test the performance of the chitosan microparticles *in vivo*, we conducted our experiments by creating critical size defects in rat femurs. Chapter 7 focuses on the methodology (section 7.2) and results (section 7.3) obtained when BMP-7 coated and encapsulated microparticles are used *in vivo*.

Chapter 8 includes a summary of the conclusions obtained from this research.

Chapter 9 presents a business plan for commercialization of this invention. This includes sections on the opportunity rationale (section 9.1), product and product line description (section 9.2), customer segment (section 9.3), detailed market analysis (section 9.4), competitors (section 9.5), key resources (section 9.6), and distribution channels (section 9.7).

Chapter 2

Literature Review

2.1 Structure and Physiology of Bone

The skeleton serves a variety of functions, which include providing structural support for the body, permit movement and locomotion by providing levers for the muscles, protect vital internal organs, provide maintenance of mineral homeostasis and acid-base balance, serve as a reservoir of growth factors and cytokines and provide the environment for hematopoiesis within the marrow spaces [10].

There are four general categories of bones – long bones, short bones, flat bones and irregular bones. Long bones are composed of a hollow shaft – the diaphysis, cone-shaped metaphyses below the growth plate and the rounded epiphyses above the growth plates. The diaphysis is composed of primarily of dense cortical bone, while the metaphysis and epiphysis are composed of trabecular meshwork bone surrounded by relatively less dense cortical bone.

The adult human skeleton is composed of 80% cortical bone and 20% trabecular bone overall [11]. Different bones in the skeleton have different ratios of cortical to trabecular bone: the ratio is 50:50 in the femoral head and 95:5 in the radial diaphysis. Cortical bone is compact structural tissue, with only 10% porosity, while trabecular bone is composed of a honeycomb-like network of trabecular plates and rods interspersed in the bone marrow compartment. Both cortical and trabecular bone are composed of repeating units of haversian system or osteon, which is primary anatomical and functional unit. They are cylindrical in shape approximately 400 mm long and 200 mm wide at the base and form a branching network within the cortical bone [11]. Each osteon has concentric layers of mineralized matrix, called concentric lamellae, which are deposited around a central canal called haversian canal, each containing a blood and nerve supply (Figure 2.1). Cortical bone is covered by a highly vascularized fibrous connective tissue, the periosteum on the outside and an inner endosteal surface. Bone formation usually exceeds bone resorption on the periosteal surface, resulting in appositional growth and therefore bones normally increase in diameter with aging. The endosteal surface has a higher rate of remodeling activity than periosteal surface, mainly due to greater biomechanical strain or greater cytokine exposure from the adjacent bone marrow. Bone resorption typically exceeds bone formation on the endosteal surface, so the marrow space normally expands with aging. Cortical bone is metabolically less active than trabecular bone. This can be understood from the fact that an estimated 21×10^6 cortical osteons are there in human adults with an total haversian remodeling area of 3.5 m^2, in comparison with approximately 14×10^6 trabecular osteons, but a total remodeling area of 7 m^2 [12].
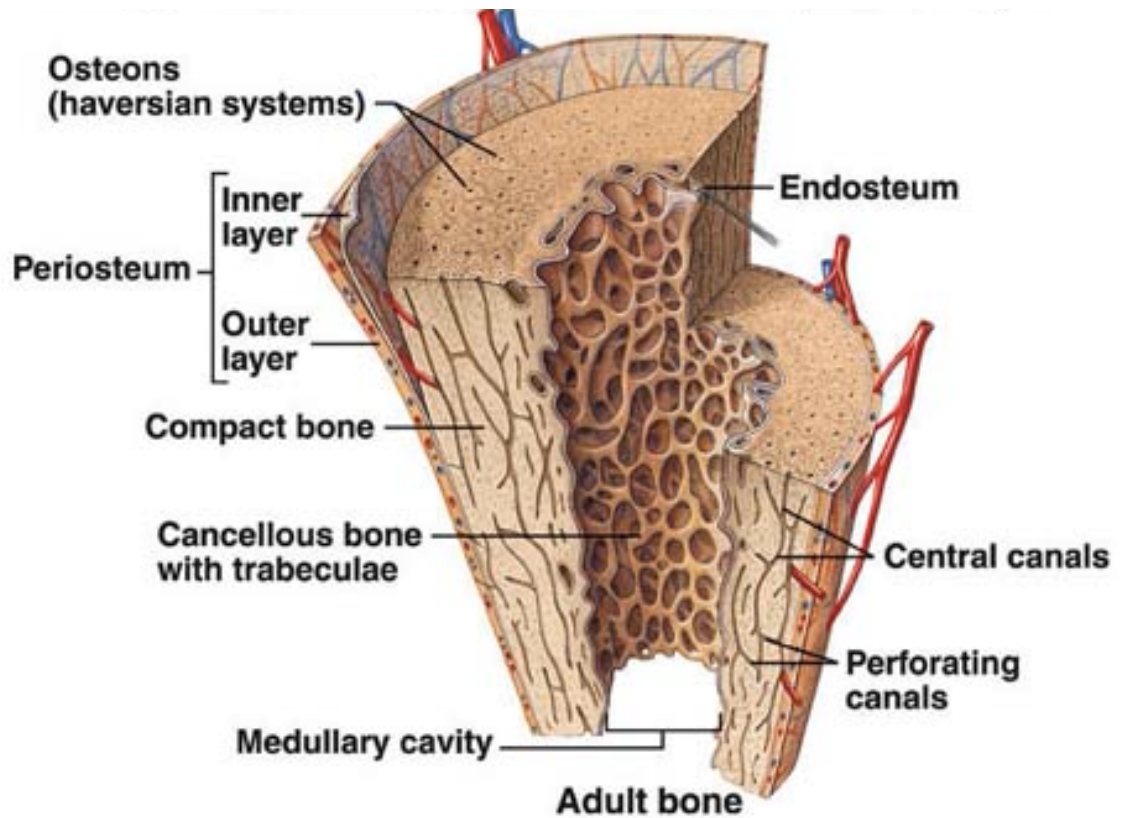
Figure 2.1: Detailed structure of bone (Courtesy: Mcgraw-Hill Companies, New York City, New York)

Cortical and trabecular bone have a lamellar pattern, in which collagen fibrils are laid down in alternating orientation [11]. The mechanism by which the osteoblasts lay down the collagen is unclear, but lamellar bone has a significant strength due to the alternating orientation of collagen fibrils. The normal lamellar pattern is absent in woven bone, in which the collagen fibrils are laid down in random manner. Woven bone is normally produced during the formation of primary bone and therefore is weaker than lamellar bone.

Bone marrow is composed of hematopoietic tissue and stromal cells [13]. Recent studies

have shown that marrow stromal cells are the progenitor cells for skeletal tissue [14].

There are five different cell types involved in bone maintenance and remodeling;

osteoclasts, osteoblasts, osteocytes, mesenchymal stem cells (MSCs), and bone lining

cells (Figure 2.2).
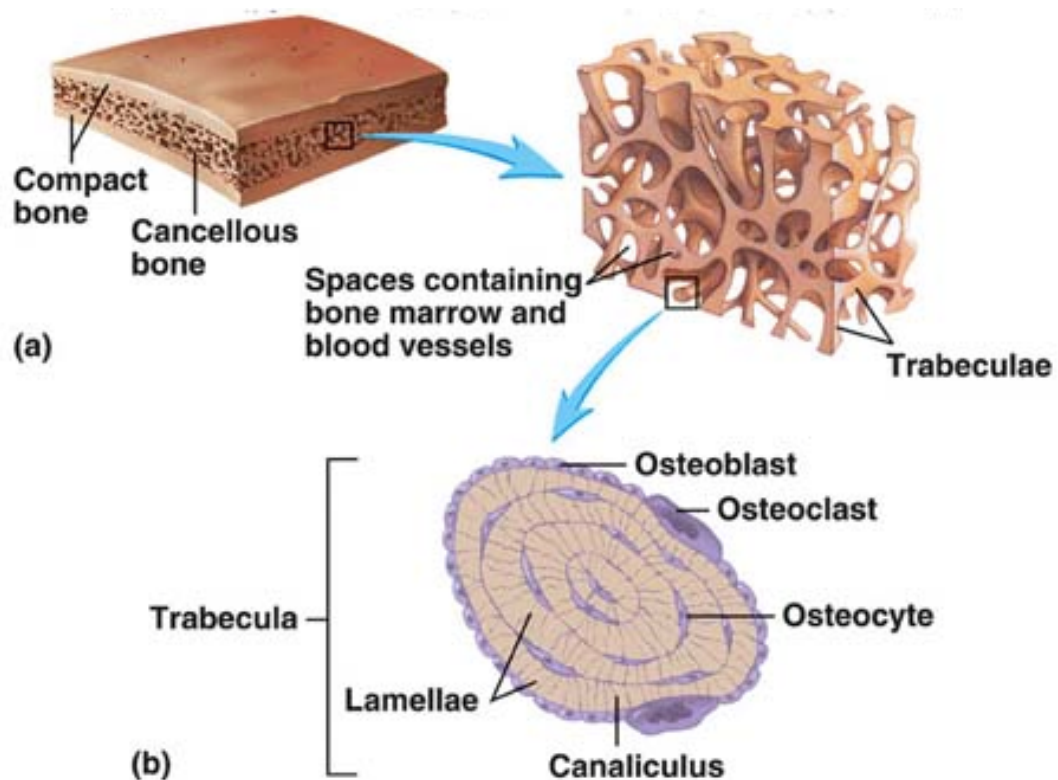
Figure 2.2: Structure and components of bone tissue (Courtesy: Mcgraw-Hill Companies, New York City, New York)

Osteoclasts are responsible for bone resorption, which is the first step in bone remodeling

process, followed by bone homeostasis [15,16]. These cells are large multi-nucleated

cells that differentiate from a fraction of monocytes found in peripheral blood [17]. They

bind to the bone matrix via interactions between integrin receptors in their cell

membranes and RGD (arginine, glycine and aspargine) containing peptides in the matrix proteins. Osteoclast-mediated bone resorption takes around 2-4 weeks during remodeling cycle. Their formation, activation, and resorption are regulated by the ratio of receptor activators of NF-KB ligand (RANKL) to osteoprotegerin (OPG), IL-1 and IL-6, colony stimulating factor (CSF), parathyroid hormone, 1,25-dihydroxyvitamin D and calcitonin [18,19]. Activated osteoclasts secrete hydrogen ions via H+-ATPase pumps and chloride channels on their cell membranes to lower the pH within the bone resorbing compartment to as low as 4.5, which helps solubilize bone mineral [20]. Resorbing osteoclasts also secrete tartarate-resistant acid phosphatase, cathapsin K, matrix metalloproteinase 9 and gelatinase from cytoplasmic lysosomes to digest the organic matrix, resulting in the formation of saucer-shaped lacunae [21]. Soon after resorption phase, the osteoclasts undergo apoptosis [22].

At the completion of bone resorption, the cavities contain a variety of cells including monocytes, osteocytes released from bone matrix and preosteoblasts recruited to begin new bone formation. The signals linking the end of bone resorption and beginning of bone formation are unclear, but derived factors such as TGF-β, IGF-1, IGF-2, BMPs, PDGF and FGF have been found to play an important role [23,24]. Bone matrix releases TGF-β, which decreases osteoclast resorption by inhibiting RANKL production by osteoblasts. Another reason for the reversal phase has been proposed to be mediated by the strain gradient in lacunae [25]. Osteoblasts are derived from mesenchymal stem cells via Wnt/ β-catenin pathway [26]. They synthesize the osteoid (non-mineralized organic matrix of the bone, i.e. type I collagen, osteocalcin, osteopontin, bone sialoprotein and bone morphogenetic proteins) and regulate mineralization of the matrix by releasing

small membrane bound vesicles that concentrate calcium and phosphate and enzymatically destroy mineralization inhibitors such as pyrophosphate or proteoglycans [27]. Osteoblasts also play an important role in vascularization process by secreting morphogens that activate angiogenesis by signaling endothelial cells. At the completion of bone formation, 50-70% of osteoblasts undergo apoptosis, with the remaining cells becoming osteocytes or bone lining cells.

Osteocytes are terminally differentiated osteoblasts entrapped in the extracellular matrix (ECM) and are involved in the maintenance of ECM and calcium homeostasis [28]. They have extensive filopodial processes that lie within the canaliculi in mineralized bone [29]. Osteocytes also sense mechanical stress and communicate signals for bone remodeling and tissue maintenance [30]. Rapid fluxes of bone calcium across filopodial gap junctions are believed to stimulate transmission of information between osteoblasts on the bone surface and osteocytes within the bone [31].

Bone lining cells are flat cells that cover all bone surfaces and are known to arise from osteoblasts that become inactive, but they retain the ability to redifferentiate into osteoblasts upon exposure to parathyroid hormone or mechanical forces [32,33]. These cells may regulate influx and efflux of mineral ions into and out of bone extracellular fluid, thereby serving as a blood-bone barrier.

ECM is another major component of bone and is composed of 20-40 % organic matrix, 50-70% mineralized matrix, 5-10% water and <3% lipids. The organic matrix is mainly type I collagen and is synthesized intracellularly as tropocollagen and then exported forming fibrils. Small fractions of 200 other non-collagenous proteins, such as

glycoproteins, proteoglycans, integrin-binding proteins and growth factors also are present in ECM. The most abundant mineral in bone ECM is hydroxyapatite $[Ca_{10}(PO_4)_6(OH)_2]$, a calcium phosphate, crystallized at the surface of collagen fibrils [27,34]. Matrix maturation is associated with the expression of alkaline phosphatase and several non-collagenous proteins, including osteocalcin, osteopontin and bone sialoproteins, as these calcium and phosphate binding proteins help regulate ordered deposition of mineral by regulating the amount and size of hydroxyapatite crystals. Osteoblasts secrete vesicles containing alkaline phosphatase, which cleaves the phosphate groups and acts as the foci for calcium and phosphate depositions. The bone mineral content provides mechanical rigidity and load-bearing strength to the bone whereas the organic content provides elasticity and flexibility.

Bones are developed by two main processes- intramembranous and endochondral ossification. Intramembranous ossification process generates flat bones and the skull structure. In this pathway, initially embryonic mesenchyme condenses in fibrous connective tissue membrane to develop primary ossification centers, which will eventually fuse to form a network of interconnected trabeculae made of woven bone. After that, periosteum is formed at the surface of trabeculae, which is further mineralized and part of intertrabecular connective tissue is transformed to hematopoietic tissue. And finally the woven bone is remodeled into a lamellar bone. In the endochondral ossification, long bones, vertebrae and pelvis are generated from cartilaginous tissue. This process starts in the fetus where mesenchymal stem cells (MSCs) differentiate into chondrocytes, converting the condensed mesenchyme into a cartilaginous model (hyaline) of bone that will expand in its extremities, while becoming hypertrophic in the

center. These hypertrophic chondrocytes will promote primary ossification by secreting molecules such as alkaline phosphatase, type X-collagen or vascular endothelial growth factor, which will induce ossification of cartilage. This tissue will be resorbed becoming a structure onto which the progenitor cells differentiate into osteoblasts that will start to deposit osteoid. After birth, secondary ossification centers develop at the extremities of long bones, allowing development and growth of bone structure.

2.2 Fracture Healing

The process of fracture healing recapitulates bone development process and can be considered a form of tissue regeneration. Following a trauma, bone heals by either indirect fracture healing, which consists of both intramembranous and endochondral bone formation or direct intramembranous (Figure 2.3). Of these, indirect form of fracture healing is the most common form as it does not require anatomical reduction or rigidly stable fracture.
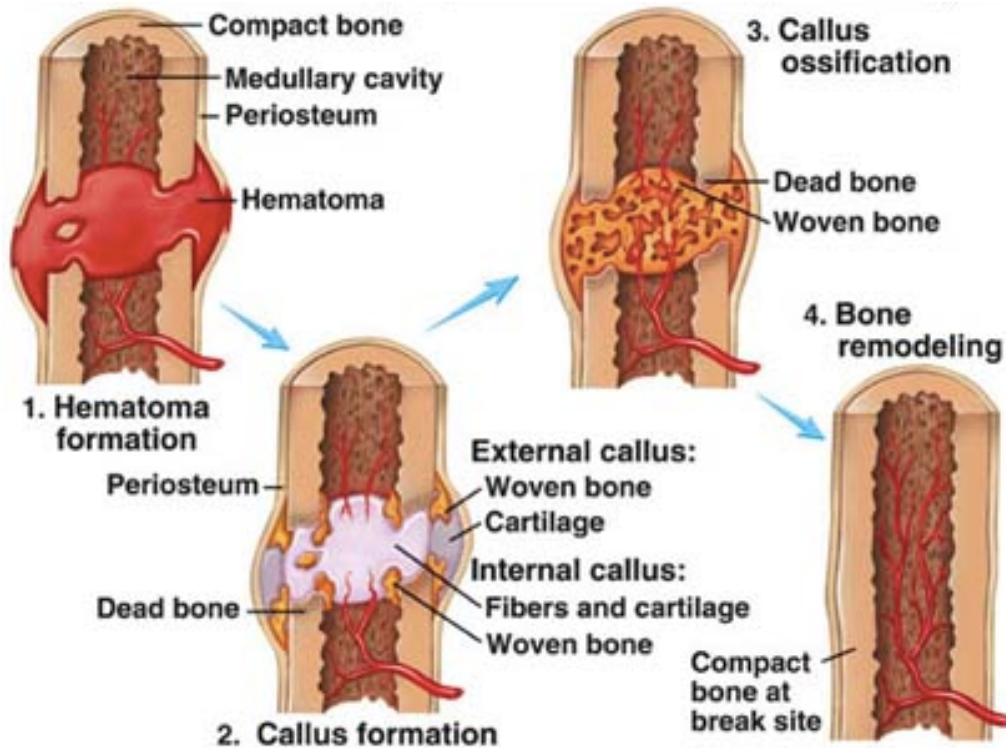
Figure 2.3: Events following a bone fracture (Courtesy: Mcgraw-Hill Companies, New York City, New York)

2.2.1 Indirect Fracture Healing

This type of healing occurs usually in non-operative fracture treatment and in some operative treatments where motion occurs at the fracture site, such as intermedullary nailing, external fixation or internal fixation of complicated comminuted fractures [35]. Although it consists of both intramembranous and endochondral ossification, the formation of cartilaginous callus which undergoes mineralization, resorption and ultimately replaced with bone are the key features to this process [36]. This healing can be divided into six steps:

I. Acute inflammatory response – A brief and highly regulated secretion of proinflammatory molecules is necessary for tissue regeneration – it peaks within first 24 h and is complete after 7 days [37]. Immediately following a trauma, a hematoma is generated which coagulates around the fracture ends and within medulla forming a template for callus formation. The initial proinflammatory response involves secretion of tumor necrosis factor α (TNF-α), Interleukins (IL-1,6,11 and 18) [38]. These factors recruit inflammatory cells to promote angiogenesis. TNF-α is expressed by macrophages and other inflammatory cells and has been shown to induce osteogenic differentiation of MSCs. Of the interleukins, IL-1 and 6 are very crucial for fracture healing. Expression of IL-1 overlaps with TNF-α and it induces production of IL-6 in osteoblasts, promotes the production of primary cartilaginous callus and also promotes angiogenesis at the injured site [39]. IL-6 on the other hand stimulates angiogenesis, vascular endothelial growth factor (VEGF) production and differentiation of osteoblasts and osteoclasts [40]

II. Recruitment of MSCs – The origin of MSCs for bone tissue regeneration is still an ambiguity and can be from soft tissue surrounding the defect, bone marrow or systemic recruitment of circulating MSCs [41]. The molecular events that lead to the recruitment of MSCs are also unclear, but BMPs have long been known to play an important role [42]. Stromal cell derived factor -1 (SDF-1) expression was also found to be increased at fracture site. SDF-1 has been shown to recruit G-protein coupled receptor CXCR-4 expressing MSCs to the injured site during

endochondral healing. Hypoxia inducible factor 1α (HIF-1α) also plays an important role in bone repair by induction of VEGF for revascularization [43].

III.   Development of cartilaginous and periosteal bony callus – Following the formation of hematoma, a fibrin rich granulation tissue, which is a new connective tissue with few blood vessels, is formed on the wound. Within this tissue, endochondral formation occurs between fracture ends and external to the periosteal sites and within 7-9 days post trauma, a soft, less stable cartilaginous callus is formed [44]. This was indicated by high expression levels of type II procollagen and proteoglycan core protein extracellular markers. At the same time, subperiosteally, intramembranous ossification response occurs adjacent to the proximal and distal ends of the fracture, generating hard callus. It is this hard callus formation, which provides the fracture with semi-rigid structure, which allows weight bearing. The MSCs are responsible for the callus formation and is followed by a cascade of molecular events, which involve collagen I and II matrix production, and several peptide molecules. Transforming growth factor β (TGF-β) members - TGF- β2, TGF- β3 are involved in chondrogenesis and endochondral ossification, whereas BMP5 and 6 have been suggested to induce cell proliferation in intramembranous ossification at periosteal site. In addition, BMPs have been shown to play a crucial role in callus formation as mice with inactivation mutation in BMP-2 are not able to form callus to heal fractures [45].

IV.   Neovascularization and revascularization at the fracture site – A good blood supply and revascularization is necessary for successful bone repair. At the endochondral ossification site, this involves not only angiogenic pathways, but

also chondrocyte apoptosis and cartilaginous degradation as the removal of cells and extracellular matrix (ECM) is necessary for ingrowth of blood vessels. Once this structural pattern is achieved, two pathways can be followed, an angiopoietin dependent pathway and a VEGF dependent pathway. Angiopoietin pathway, with primarily angiopoietin 1 and 2, is induced initially to promote formation of vessels from the pre-existing ones in the periosteum [46]. Whereas in the VEGF pathway, it promotes vascular regeneration. Both osteoblasts and hypertrophic chondrocytes have shown high expression levels of VEGF, indicating promotion of blood vessels and transformation of avascular cartilaginous tissue to vascularized osseous tissue. VEGF is known to promote vasculogenesis, i.e aggregation and proliferation of endothelial MSCs into vascular plexus and angiogenesis, i.e. growth of new vessels from already existing ones. Several other factors have been shown to have pro-angiogenic effect, such as the synergistic interaction of BMPs with VEGF and the role of mechanical stimuli to enhance angiogenic activites.

V. Mineralization and resorption of cartilaginous callus − The primary soft cartilaginous tissue should be replaced by hard bony callus for bone regeneration. Wnt-family of molecules is thought to regulate differentiation of pluripotent MSCs into the osteoblastic lineage and to positively regulate osteoblastic bone formation. Resorption of mineralized cartilage is initiated by macrophage colony stimulating factor (M-CSF), receptor activator of nuclear factor kappa B ligand (RANKL), osteoprogegerin (OPG) and TNF-α and they also recruit bone cells and osteoclasts to form woven bone. TNF-α's most important role is apoptosis of

chondrocytes. Calcification mechanism involves mitochondria, which accumulates calcium-containing granules created in the fracture environment. These calcium granules are transported into the ECM, where they are precipitated with phosphates and form initial mineral deposits. The peak of hard callus formation is reached 14 day post trauma in small animals as proved by ECM markers such as type I procollagen, osteocalcin, alkaline phosphatase and osteonectin [44].

VI. Bone remodeling – Despite the formation of hard callus, biomechanical properties of natural bone are not restored and in order to achieve this, fracture healing cascade initiates a second resorptive phase, this time to remodel the hard callus to a lamellar bone structure with central medullary canal. During this phase, IL-1, TNF- α and BMPs expression increases, while TGF-β expression decreases [47]. Remodeling is carried out by balancing bone resorption process by osteoclasts and lamellar bone formation process by osteoblasts. Bone remodeling is shown to be a result of production of electrical polarity created when pressure is applied in crystalline environment [48]. Axial loading of long bone creates ne electropositive convex surface and one electronegative concave surface, activating osteoclasts and osteoblasts. Due to these actions, external callus is replaced by lamellar bone and internal callus results in a medullary cavity resulting in diaphyseal portion of bone. Although this process is initiated 3-4 weeks in animal and human models, remodeling may take years to be completed.

In cases, when neither adequate blood supply nor mechanical stability is achieved, it results in strophic fibrous non-union and in cases with good vascularity but unstable

fixation, healing process progresses to form a cartilaginous callus, but results in hypertrophic non-union or pseudoarthritis.

2.2.2 Direct Fracture Healing

For this process to occur, it requires a correct anatomical reduction of fracture ends, without any gap formation, and a stable fixation resulting in substantial decrease in interfragmentary strain. When these conditions are met, direct bone healing can occur by direct remodeling of lamellar bone, the haversian canals and blood vessels via two processes:

I. Contact healing – If the gap between bone ends is less than 0.01 mm and interfragmentary strain is less than 2%, contact healing follows [49]. In this process, bony union and restoration of haversian system occurs simultaneously in longitudinal direction. Re-establishment of haversian system allows penetration of blood vessels carrying osteoblastic precursors. Osteons mature by remodeling to lamellar bone resulting in fracture healing without periosteal callus formation.

II. Gap healing – This type of healing occurs when defect is less than 800 μm-1 mm [50]. In this process, initially lamellar bone oriented perpendicular to the long axis is created, therefore requiring a secondary osteonal reconstruction. In this process, primary bone is replaced by longitudinal revascularized osteons carrying osteoprogenitor cells, which differentiate into osteoblasts and produce lamellar bone on each surface of the gap [51]. This lamellar bone is laid perpendicular to the long axis and therefore is mechanically weal and therefore undergoes secondary remodeling to restore biomechanical and anatomical properties.

2.3 Bone Tissue Engineering

Great number of bone defects do not heal properly using standard treatments [52] and this can be due to severity of an injury, extent of soft tissue damage, inadequate internal fixation, advanced age or co-morbidities such as diabetics [52]. The National Center for Health Statistics' National Health Interview Survey provides information on the percentage of fractures in the United States [53]. Of a total of 5,946,000 fractures per year, the average annual number of lower leg fractures (tibia, fibula and ankle) in the United States was 581,000. Approximately 10% of the tibial fractures result in non-unions [54]. The majority of non-union fractures (62%) occur in tibia, while 23% occur in the femur, 7% in the hemerus and 7% in the forearm [55]. For all critical or non-union bone defects, a biomaterial must be filled at the defect site. The current gold standard treatment is using an autogenous bone grafting. In this method, bone is removed, usually pelvis or iliac crest in the patient and grafted at the defect site. However, the complication rate is very high at around 30% and includes donor site morbidity, limited availability, extended surgical and anesthesia time, prolonged hospitalization and rehabilitation, risk of deep infection, hematoma, and inflammation [56-63]. Second preferred method is usage of allografts. They are derived from human cadavers and similar to autografts, their success is also attributed to physical and biological similarity in donor and host tissue. However, allografts are associated with improper methods of tissue recovery leading to disease transmission (rate of incidence as high as 13%) [64-66], reduced biological and mechanical properties following sterilization and storage and limited availability. The last type of bone graft would be a xenograft, a tissue obtained from a non-human source. After almost two decades of investigation and clinical trials, xenografts are widely

considered unsuitable for transplantation due to risk of disease or virus transmission, toxicity associated with sterilization, immunogenicity and finally host rejection [67-69].

All these concerns motivated the development of bone graft substitutes in recent years. A number of different materials are being tested to observe their efficacy in bone regeneration [70-74]. Advantages in utilizing these include: elimination of disease transmission risk, fewer surgical procedures, reduced risk of infection or immunogenicity and abundant availability of synthetic materials. Therefore, an ideal bone graft substitute must be capable of physiochemical biomimetic environment while biodegrading as the natural tissue builds and promoting the desirable physiological responses [75-79]. For a biomaterial to act as a bone scaffold, it should possess the following properties: provide mechanical support at the affected site, act as a scaffold for osteoid deposition, contain porous architecture to allow vascularization and bone in-growth, support and promote osteogenic differentiation in non-osseous, synthetic scaffold, promote scaffold-host tissue integration, degrade in a controlled fashion to facilitate load transfer to developing bone, non-toxic degradation products, should not incite chronic degradation response, capable of sterilization without loss of bioactivity and able to deliver bioactive molecules or drugs in a controlled manner to accelerate bone healing [80-82].

2.4 Chitosan as a Biomaterial

Chitosan is a natural polymer formed by alkaline deacetylation of chitin, the second most abundant natural polysaccharide, primarily obtained from shellfish, such as crab and shrimps. Chemically it comprises of β (1-4) linked D-glucosamine residues with N-acetyl-glucosamine side chains that makes it structurally similar to glucosaminoglycans

(GAGs), which are usually the interacting molecules with osteoblasts [83-85], make it particularly attractive as a biomaterial for bone defects. Chitosan has been found to provoke least foreign body response, leading to just normal granulation and neutrophils accumulation, which ultimately result in triggering local cell proliferation and integration of the scaffold with the host [86,87]. Chitosan has already been studied for a number of biomedical applications including wound dressing, drug delivery system, and space filling implants and has already gained Food and Drug Administration approval for human use in wound dressing [88-92]. Chitosan's degree of deacetylation has often been cited as an important parameter that determines physiochemical and biological properties such as crytallinity, hydrophilicity, degradation and cell response [93-98]. Chitosan's molecular weight ranges from 300 to over 1000 kD with a degree of deacetylation from 50% to 95%. Chitosan is insoluble in solutions above pH 7.0, however the free amino groups of glucosamine are protonated in dilute acids (pH<6.0). Chitosan can also be degraded *in vivo* by lysozymes through hydrolysis of acetylated residues, but studies have shown that degradation rate is dependent on the degree of deacetylation, which is determined by the ratio of glucosamine/N-acetyl glucosamine. The highly deacetylated chitosan (>80%) has the lowest degree of degradation; whereas the lesser deacetylated molecules have much faster degradation [99]. Finally the degradation products are varying length of oligosaccharides. Degradation is an important property of a bone scaffold material because in order for the bone to heal completely, the scaffold material has to be replaced completely by the new natural bone. All the properties it possesses- biocompatibility, biodegradability, wound healing capabilities and antibiotic properties makes it an attractive biomaterial for bone regeneration. However, the methods of

preparing chitosan scaffolds in the previous studies do not fulfill all the necessary criteria for bone tissue engineering. Therefore, a better understanding of the already used techniques is necessary to determine the advantages and disadvantages associated with them.

2.5 Growth Factors for Bone Tissue Engineering

One of the techniques to improve osteoconductivity of chitosan scaffolds is to incorporate biologically active molecules, which play a crucial role in bone regeneration. As discussed previously, growth factors are expressed in all the stages of fracture healing. Some of the important growth factors include TGF-β, IGF-I and II, PDGF, FGF and various types of BMPs.

BMPs are the members of TGF-β superfamily and are known to be osteoinductive [100,101]. BMP was first identified by Urist in 1965, when he observed that demineralized bone matrix (DBM) induces ectopic bone formation when implanted under skin of rodents and there was a recapitulation of all the events that occur during skeletal development [102]. BMPs are known to be produced by MSCs, osteoblasts and chondrocytes and they induce a cascade of cellular pathways that promote cell growth, migration and differentiation of MSCs to repair injury, stimulate angiogenesis, as well as synthesis of ECM and play a regulatory role in tissue hemeostasis [103]. Studies have shown that in fracture healing, BMP-2 mRNA shows maximum expression within 24 h of injury, indicating an important role in initiating the repair cascade. BMP-3, BMP-4, BMP-7 and BMP-8 have been shown to be expresses during bone repair from days 14-21, when the resorption of calcified cartilage and osteoblastic recruitment are most active,

and bone formation occurs. BMP-7 has the capacity to select a cell population from bone marrow and assign it a skeletogenic potential under *in vitro* and *in vivo* environments [104-106]. BMP-5 and BMP-6 and other members of TGF superfamily are expressed from days 3-21 during fracture healing in mice, suggesting they have a regulatory effect on both intramembranous and endochondral ossification. BMP-2 to BMP-8 show high osteogenic potential, however BMP-2, BMP-6 and BMP-9 are the most potent inducers of MSCs differentiation to osteoblasts, while other stimulate maturation of osteoblasts [107].

Another important growth factor is insulin like growth factor – I and II. IGF-I and IGF-II are delivered by osteoblasts, chondrocytes, endothelial cells and bone matrix and these growth factors are detected by MSCs and bone cells in autocrine/paracrine manner by IGF binding proteins (IGFBPs), which modulate their action by intracellular tisone kinase pathway [108]. IGF-II is the most abundant GF in bone matrix. However, IGF-I is 4 to 7 times more potential in synthesis of bone matrix (type I collagen and non-collagen matrix proteins) [109]. *In vitro* studies have indicated that IGF-I mRNA was expressed during MSCs recruitment and proliferation, while IGF-II mRNA was expressed later during endochondral bone formation by osteoblasts and chondrocytes [110]. Therefore, IGFs are necessary to promote bone formation, repair and MSCs cell proliferation and differentiation.

However, clinical applications are very restricted, with BMP-2 being used for open tibial and spinal fractures and BMP-7 for non-unions in tibia [111]. Both the BMPs are currently being used with collagen as a carrier. New strategies that are still being investigated are local and controlled release of growth factors from bone graft substitute

that can be injected at the defect site. This technique would eliminate many clinical problems being faced today in fracture treatment, such as (1) the need for exposure of the fracture (2) risk of infection, and (3) side effects caused by carrier.

As it is known, the organic fraction of bone ECM consists mostly of fibrillar proteins (collagen type I), glycoproteins (osteonectin, fibronectin etc.), sialoproteins (BSP, osteopontin) and proteoglycans, consisting of a core protein with covalently attached glycosaminoglycans (chondroitin sulpfate, dermatin sulfate, heparin sulfate and heparin). Growth factors interact with the GAG units and this process is critical for morphogenetic processes during tissue regeneration. [112-114]. The interaction between growth factors and GAGs is mediated by electrostatic interactions, Vander Waals interactions and hydrogen bonds. Localized growth factor binding results in formation of stable gradients, which results in directed migration of the respective cell types [115]. Other ECM components like fibronectin, vitronectin, tenascin, thrombospondin, fibrillin and collagen type II have been also found to interact with BMPs [116].

2.6 Controlled Growth Factor Delivery

Despite the knowledge on growth factor biology in bone regeneration, possibility of large-scale production of growth factors, first clinical trials with a number of promising growth factors like VEGF, BMPs have not shown significant effects or were of limited efficiency [117-119]. In this trial, pure growth factors were injected as bolus. Such uncontrolled delivery resulted in systemic rather than localized response [120]. Furthermore, in addition to their distribution in the body, the relatively short half-live of growth factors in the circulation may have resulted in initial excess levels followed by a

deficit of growth factors [121-123]. Several animal studies have shown that a narrow therapeutic window of growth factors dose acts positively towards regeneration, whereas too low or too high doses will most probably lead to severe side effects [124,125]. Therefore, in order to maintain physiologically relevant doses of growth factor and preserve its activity over a prolonged period of time, localized delivery of growth factors is an ideal solution. For growth factor administration, it can be either freely embedded or bound to it. In the former approach, the release of growth factor is driven by passive diffusion or coupled to material degradation. Release kinetics can be varied by either altering material degradation rate or by changing growth factor quantity [126].

The efficacy of factor delivery is significantly enhanced by delivery of growth factors by three-dimensional scaffolds [127,128]. Two distinct strategies for delivery of growth factors by biomaterials have been pursued: (i) chemical immobilization of growth factors into or onto the matrix and (ii) physical immobilization of growth factors in the delivery system (Figure 2.4). The techniques currently being used for physical encapsulation of growth factor include solvent casting and particulate leaching, freeze-drying, phase separation, melt molding, phase emulsion, and gas foaming [129]. Table 2.1 lists the advantages and disadvantages associated with these techniques [130-140]. An important factor to consider is to minimize the exposure of growth factors to harsh conditions during fabrication in order to protect the bioactivity of the proteins. Many other physical and chemical factors also influence the release kinetics such as the polymer molecular weight, distribution, hydrophobicity and porosity. The encapsulation efficiency and mechanism of growth factor encapsulation depends on the hydrophobic-hydrophobic or hydrophilic- hydrophillic interactions among the proteins and polymer. It is also

dependent on the complexity of the structures of the carrier, for example, microparticles with a core-shell structure prevented loss of growth factor during fabrication and washing processes resulting in better encapsulation efficiency [141]. It is necessary that the carrier material be fabricated in conditions that favor incorporation of the growth factor; temperature, pH, and chemicals composition playing an important role in protein stability.
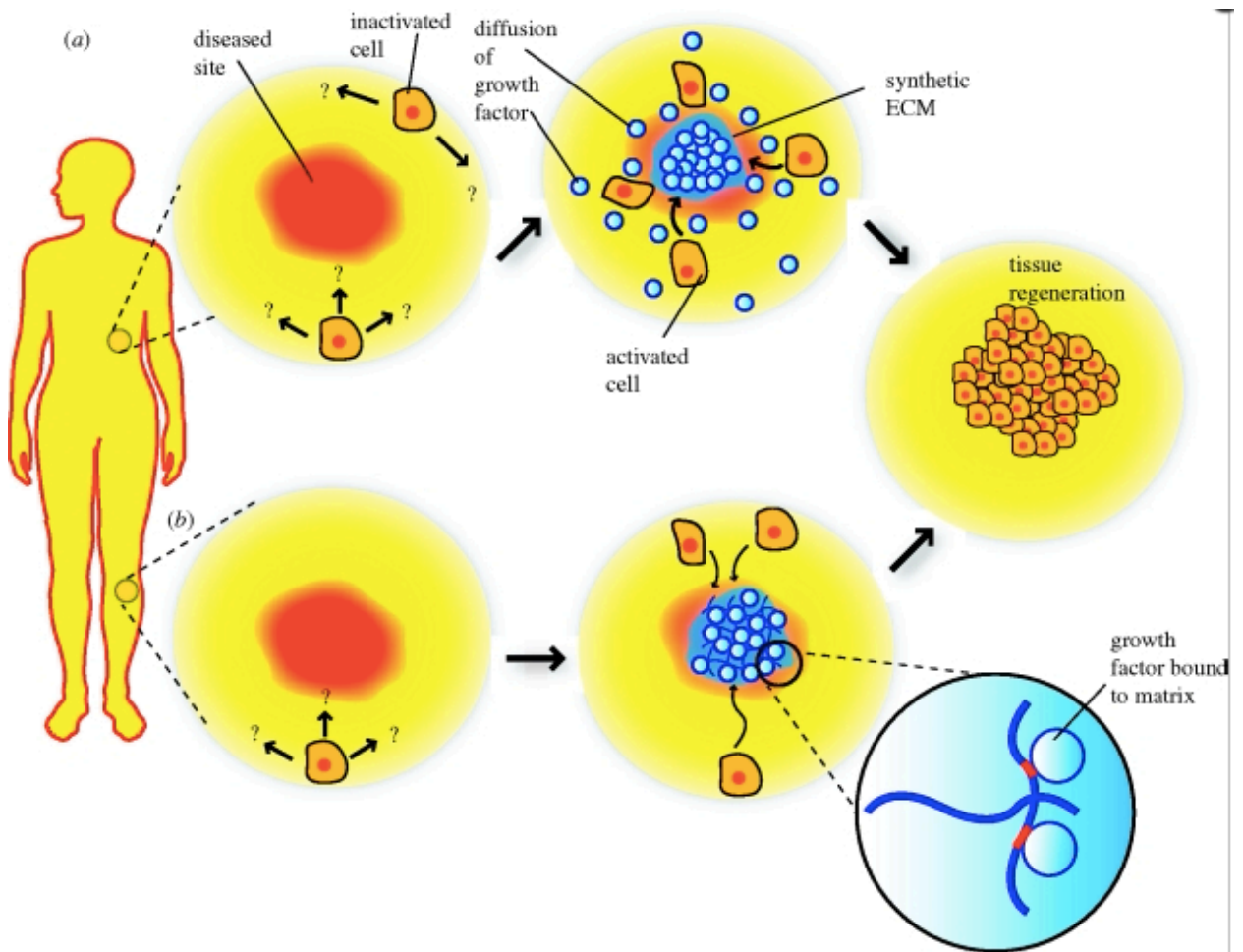
Figure 2.4: Two tissue engineering approaches using synthetic ECM to present growth factors to tissue (a) physical encapsulation of growth factors to target specific cell population to migrate and direct tissue regeneration (b) chemical entrapment of growth factors [140].

Table 2.1: Advantages and disadvantages associated with various fabrication techniques when incorporating growth factors

Technique	Advantages	Disadvantages
Freeze drying	High porosity and interconnectivity	Limited pore sizes range (15-35 μm), reduced mechanical properties
Phase separation	High porosity	Limited pore size(1-10 μm), residual solvents
Gas foaming	Free of organic solvents, control over porosity	Low pore interconnectivity
Solvent casting/particulate leaching	Control over porosity, pore size and crystallinity, high porosity	Residual solvents and porogen materials, limited mechanical properties
Melt molding	Control over macrogeometry, porosity and pore size, free of harsh organic solvents	High temperatures
Phase emulsion	Control over porosity, pore size and interconnectivity	Limited polymer types and mechanical properties, residual solvents

2.7 Drug Delivery

Gram-positive organisms are considered to be a major cause of bone infections, especially *staphylococci* [142]. This genus of bacteria is a principal causative agent for mainly two types of bone infection – septic arthritis and osteomyelitis. These infections involve the inflammatory destruction of joint and bone [143,144]. It is a known fact that cytokines play a prominent role in modulating bone turnover, and perturbation of their levels has a profound effect on this process. Infection of bone by *Staphylococcus* species initiates local and systemic production of TNFα, IL-1 and IL-6, which shifts the homeostatic balance of bone turnover, increasing osteoclast differentiation and diminishing osteoblasts-mediated bone matrix production and mineralization, thereby driving bone destruction [145]. These species have also been found to interact directly with bone cells. *Staphylococcus epidermidis* is also able to invade and grow within cultured osteoblasts *in vitro*, where it will be shielded from immune effector mechanism and antibiotics [146]. *S. epidermidis* is a gram-positive bacterium associated with normal human flora, particularly skin flora. Although *S. epidermidis* are not pathogenic, they are the most common coagulase-negative *Staphylococcus* species in many types of infection, including osteomyelitis, and infection of prosthetic joints. [147-150]. *S. epidermidis* organisms associated with the devices tend to produce a slimy material that mediates adherence of these organisms to the smooth surfaces of prosthetic devices [151,152]. Surveillance data from the Health Protection Agency on surgical site infection between 1997-2005 found *S. aureus* to be the causative organism in 41.4% of hip prosthesis, 33.5% of knee prosthesis, 53% of open bone reduction of bone fracture and 59.1% of hip hemiarthroplasty infection. *S. epidermidis* is the most common coagulase-negative

Staphylococcus species in many types of infection, including osteomyelitis and infection of prosthetic joints and it accounts for 15.1%, 20.7%, 7.5% and 6.3% of the infections caused by *S. aureus* [153]. Clinical evaluations have demonstrated that bacterial adhesion to an implant is an important step in development of an infection [154,155]. One important observation in regards to microbial infection is that, the initial adhesion of the bacteria to the surface of the biomaterial is a very crucial step in pathogenesis of infection. They form biofilms on the biomaterial and that protects the bacteria from immune system and antibiotics. Therefore the best way to treat the infection is to prevent colonization of microorganism in the early stages [156,157]. Biomaterials that have antibacterial properties and are capable of controlled release of antibiotics at the site of action would be the best approach to reach deep inside the tissue with an effective drug concentration [158]. Chitosan has been demonstrated to possess antibacterial activity against many bacteria, filamentous fungi and yeast [159]. Research suggests that the antibacterial activities of chitosan rely on numerous intrinsic and extrinsic factors like pH, microorganism species, presence and absence of metal cations, pKa, molecular weight and degree of deacetylation [160-163]. Chitosan has a wide spectrum of activity against gram-positive and gram-negative bacteria, but lower toxicity against mammalian cells [164]. All these properties of chitosan- biocompatibility, biodegradability, wound healing capabilities and antibacterial properties make it an ideal material for preparing scaffold materials to be used in bone tissue engineering. Therefore, as a measure of prophylaxis, the surgeons are keenly interested in developing or using materials that possess antibacterial properties.

The activity of bone healing also occurs at the same time and is accompanied by many growth factors, molecular signaling and various cellular activities [165,166]. These processes suggest that it would be beneficial to develop a system which could simultaneously and timely deliver both the growth factor and the drug in a sustained manner to help both the above mentioned processes [167,168]. For drug delivery systems, there is particular interest in developing microparticle system in which the growth factors and drugs are encapsulated in the microparticles for efficient release over a long period of time [169]. The core-shell structure of the microparticles can overcome the problem of burst release and at the same time protect the growth factor from harsh environmental conditions. Two main challenges in developing this system are to control the release behavior of the drug and growth factor simultaneously and to optimize the dosage of the drug and growth factor in order to observe efficient bone regeneration. Other parameters that need to be considered include the maintenance of effective concentration, prolong their availability and to reduce the effect of high burst doses [170-173].

Cephalosporins are the commonly used antibiotics to treat osteoarticular infections, given their broad range of activity spectrum [174]. Cefazolin is a semisynthetic cephalosporin with good *in vitro* activity against resistant strains of staphylococci (MIC_{90} 1mg/L), excellent tolerance and bone diffusion [175,176]. Several authors recommend the use of cefazolin for treating bone and joint infections, particularly those due to *S. aureus* [177,178].

Serious infections caused by resistant strains are treated with vancomycin (glycopeptide antibiotic with high activity against gram-positive bacteria) [179]. Therefore, cefazolin and vancomycin along with *S. epidermidis* were chosen for our study.

Chapter 3

Fabrication and Characterization of Chitosan-tri-polyphosphate Microparticles using Mild Environmental Conditions

In this chapter, experiments conducted address hypothesis I. In order to do so, microparticles are fabricated using emulsification and coacervation method. IGF-1 growth factor is encapsulated in both types microparticles and release is studied to determine the influence of organic solvents used during microparticles fabrication. *In vitro* degradation study is conducted using coacervation microparticles.

3.1 Materials

Chitosan (85% deacetylated), sodium tripolyphosphate (TPP), acetic acid, phosphate buffer saline (PBS) were purchased from Sigma Chemicals (USA). Insulin like Growth Factor-1 (IGF-1) was purchased from Invitrogen (USA), IGF-1 ELISA kit (DY291) was supplied by R&D systems (USA) and LIVE/DEAD cytotoxicity/viability assay (Invitrogen, USA).

3.2 Methods

3.2.1 Fabrication of Chitosan Microparticles by Emulsification and Coacervation Methods

Microparticles were prepared by emulsification and coacervation method. Emulsification procedure followed was similar to the method described by Jayasuriya et al. [180-182]. In the coacervation method, 2% (w/v) chitosan was prepared by dissolving in acetic acid (1% v/v) at room temperature. The mixture was passed through a nylon mesh to remove insoluble substances. This mixture was then added drop wise to the TPP solution. The microparticles were allowed to cross-link overnight and then were air-dried. For optimizing the microparticles preparation, various parameters varied include the amount of TPP, temperature at which the microparticles were being prepared and needle size. IGF-1 was dissolved in water and was added to the chitosan solution to encapsulate the growth factor.

3.2.2 Characterization of Chitosan Microparticles

The surface morphology and particles size was analyzed using the scanning electron microscope (SEM Hitachi S-4800, Hitachi Ltd., Japan). The samples were prepared by fixing the microparticles using the double sided tape and sputter coating with gold before analysis. The SEM operated at 15 kV voltage and 10 μA current. Size distribution data was obtained from measuring diameter of particles obtained using SEM images (n=12), with each image having a minimum of 10 particles.

3.2.3 Degradation Study

The optimized microparticles were also tested for degradation *in vitro*. In order to do so, the microparticles were suspended in PBS of pH 7.4 and 5.1 for a period of 30 weeks. Lysozyme is added to PBS at a concentration of 10mg/L and the samples were incubated at 37°C under continuous shaking at 50 rpm. Lysozyme is usually one of the enzymes involved in degradation of chitosan *in vivo*. The averaged pH changes for microparticles immersed in PBS solutions of pH 7.4 and 5.1 were plotted for 30 weeks.

3.2.4 Determination of IGF-1 Encapsulated in the Microparticles

Twenty mg of microparticles containing IGF-1 were dissolved in 2 ml of 1% acetic acid and kept in incubator at 37°C for 20-24 h. The microparticles dissolved completely and this sample was assayed by IGF-1 ELISA kit according to manufacturer's protocol. Triplicates of each sample were analyzed. Encapsulation efficiency (EE) was calculated as follows:

$$EE = \frac{\text{Actual amount of IGF-1 encapsulated into the microparticles}}{\text{Theoretical amount of IGF-1 added for encapsulation}} * 100\%$$

3.2.5 *In vitro* Release Study of IGF-1

Microparticles (20 mg) were suspended in PBS (pH 7.4). The suspension was incubated at 37°C with continuous rotation at 25-50 rpm for a period of two weeks. At predetermined time points, PBS in the vials was collected and replaced with 2 ml of fresh PBS to maintain the sink conditions. Samples were stored at -20°C until further analysis. The IGF-1 remaining in the microparticles after the study period was determined by dissolving the microparticles in 1% (v/v) acetic acid at 37°C for 24-48 h. To quantify the IGF-I being released ELISA was used. Manufacturer's protocol was followed to do the

ELISA (R & D Systems). Triplicates of each sample were used to do the assay and the results are expressed as mean $\pm$ standard deviation (SD).

3.3 Results

3.3.1 SEM Characterization of Chitosan Microparticles and Degradation Study

SEM images of the microparticles fabricated by emulsification method at room temperature showed that they were in the size range of 50-80 μm. Their shape was a little distorted but overall shape was spherical (Figure 3.1a). The microparticles prepared by coacervation method were spherical. The size range of these microparticles was between 400-700 μm (Figure 3.1b). SEM data has shown (Figure 3.1c) that the surface of the microparticles is groovy and rough. SEM images of microparticles prepared by varying parameters did not show much of a difference in shape and size but the microparticles appear to be smoother when prepared at below room temperature when compared to the microparticles prepared at room temperature. The size of the microparticles obtained from one needle size had consistency and thus less variation in size (Figure 3.2). This is advantageous as reproducibility of microparticles is necessary, which will result in repeatability of the release behavior.
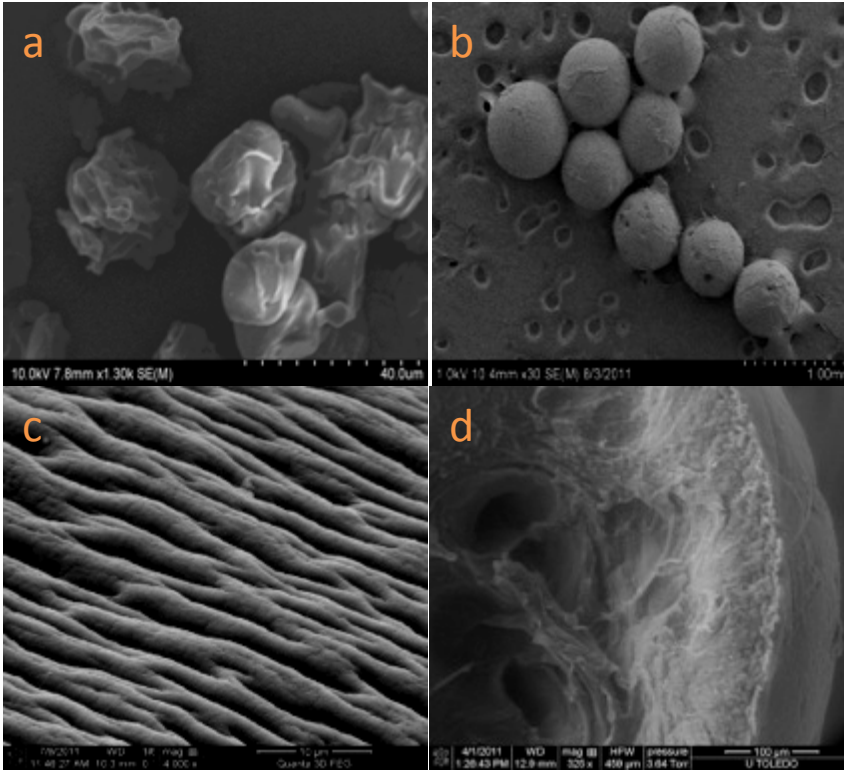
Figure 3.1: SEM images of a) microparticles prepared by emulsification method; b) IGF-1 encapsulated microparticle preparation using 30G needle; c) surface morphology of microparticles prepared by ionic cross-linking method; d) cross-section of microparticle shows the internal less dense structure.
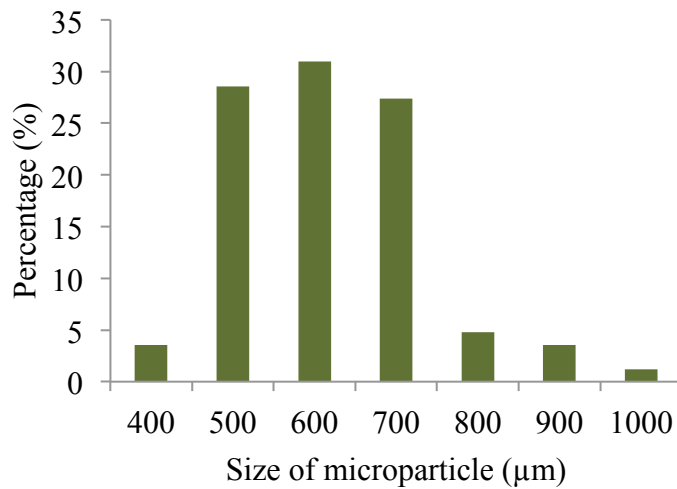
Figure 3.2: Size distribution of microparticles for n = 12 prepared using coacervation method at low temperatures using 27G needle.

The degradation study was conducted to determine the stability of the microparticles *in vitro*. The data shows that there is not a significant difference in the pH of the solution even after 30 weeks (Figure 3.3). There was also not much change in the physical structure of the microparticles immersed in PBS solution of pH 7.4 even after 30 weeks, but the particles suspended in PBS solution of pH 5.1 degraded in 15 weeks (Figure 3.4). At the lower pH, there was a higher percent of swelling observed when compared to that at pH 7.4, indicating the uptake of solution.
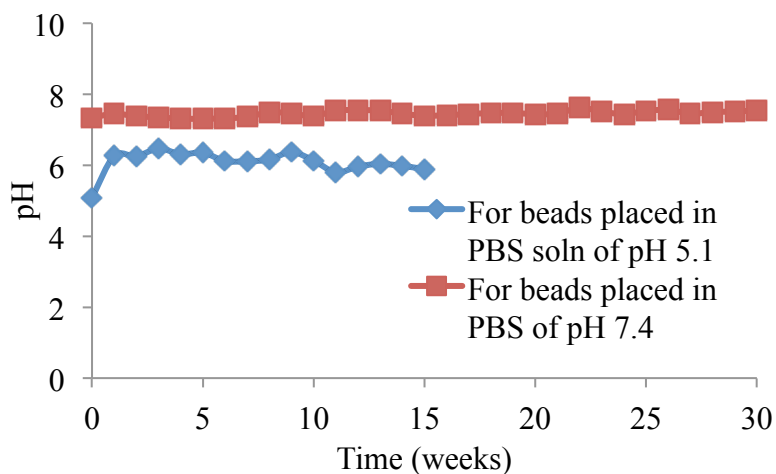
Figure 3.3: pH observation during the 30 weeks period when microparticles were placed in PBS solution (n = 3) of pH 5.1 and pH 7.4.
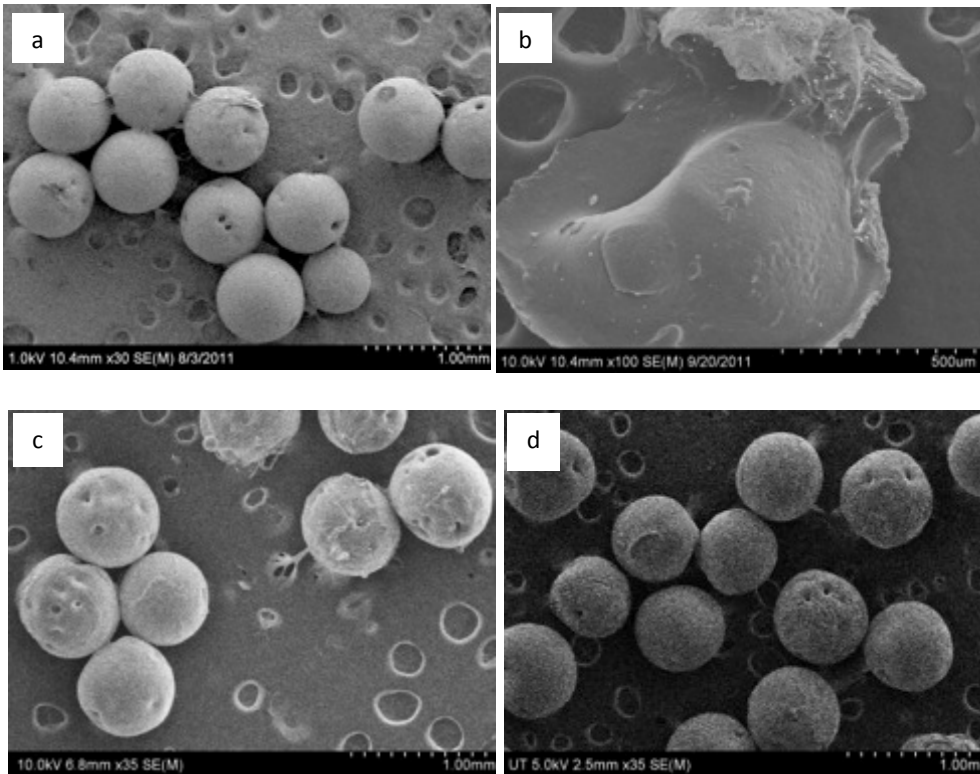
Figure 3.4: SEM images of a,b) coacervation chitosan microparticles placed in PBS solution of pH 5.1 containing 10 mg/L lysozyme at week 0, and week 10 respectively; c,d) coacervation microparticles in PBS solution of pH 7.4 containing 10 mg/L lysozyme at week 0 and week 30 respectively.

3.3.2 *In vitro* Release of IGF-1 from Microparticles from Emulsification and Coacervation Microparticles

The amount of IGF-1 encapsulated in both types of microparticles was determined by dissolving the IGF-1 encapsulated microparticles in acetic acid and it was found that the amount of IGF-1 encapsulated in emulsification microparticles (70.02 ng) was approximately 50% less than that encapsulated in coacervation microparticles (168.7 ng). This result indicates that although the same amount of IGF-1 was added for encapsulation, IGF-1 was not encapsulated in emulsification microparticles, indicating the adverse effect of the organic solvents used during microparticle preparation, which

denatures IGF-1. At the end of 14 days time period, it was found that only 3.31% of the encapsulated proteins were released, whereas for coacervation microparticles, 30.68% of growth factor was released (Figure 3.5). This result indicates that there is a 10 times increase in the percent of IGF-1 release, which may either indicate growth factor degradation in emulsification microparticles or slower release of growth factors.
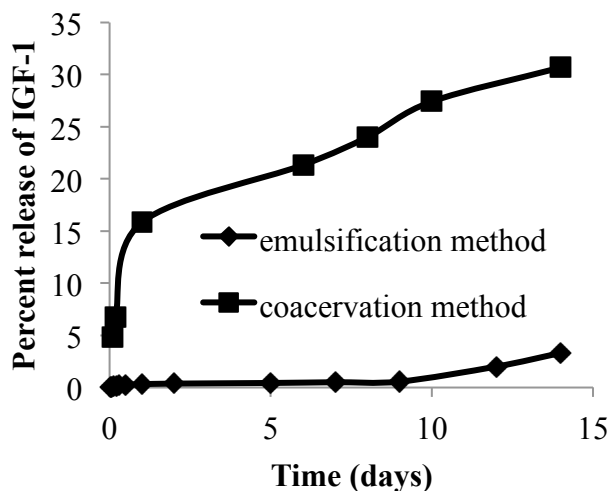
Figure 3.5: Cumulative release behavior of IGF-1 from emulsification and coacervation particles prepared at room temperature.

3.4 Discussion

Chitosan is being widely investigated as a promising implantable biomaterial with a number of applications in tissue engineering [183]. The most intriguing properties that attract chitosan to researchers are its tissue compatibility, biodegradability and functionality [184-186]. Diverse efforts have been made to obtain chitosan-TPP cross-linked microparticles to explore its potential as a delivery system. Optimizing the fabrication conditions and the comprehensive properties of these microparticles is still an

ongoing important research topic to obtain better bone scaffolds, as these parameters influence the loading and encapsulation efficiency of the growth factors, release profiles as well as govern the interaction of the particles with the biological tissue. This study was primarily aimed at understanding the influence of two different methods of microparticles preparation on the stability of the encapsulated growth factor.

Microparticles prepared at room temperature indicated that the microparticles had a rough surface, which is an important parameter known to influence cell attachment, including bone cells [187]. The microparticles were also found to possess internally less dense structure, which is advantageous for delivery of proteins as well as play an important role in its degradation [188-190]. The microparticles thus fabricated have very good physical characteristic for protein encapsulation and cell attachment and proliferation, which were proved experimentally.

Lysozyme is an amphoteric enzyme that includes ionizable groups at its active site. Therefore, variation in the pH of the PBS solution may result in changes in the ionic form of the active site, thus affecting its activity. Studies have also found that its activity also depends on the substrate on which it is acting (in our case, chitosan microparticles). The maximum activity of native lysozyme was observed at pH 4.5, but depending on the substrate, its activity was found to be optimum between pH 4-7 [191]. Previous studies also indicate the fact that the substrate specificities of lysozyme in degradation of soluble chitosan are independent of pH between 4.5 and 7. [192]. Lower pH 5.1 was considered for this study to stimulate an environment induced by macrophages accumulating around the polymer *in vivo* after implantation. Degradation study indicates that in the presence of lysozyme and at lower pH 5.1, microparticles degrade faster in comparison with that at

higher pH 7.4. Lysozyme contains a hexameric-binding site, which is a hexasaccharide sequence that presents 4 or more acetylated units, necessary for the initial degradation of partially N-acetylated chitosan [193]. Apart from the activity of lysozyme on the microparticles, pH also has a direct influence on microparticle degradation. At low pH, the free amine groups in chitosan will be protonated, resulting in high positive charge and also charge number on TPP reduces. This hydrolysis of chitosan-TPP bonds lead to microparticle degradation at a faster rate at low pH [194]. The pH study over the period of 30 weeks did not indicate drastic change in the overall pH of the solution. This is advantageous as a sudden change (or drop) in the pH *in vivo* can induce rapid inflammatory response, which can harm bone cells at the implant site. Moreover, the rapid drop in pH *in vivo* may accelerate polymer's degradation rate, thus resulting in premature loss of mechanical properties before new bone formation occurs. Therefore, it is critical to ensure that there are no adverse changes in pH at the defect site for its effective application in orthopedics.

In order to develop a better method to fabricate microparticles for growth factor encapsulation, we compared microparticles prepared using emulsification and coacervation methodology. Emulsification process can be harmful to the stability of the protein due to the presence of multiple organic-aqueous interfaces and also the presence of organic solvents itself can denature number of protein molecules [195,196]. In case of coacervation microparticles, initial burst release was observed till day 1 where 15% of IGF-1 was released but later, we observed a sustained released till day 14. The release of proteins from these microparticles suspended in PBS solution of pH 7.4 and the degradation study indicates that the release of IGF-1 is mainly due to desorption and

diffusion and not by degradation or erosion of microparticles. The proteins adsorbed on the surface of the chitosan particles are first released in the process of desorption and contribute mainly to the burst release phase while the next phase, IGF-1 encapsulated in the microparticle is released mainly by diffusion and minor contribution by degradation process [197-199], together contributing to the controlled release.

Chapter 4

Factors Determining the Sustained Release of Growth Factors from Chitosan Microparticles

In this chapter, experiments conducted address Hypothesis II. IGF-1 growth factor is used in this study to optimize the various parameters that determine its release kinetics from coacervation microparticles. Bioactivity of the release growth factor was determined using cell attachment and proliferation assays.

4.1 Materials

Chitosan (85% deacetylated), sodium tripolyphosphate (TPP), acetic acid, PBS, glutaraldehyde and silver nitrate were purchased from Sigma Chemicals (USA). Insulin like Growth Factor-1 (IGF-1) and LIVE/DEAD cytotoxicity/viability assay were purchased from Invitrogen (USA). IGF-1 ELISA kit (DY291) was supplied by R&D systems (USA), RNeasy Mini Kit (Qiagen, USA), Verso cDNA kit (Thermo Scientific, USA) and SYBR green master mix kit (Applied Biosystems, USA).

4.2 Methods

4.2.1 Release of IGF-1 by Coacervation Microparticles Prepared by Varying Conditions

Microparticles (20 mg) were suspended in PBS (pH 7.4). The suspension was incubated at 37°C with continuous rotation at 25-50 rpm for a period of two weeks. At predetermined time points, PBS in the vials was collected and replaced with 2ml of fresh PBS to maintain the sink conditions. Samples were stored at -20°C until further analysis. The IGF-1 remaining in the microparticles after the study period was determined by dissolving the microparticles in 1% (v/v) acetic acid at 37°C for 24-48 h. To quantify the IGF-I being released ELISA was used. Manufacturer's protocol was followed to do the ELISA (R & D Systems). Triplicates of each sample were used to do the assay and the results are expressed as mean $\pm$ SD.

The following parameters were varied to determine their effect on release:

- Different amounts of IGF-1 were added to determine the optimum amount for efficient encapsulation given the amount of chitosan and TPP percent.
- The microparticles were suspended in PBS solutions of different pH to study its effect on release.
- Different TPP amounts were used for cross-linking the amine groups in chitosan
- The effect of temperature was studied by preparing the IGF-1 encapsulated microparticles at room temperature and below room temperature.

4.2.2 Bioactivity of IGF-1 Released *in vitro* from Coacervation Microparticles

To confirm the bioactivity of the IGF-1 released from chitosan microparticles formed by coacervation method, osteoblasts (OB-6) cells were used for assays *in vitro*. IGF-1 has been found to play an important role in stimulating osteoblast proliferation and matrix mineralization Therefore live/dead assay was performed in order to check the effect of IGF-1 encapsulated microparticles on proliferation of viable cells.

4.2.2.1 Osteoblast Cell Culturing

In vitro studies were performed with coacervation microparticles prepared using 2% chitosan and 50% TPP with 0.05% IGF-1 encapsulated (as observed from release data, this amount was found to be optimum). IGF-1 was encapsulated during microparticle preparation. Dr. Beata L Czernik of the Department of Orthopedic Surgery at The University of Toledo kindly provided pre-osteoblast OB-6 murine cell line vial, which was used for propagation and our further studies. α-MEM medium supplemented with 15% fetal bovine serum (FBS) and 1% penicillin/streptomycin was used for culturing cells at $37^{o}C$ in humidified atmosphere of 5% CO_2. For all the experiments, microparticles were sterilized under UV light for 45 min. In a 24-well plate, 25 mg microparticles were added to each well and then seeded with a cell suspension containing 10^5 cells/ml. The microparticles were soaked in the medium for 45 minutes prior to seeding them with cell suspension. This was done particularly because the particles absorbed some medium and swelled and later they settle to the bottom of the well plate. Thus prior to addition of cell suspension, it was ensured that the particles settled to the bottom of the well plate.

4.2.2.2 Cell Attachment and Proliferation Assay

Attachment of cells to the microparticles was determined using a phase contrast light microscope (FSX 100, Olympus). On day 3, 5, and 7, the medium was aspirated, washed twice with 1X PBS and then cells were fixed using 2.5% glutaraldehyde. After fixing, the microparticles were washed thoroughly in water and then cells were observed under light microscope. The viability and proliferation of attached cells on the chitosan microparticles was confirmed by intracellular esterase activity as indicated by the green fluorescence of calcein that had been enzymatically converted from calcein AM (acetomethoxy derivative). Dead cells were simultaneously recognized by their red fluorescence caused by the binding of nucleic acids to ethidium homodimer 1 that has entered the cells through damaged membranes. Chitosan microparticles without growth factor, cells in medium without growth factor, and medium containing IGF-1 without microparticles were used as controls. Medium was changed every three days. Live/Dead viability/cytotoxicity assay was performed according to the manufacturer's protocol on day 5 and day 10 by transferring the microparticles to a new well in order to distinctly see the cells attached to microparticles only.

4.2.3 Statistical Analysis

Data are reported as means $\pm$ standard deviation for n = 3 unless otherwise stated. One-way analysis of variance (ANOVA) was followed by Tukey's Honest Significant Test (HSD) to determine the statistical significance among means of different groups. Two-way ANOVA analysis was also conducted followed by Tukey's HSD. A probability

value of P<0.05 or 0.001was used to determine significance, which was specified each time.

4.3 Results

4.3.1 *In vitro* Release of IGF-1 from Microparticles

4.3.1.1 Effect of the Amount of IGF-1 used during Encapsulation on Encapsulation Efficiency

Direct proportionality is observed between the amount encapsulated and the amount released till 0.05% w/v IGF-1 but then a decrease is observed as the amount encapsulated is increased further to 0.2% w/v (Figure 4.1a). The release data showed that there is a significant difference ($P < 0.05$) between the cumulative amount released by day 14 between 0.05% and 0.2% w/v IGF-1 encapsulated microparticles. The encapsulation efficiency (Table 4.2) of the particles showed that 0.05% w/v IGF-1 particles have almost equal amount of IGF-1 encapsulated than 0.2% w/v IGF-1, while 0.1% indicated that a higher amount of IGF-1 is encapsulated.

4.3.1.2 Effect of TPP Concentration on IGF-1 Release from Microparticles

The release profile shows that as the TPP amount increased, the IGF-1 being released from the microparticles decreased (Figure 4.1b). In 50% TPP-chitosan microparticles, in comparison with other groups, we could observe maximum release of 75.2% IGF-1 by day 14, but by day 2 itself, we observe that 42.2% of IGF-1 has been released. On the other hand, in case of 60% TPP-chitosan microparticles, we observe that by day 14, only

39.2% of IGF-1 is released, but by day 2, only 14.8% of IGF-1 is released and in case of 80% TPP, it was observed that the cumulative release percent decreased to 15.6%.

4.3.1.3 Effect of pH on Release of IGF-1

The release behavior of microparticles studied in PBS solution of different pH showed significant difference in the release ($p<0.05$) between pH 5.1, 7.4 and 10.7 on day 14. The result showed that at a lower pH, the release was largest and the release decreased with increase in pH (Figure 4.1c). This can be explained by the indicative difference in the swelling behavior *in vitro.* For pH 5.1, the microparticles swelled significantly in the first 2 h indicating a burst release and later swelling degree did not change greatly, thus indicating a steady release over the time period.

4.3.1.4 Effect of Temperature on IGF-1 Encapsulation and Release

A significant difference ($p<0.05$) is observed in the release of IGF-1 between microparticles prepared at room temperature and that prepared below room temperatures ($0^{o}C$-$5^{o}C$) (Figure 4.1d). This can be explained by the significant difference observed in the encapsulation efficiency of the growth factor into the microparticles prepared at different temperatures (Table 4.2).
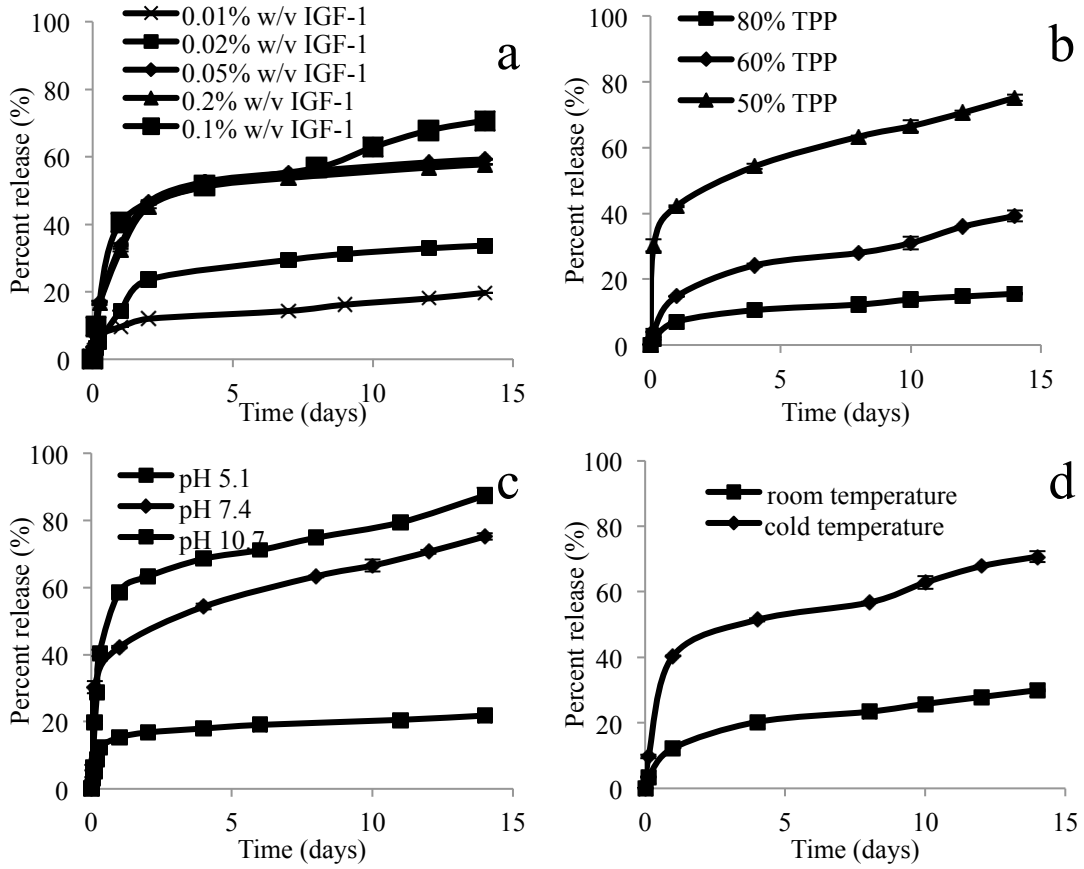
Figure 4.1: Coacervation particles prepared at lower temperature a) with different concentrations of IGF-1 encapsulation b) different percent of TPP concentration c) different pH of TPP solution d) Different temperatures of microparticle preparation.

Table 4.1: Encapsulation efficiency of IGF-1 in ionic cross-linked microparticles.

Parameters		Encapsulation efficiency
IGF-1 amount used for encapsulation (w/v %)	0.01%	58.10%
	0.02%	49.8%
	0.05%	49.57%
	0.2%	14.9%
Temperature	At below room temperature	59.57%
	At room temperature	38.3%
TPP percent	50%	56.97%
	60%	49.86%
	80%	40.09%
pH of PBS solution	5.07	44.5%
	7.4	49.8%
	10.7	47.09%

4.3.2 Bioactivity of IGF-1 Released *in vitro* from Coacervation Microparticles

4.3.2.1. Cell Attachment and Viability

Light microscopy images taken on day 3 (Figure 4.2a) showed that the cells attached to the microparticles had round morphology and were just beginning to attach, while on day 5 and day 7, the cells appeared to flat and were spreading well with higher cell-substrate contact area (Figure 4.2b, c).

The number of viable cells increased, as observed by the live dead cell assay during the ten-day culture period, except for the control with just the cells, which showed a number of dead cells (cells with red stained nuclei) by day 10, which is probably due to overpopulation of the cells (Figure 4.3). Proliferation of cells on three-dimensional microparticles (with and without IGF-1) increased through the ten-day period, with most number of live cells (cells with green cytoplasm) observed on day 10 (Figure 4.4). Microparticles are three-dimensional and in order to capture all the cells attached on its surface, a number of images beginning from the top of the microparticle need to be taken and thus Figure 4.4 show four such images. There was also a difference seen in the number of viable cells attached to the IGF-1 encapsulated particles than to particles with no growth factor on day 5 and 10 (Figure 4.5 and Figure 4.6), thereby proving that the IGF-1 being released from the microparticles is biologically active and is helping in the proliferation of osteoblasts.

Image J software was used to analyze the % area of microparticle occupied by cells to determine any significant difference in the cell attachment and as it can be seen from Figure 4.7, a significant increase in cell attachment was found on microparticles with IGF-1 on day 5 and day 10 ($p<0.05$) in comparison with cells attached to microparticles without IGF-1. This indicates that the IGF-1 being released from the microparticles is biologically active and is beneficial for attachment and proliferation of pre-osteoblasts.
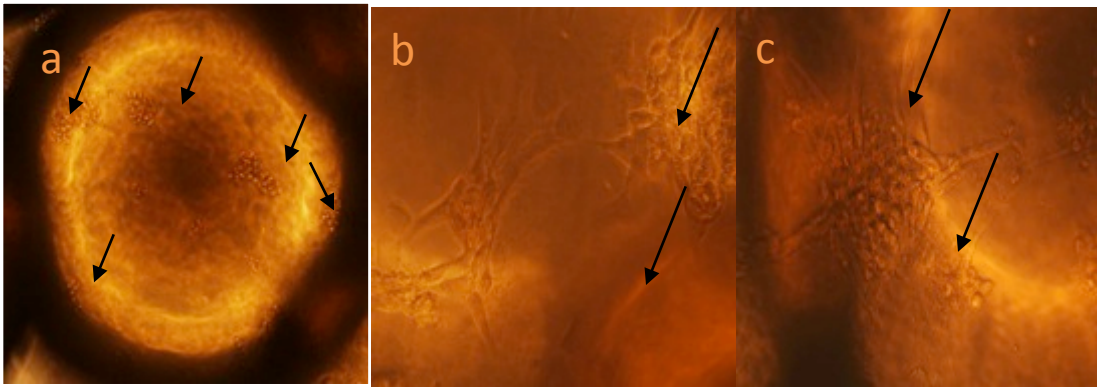
Figure 4.2: Phase contrast microscope image of attachment of osteoblasts to chitosan microparticles prepared by coacervation method on a) day 3 shows that cells are round in morphology b, c) day 5 and day 7 respectively image shows that cells are attached and spreading.
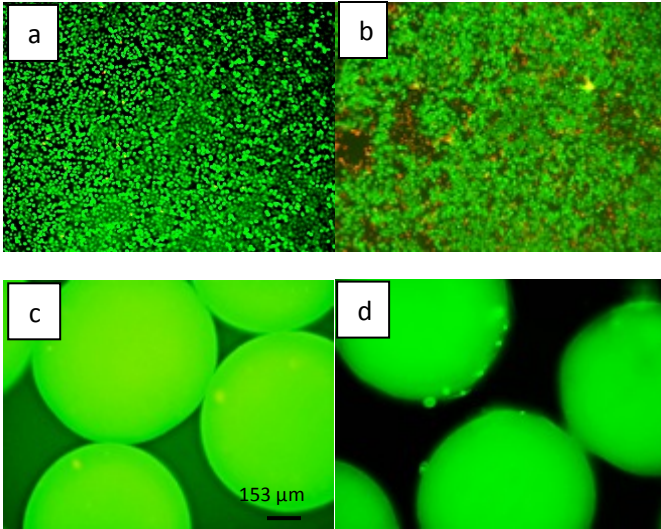
Figure 4.3: Live dead assay images of a) Cells only (control) on day 5 b) Cells only on day 10 c) microparticles only (control) d) microparticles seeded with OB-6 cells on day 5.
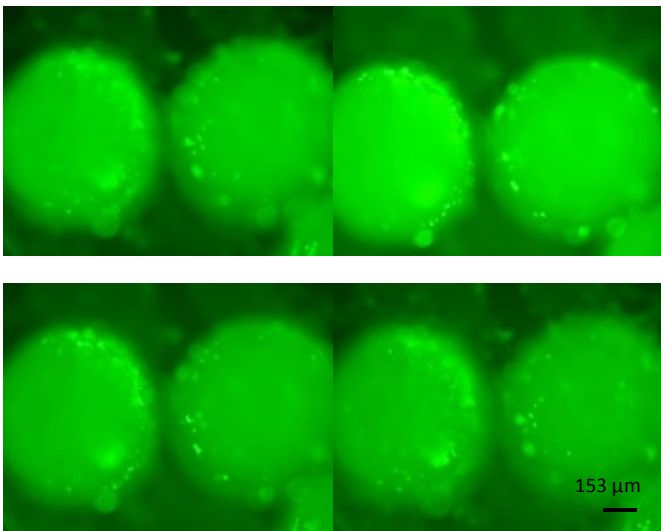
Figure 4.4: Four different views starting from top to the bottom of the three dimensional microparticles showing OB-6 cells attached to microparticles without growth factors as demonstrated by live dead assay on day 10.

153 µm
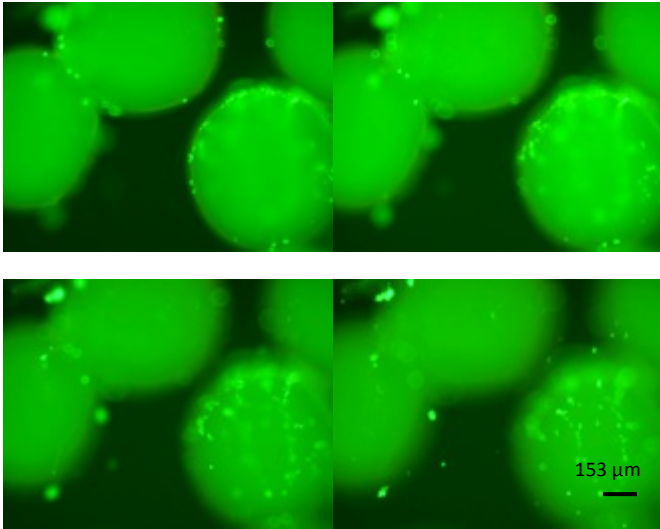
Figure 4.5: Four different views starting from top to the bottom of the three dimensional microparticles showing OB-6 cells attached to IGF-1 encapsulated microparticles as demonstrated by live dead assay on day 5.

153 µm
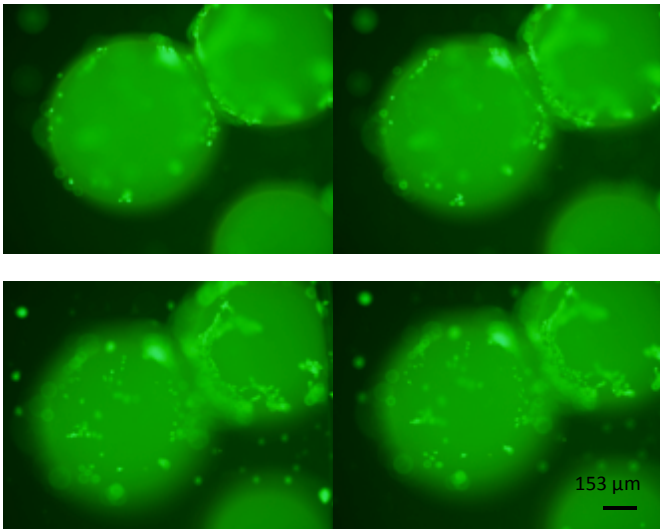
Figure 4.6: Four different views starting from top to the bottom of the three dimensional microparticles showing OB-6 cells attached to IGF-1 encapsulated microparticles as demonstrated by live dead assay on day 10.
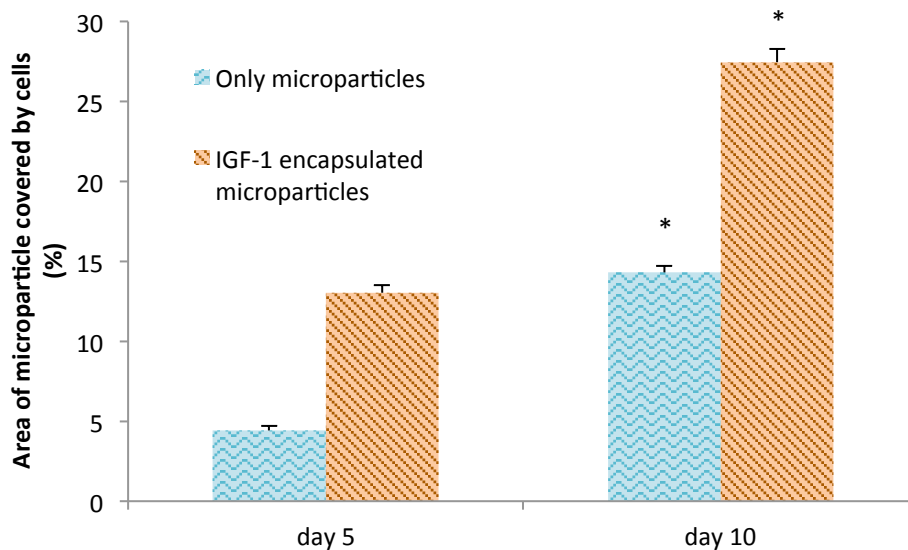
Figure 4.7: Area occupied by the cells on the microparticles with and without IGF-1 on day 5 and 10. Live/dead assay images were used to analyse and calculate the area occupied by using image J software.

4.4 Discussion

Two mechanisms control the encapsulation of IGF-1 in chitosan microparticles. Physical entrapment of IGF-1 in the mesh like structure of the microparticle and the hollow structure inside the microparticle also helps in encapsulating some IGF-1, which flows in during the process of diffusion as the microparticle swells in TPP solution. This indicates that there is a saturation level for the amount of IGF-1 that can be encapsulated in the 700 μm size microparticles. Some of the IGF-1 can escape to the TPP solution where it attains negative charge (isoelectric point = 8.6) [200,201]. Thus partially, IGF-1 can be incorporated due to electrostatic interactions between the negatively charged IGF-1 and positively charged chitosan molecules. There are ionic interactions between the chitosan molecules and the TPP, which chemically constitute the microparticle. This explains the

reason for saturation of positive sites in the molecule and thus a saturation level for the amount of IGF-1 that can be incorporated for a given amount of chitosan-TPP in a microparticle, thereby limiting the amount of IGF-1 that can be encapsulated.

The action of growth factors is concentration dependent as it decides the distance around the tissue that gets influenced by that growth factor. Very little concentration of the drug might not be sufficient to activate the osteoblasts while too much of IGF-1 can saturate cell receptors and disrupt cell guidance [202]. Studies have shown that certain concentration of IGF-1 have shown significant increase in bone matrix formation and stimulated bone formation [203, 204] and this concentration was found to coincide with the concentration of IGF-1 being released by day 14 from the microparticles encapsulated with 0.05% w/v IGF-1.

In the experiment to determine the effect of varying amounts of TPP used for cross-linking, we can understand that chitosan and TPP cross-link to form interconnected mesh like network and the density of this network depends on the concentration of TPP and chitosan. The growth factor encapsulated before cross-linking gets distributed in the mesh like network and its movement through this network occurs based on its hydrodynamic diameter. When the hydrodynamic diameter of the growth factor is smaller than the average mesh size, release occurs through diffusion and when the diameter is greater than or equal to the mesh size, release occurs via enzymatic degradation of the chitosan microparticle [94]. The cross-linking density in the microparticle is determined by the concentration of TPP and chitosan, thus higher the concentration of TPP, smaller is the mesh size thus restricting the motion of growth factors through it [205].

In the experiment to determine the effect of pH on growth factor release, we could clearly observe a difference in the release profile at pH 5.1, 7.4 and 10.1. This can be explained from the fact that chitosan-TPP complex has a pI value of 7.5 [206]. According to Henderson-Hasselbalch equation, it can be concluded that at acidic pH, this complex attains a positive charge. Thus chitosan molecules attain an extended conformation at lower pH due to charge repulsion of highly protonated amino groups, which subsequently yield an increase in the mesh size. IGF-1, which is physically entrapped in the microparticle and has a pI of 8.6 is also conveniently released due to its positive charge. At pH 7.4, the chitosan-TPP complex behaves like a zwitterion. Therefore swelling behavior is not observed and IGF-1 is released in sustained manner. At pH 10.7, the complex attains a negative charge and the chitosan molecules become increasingly globular decreasing the mesh size and the entrapped protein could not be released easily [206,207].

The experiment to determine the influence of microparticle preparation temperatures also indicated a difference in the release profile and amounts. This result is in agreement with the fact that the protein integrity is dependent on the temperature [208].

The *in vitro* study proves the bioactivity of the released growth factor. Studies have shown that 2D substrates differ from 3D scaffolds in the manner they support cell migration, localization and function [209-212]. Literature also supports that surface topography and dimensions have a regulatory effect on cell behavior. Groovy surface is known to influence osteoblast movement independent of the surface material [213]. Surface roughness modulates the production of growth factors and cytokines, thus influencing proliferation, differentiation and matrix production by osteoblasts [214]. Also

the cell binding properties of chitosan may be explained by its polycationic nature, which is obtained by deacetylation because of which the cells that carry a negative charge at physiological pH binds to it [215].

Chapter 5

Influence of BMP-7 Containing Chitosan Microparticles on Pre-osteoblasts: *In vitro* Study

In this chapter, the experiments conducted address Hypothesis III. BMP-7 growth factor was incorporated into the chitosan microparticles to determine its influence on pre-osteoblasts.

5.1. Materials

Chitosan (85% deacetylated), sodium tripolyphosphate (TPP), acetic acid, PBS, 2.5% glutaraldehyde in 0.1M buffer and silver nitrate were purchased from Sigma Chemicals (USA). Human recombinant bone morphogenetic protein 7 (BMP-7) were purchased from PeproTech (USA). LIVE/DEAD cytotoxicity/viability assay was purchased from Invitrogen (USA). BMP-7 ELISA kit (DY354) was supplied by R&D systems (USA), RNeasy Mini Kit (Qiagen, USA), Verso cDNA kit (Thermo Scientific, USA) and SYBR green master mix kit (Applied Biosystems, USA).

5.2. Methods

5.2.1 Release Kinetics

The microparticles were fabricated using a coacervation technique using chitosan as a base polymer and cross-linking with tripolyphosphate (TPP). 2% chitosan was prepared by dissolving in acetic acid (1% v/v) at room temperature. The mixture was passed through a nylon mesh to remove insoluble substances. This mixture was then added drop wise to the 50% TPP solution kept on ice bath and continuous stirring at 250 rpm. The microparticles were allowed to cross-link for 5 h and then were air-dried. BMP-7 for the release study was encapsulated in two ways. In the first method, BMP-7 was added to the chitosan solution, which is then added to TPP solution to cross-link and form the microparticles (BMP-7 encapsulated microparticles). In the second method, BMP-7 was added to the dried microparticles, which adsorbed the BMP-7 and then were again dried before using for the release study (BMP-7 coated microparticles). 20 mg of both types of microparticles were suspended in PBS (pH 7.4) and incubated at 37°C with continuous rotation at 25-50 rpm for a period of two weeks. At predetermined time points, PBS containing the released BMP-7 was collected and replaced with 2 ml of fresh PBS to maintain the sink conditions. Samples were stored at -20°C until further analysis. The BMP-7 remaining in the microparticles after the study period was determined by dissolving the microparticles in 1% (v/v) acetic acid at 37°C for 24-48 h. To quantify the BMP-7 released, enzyme linked immunosorbent assay (ELISA) was used. Manufacturer's protocol was followed to do the ELISA (R & D Systems). Triplicates of each sample were used to do the assay and the results are expressed as mean $\pm$ SD.

5.2.2 Morphology Study by Scanning Electron Microscopy

Sterilized microparticles (25 mg) were seeded with cell suspension containing 10^5 cells/ml in a 24-well plate and incubated at 37°C with 5% CO_2. Medium was changed every three days. The morphology of the osteoblast adhered to the chitosan microparticles was determined using scanning electron microscopy (SEM). The samples were fixed in 2.5% glutaraldehyde followed by dehydration in graded ethanol series – 20%, 30%, 50%, 70%, 80%, 90%, 95%, 100% v/v respectively for 5 min in each concentration, followed by three 10 min changes of 100% ethanol. Samples were critical point dried (CPD) and then immediately the samples were sputter coated with gold/palladium (80/20). Specimens were examined using a Hitachi S-4800 scanning electron microscope fitted with SE detector. The microscope was operated in normal current –SE detection mode. The cells attached to the chitosan microparticles were viewed at 5 kV accelerating voltage and 2 µA current. The SEM images obtained were analyzed by Image J software to determine the area occupied by the cells on the microparticles. For each sample, triplicates were used and in each of the triplicates, n=10 images were analyzed to obtain average area.

5.2.3 Cell Viability

The viability of attached cells on the chitosan microparticles was confirmed by intracellular esterase activity as indicated by the green fluorescence of calcein that had been enzymatically converted from calcein AM. Dead cells were simultaneously recognized by their red fluorescence caused by the binding of nucleic acids to ethidium homodimer 1 that has entered the cells through damaged membranes. For the assay, 25 mg microparticles sterilized under UV light for 45 min in a 24 well-plate. The

microparticles were seeded with cell suspension containing 10^5 cells/ml. Medium was changed every three days. In order to specifically determine the cells attached to the microparticles, the microparticles were transferred to another well after washing them with PBS and then live/dead viability/cytotoxicity assay was performed according to the manufacturer's protocol on day 5 and 10. The percent area of microparticle covered with cells was determined using Image J software. The area of the microparticle was calculated considering it circular (projection of sphere would be a circle) and since only half of the surface is visible at a time, only half of that area was considered in the calculations.

5.2.4 Quantification of DNA

Murine osteoblasts (OB-6) were seeded at a density of 100,000 cells/ml in 24 well-plates. Cells were incubated at 37°C with 5% CO_2 atmosphere for 5 and 10 days. The data presented for the DNA assay is an average of 3 experiments conducted with same parameters and for each experiment there were triplicates for each sample. In order to quantify the total number of cells grown in the well plate in the presence of growth factors being released from the microparticles, the assay was done in the same well to obtain the DNA from the cells attached to the well plate and the microparticles, and in order to quantify the cells attached and proliferating only on the microparticles, the microparticles were transferred to another well plate and then the DNA was extracted and quantified. At each time point, the microparticles were washed thoroughly in PBS before doing the DNA assay to make sure that there is no fetal bovine serum (FBS) or media left absorbed in the microparticles, as they hinder with the DNA extraction process and reduce the yield. In both the types of experiments, the remaining part of the experiment

remained the same. DNA kit from Qiagen was used to extract DNA from the osteoblasts. After washing with PBS, 20 μl of each proteinase K and RNAse was added to the wells with microparticles followed by addition of 100 μl of PBS and lysis buffer respectively. The solutions were mixed and then kept in water bath maintained at 55°C for 10 min to maximize the efficiency of the added enzymes. 200 μl of ethanol was added to the above mixture and then the total mixture was transferred to the spin column supplied in the kit. Then the procedure mentioned in the kit is followed to obtain maximum DNA. The quantity and purity of the obtained DNA is analyzed using Nanodrop-1000, version 3.6.0.

5.2.5 Real Time RT-PCR Analysis

Cells were seeded at 2 x 10^5 cells/ml and cultured in the presence of microparticles (with and without BMP-7) for 5, 7 and 14 days. Total RNA was isolated using RNeasy Mini Kit following manufacturer's instructions. The purity and concentration of total cellular RNA was determined using Nanodrop-1000, version 3.6.0. The minimum RNA amount obtained was considered as a base for calculations to reverse transcribe complementary DNA (cDNA) using the Verso cDNA kit according to manufacturer's protocols. The forward and reverse primers for the selected genes were designed from Integrated DNA Technologies (IDT, USA) and are listed in Table 5.1. Expression was quantified using real time Reverse Transcription-Polymerase Chain Reaction (real time RT-PCR) analysis with SYBR green master mix kit. Data analysis was carried out using Applied Biosystems StepOne Plus thermal cycler and detection system. The real time RT-PCR analysis was carried out for two independent experiments with each sample run in duplicates. The gene expression levels were normalized to the expression of the

housekeeping gene GAPDH and were expressed as fold changes relative to the expression of the genes in cells only on the respective days.

5.2.6 Determination of Mineralization by Von Kossa Staining

Von Kossa staining was carried out to characterize mineralization of differentiated osteoblasts. Microparticles were plated and treated as mentioned above with 2×10^5 cells/ml in a 24 well plate. On day 5 and 10, the cultures were washed thrice with 1X PBS solution and then the cells were fixed in 2.5% glutaraldehyde in 0.1 M sodium cacodylate buffer for 1 h. Later, the microparticles were washed thoroughly in water and then 2% silver nitrate solution was added and the plate was placed on aluminum foil and kept under light for 10 min after which the plate was rinsed with water and dried for image analysis using bright field microscopy. The images were analyzed using Image J software to determine the area of mineralization in each image. For each group, triplicates were used and for each one of the triplicate, n=10 images were used to calculate the area of mineralization.

5.2.7 Statistical Analysis

Data are reported as means $\pm$ standard deviation for n=3 unless otherwise stated. IBM SPSS (service product for statistical solution) one-way and two-way analysis of variance (ANOVA) followed by posthocTukey's Honest Significant Difference (HSD) test was performed to determine the significant difference among the various groups. A probability value of $p < 0.05$ or $p < 0.001$ was used to determine significance, which was specified each time.

5.3 Results

5.3.1 BMP-7 Release Kinetics

The release study indicated that by day 18, nearly 98% of the BMP-7 was released from the coated microparticles, while only 36% of the BMP-7 encapsulated in the microparticles was released (Figure 5.1). SPSS two way ANOVA indicated that there is a significant difference ($p < 0.001$) in the release of BMP-7 incorporated in the two different ways at all the time points from t=0 to t=18. The release from the microparticles can mainly be attributed to two processes, diffusion and desorption. The proteins adsorbed on the surface are released due to desorption first and the process of diffusion releases the encapsulated protein.
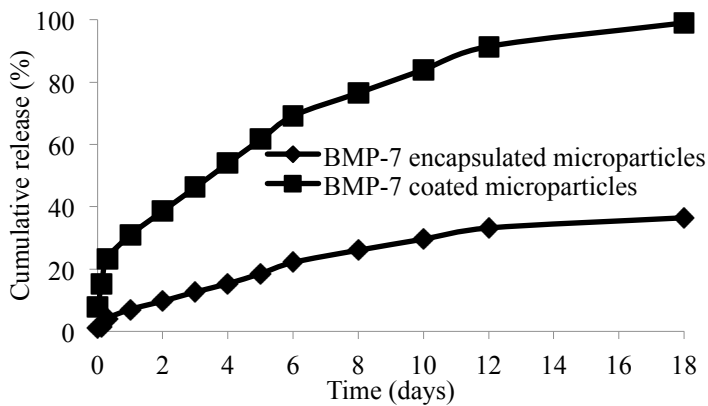
Figure 5.1: Cumulative release profile of BMP-7 encapsulated microparticles and BMP-7 coated microparticles over a period of 18 days.

5.3.2 Morphology Study

On day 5, the cells appeared to be circular and elongated, with their body raised above the surface of all the three types of microparticles. On BMP-7 coated and encapsulated microparticles, the cells appeared to be growing in a number of small colonies throughout the surface of the microparticle, while on the normal chitosan microparticle with no growth factors; they appeared to be growing in lumps only at particular locations on the microparticles (Figure 5.2). Although the surface of the three different types of microparticles- normal chitosan microparticle with no growth factor, BMP-7 coated microparticle and BMP-7 encapsulated microparticle appeared to be similar, the cells showed distinct difference in the proliferation rate on the three different surfaces on day 10. On BMP-7 coated microparticles, the cells were flattened and well spread covering majority of the 700 μm diameter microparticle. The cells were found to have very thin edges and filopodia adhered to the surface of the microparticle (Figure 5.3). The cells were found to be closely associated with the surface of the chitosan microparticle. Even on BMP-7 encapsulated microparticles, the cells appeared to be flattened but the spreading of the osteoblasts was not as extensive as that of cells on BMP-7 coated microparticles (Figure 5.4). While on microparticles with no growth factors, the cells appeared flattened, with even lesser area of the microparticle occupied (Figure 5.2). The cell body also appeared to be raised above the surface of the microparticle.
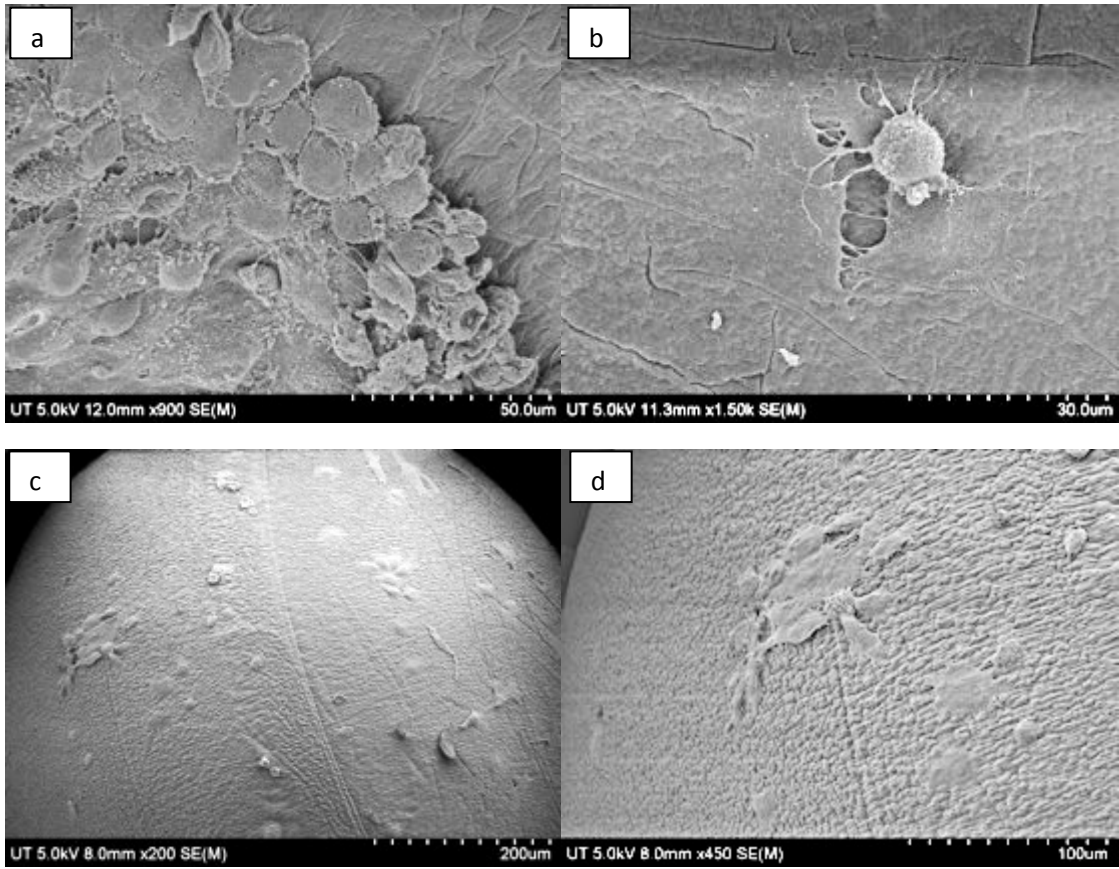
Figure 5.2: SEM image of mouse osteoblasts attached and proliferating on normal chitosan microparticle without any growth factor as observed on day 5 – a, b) lower magnification at a scale of 50 μm and higher magnification at a scale of 30 μm and on day 10 c, d) lower and higher magnification at scale of 200 μm and 100 μm respectively.
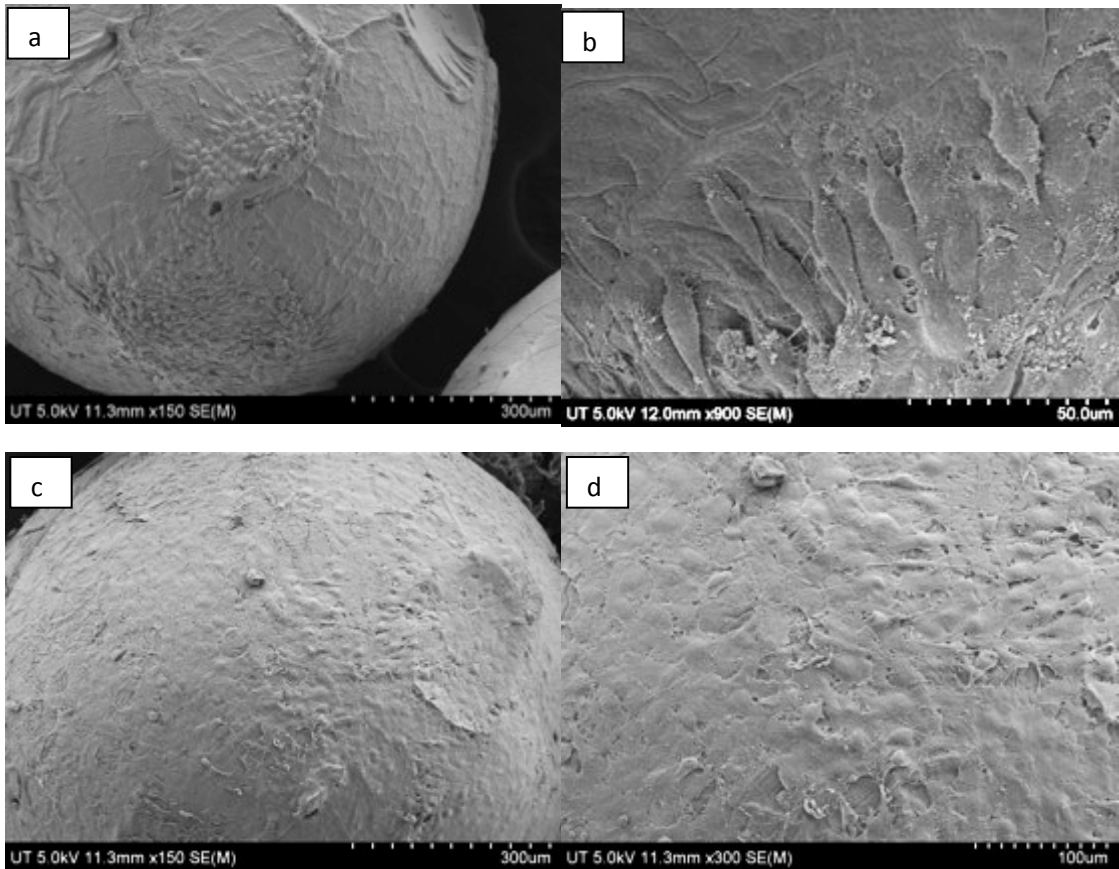
Figure 5.3: SEM image of mouse osteoblasts attached and proliferating on BMP-7 coated chitosan microparticle as observed on day 5 – a, b) lower magnification and higher magnification at a scale of 300 μm and 50 μm respectively and on day 10 c, d) lower and higher magnification at a scale of 300 μm and 100 μm respectively.
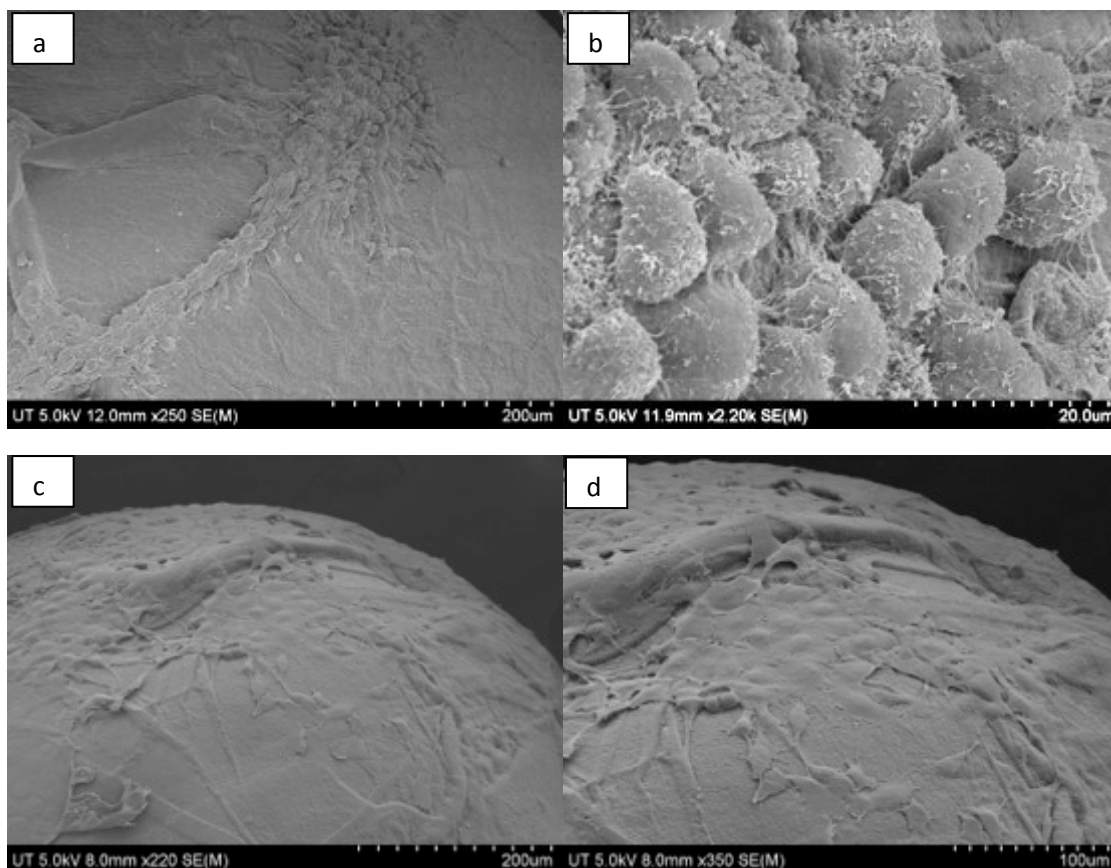
Figure 5.4: SEM image of mouse osteoblasts attached and proliferating on BMP-7 encapsulated chitosan microparticle as observed on day 5 – a, b) lower and higher magnification at a scale of 200 μm and 20 μm respectively and on day 10 c, d) lower and higher magnification at a scale of 200 μm and 100 μm respectively.

5.3.3 Cell Viability Assay

The viability of osteoblasts attached to the three dimensional chitosan microparticles was determined by live/dead assay. A significant increase ($p < 0.001$) is observed in the number of cells adhered onto the microparticles on day 10 in comparison with day 5, indicating the biocompatibility of chitosan-TPP microparticles (Figure 5.5). The results thus suggest that the minor amounts of acetic acid used and the presence of TPP is not detrimental for the osteoblasts. ANOVA analysis by SPSS pairwise comparison indicated that on day 5, a significant difference ($p < 0.05$) exists in the number of viable cells

attached to normal microparticles without any growth factor (Figure 5.6) and BMP-7 coated microparticles (Figure 5.7). No significant difference was observed in the number of cells attached to BMP-7 encapsulated and normal (p=0.445) as well as BMP-7 coated microparticles (p=0.147). This result suggests that bioactive BMP-7 is released at a much faster rate from microparticles which have BMP-7 coated, which enhances cell attachment and proliferation. But on day 10, a significant difference was observed among all the three types of microparticles (p<0.001). Day 10 result suggests that bioactive BMP-7 is released from both the BMP-7 coated (Figure 5.8) and encapsulated microparticles (Figure 5.9), indicating increased cell proliferation. Tukey's posthoc analysis indicates that a significant difference exists in the number of viable cells proliferating on BMP-7 coated microparticles in comparison with BMP-7 encapsulated (Figure 5.8) and normal microparticles (p<0.001) and also between BMP-7 encapsulated and normal microparticles (p<0.05).

The significant difference in viable cell attachment to various particles was determined by considering the degree of cell spreading on the surface area of the microparticle as shown in Figure 5.5. The graph takes into consideration only the cells attached to one of the hemisphere of the microparticle as the microscopy provided us with that part of the image only. This analysis indicates that 56% of the hemisphere of the chitosan microparticle coated with BMP-7 is covered by osteoblasts which are in agreement with the SEM images. As expected, the BMP-7 presence influenced the cell attachment and specifically proliferation on the surface of the microparticle. The concentration of the bioactive BMP-7 available to the cell also influenced the spreading of the osteoblasts with higher concentration supporting greater degree of cell spreading. For instance,

56.2% of the osteoblasts attached to microparticles with BMP-7 coated, but only 40.4 %

of cells attached to BMP-7 encapsulated microparticles. The 56.2% account for an

average of 4.33 x 10^5 μm^2 of the surface area of the hemisphere, for BMP-7 encapsulated

microparticles it accounts to 3.11 x 10^5 μm^2, for microparticles without any growth

factors it accounts for 1.02 x 10^5 μm^2.
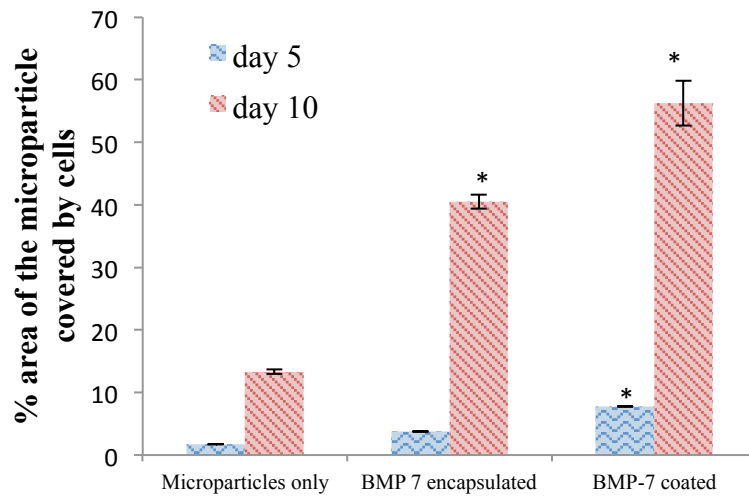
Figure 5.5: Area occupied by the cells on the microparticles on day 5 and 10. The area is
calculated using image J software.
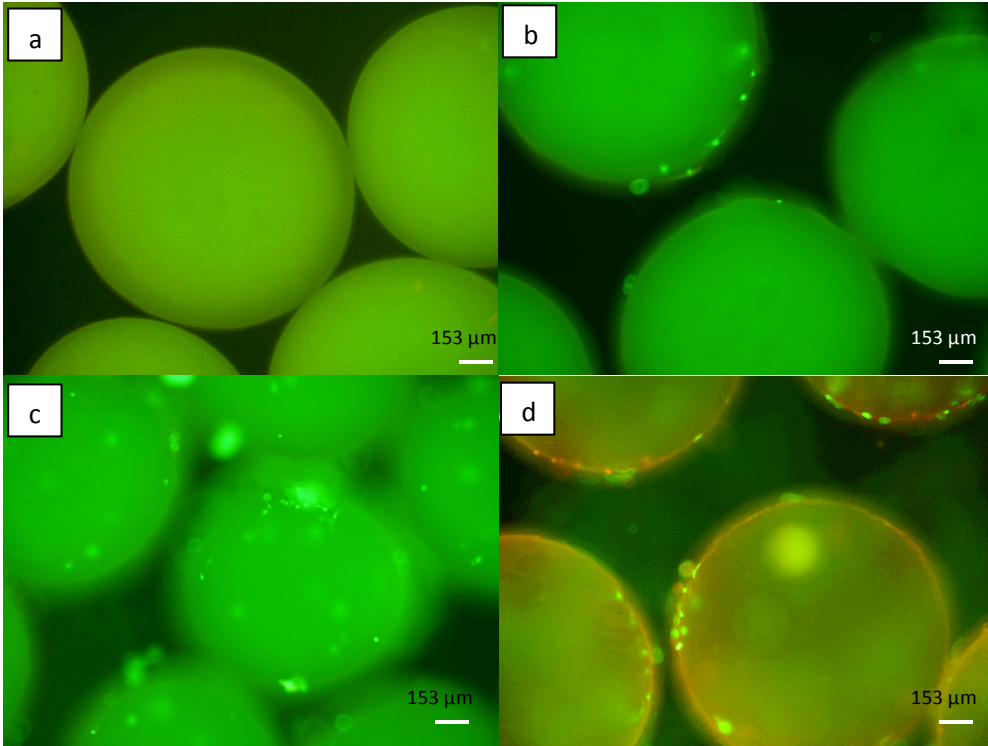
Figure 5.6: Live/dead fluorescence image of microparticles a) without cells (control) b) without any growth factors on day 5 c) encapsulated with BMP-7, seeded with OB 6 cells on day 5 d) without any growth factor on day 10. Microparticles are three-dimensional and therefore in order to capture all the cells attached throughout the surface of the particle, different views were considered starting from periphery of the particle to its upper surface.
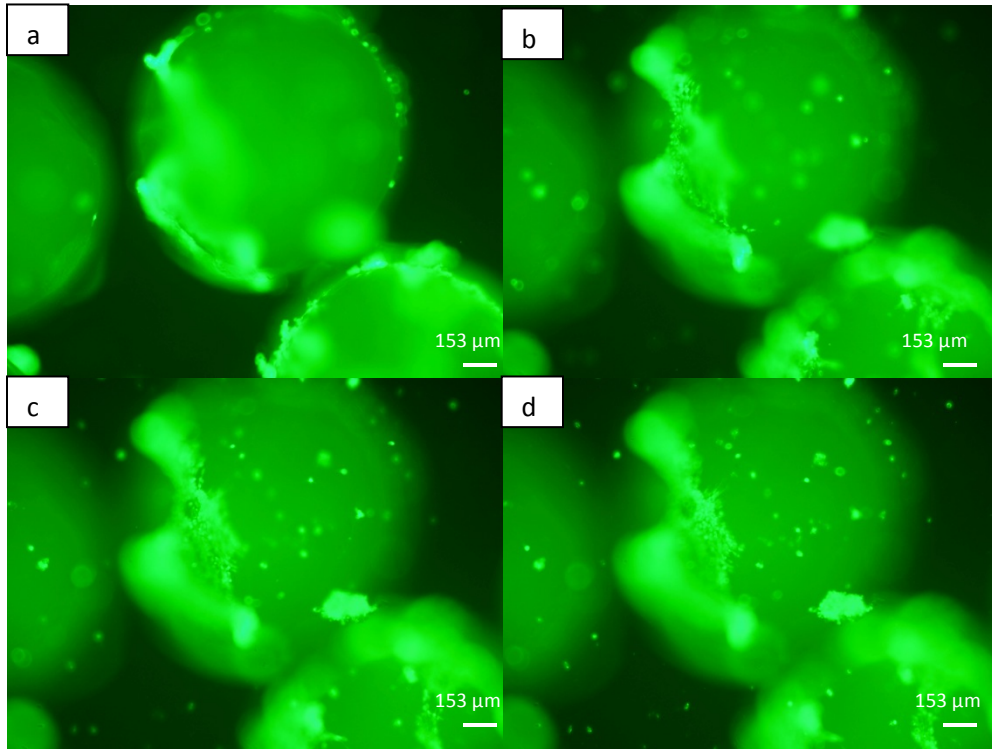
Figure 5.7: Live/dead fluorescence image of microparticles coated with BMP-7 seeded with OB 6 cells on day 5. Microparticles are three-dimensional and therefore in order to capture all the cells attached throughout the surface of the particle, different views were considered starting from the periphery of the particle to its upper surface.
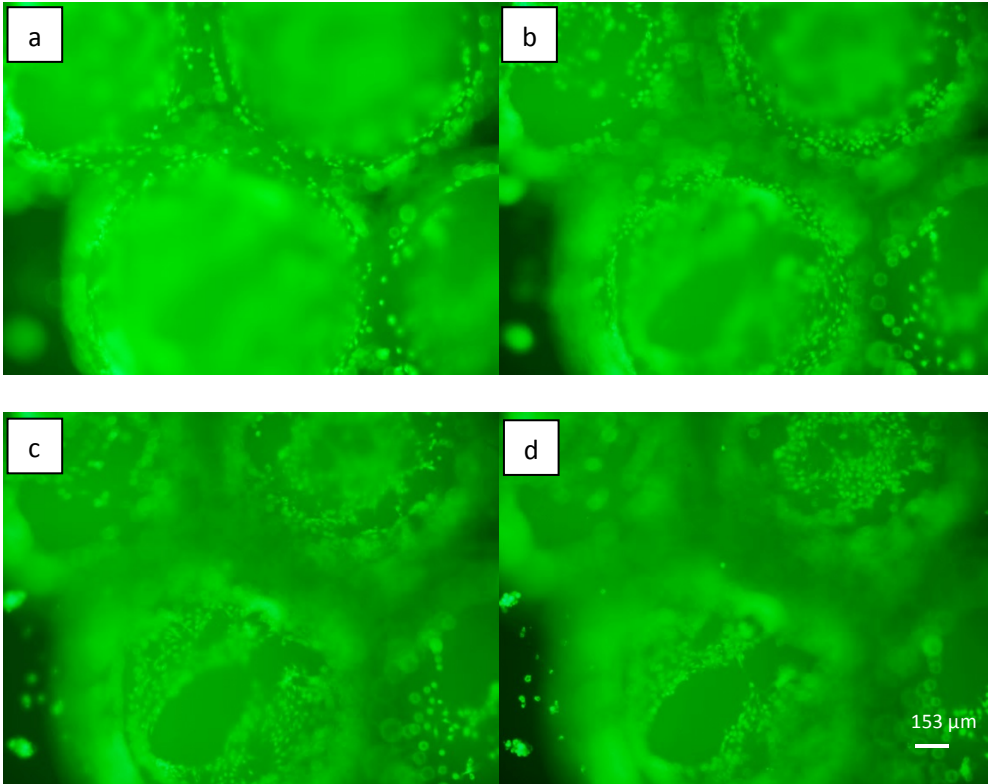
Figure 5.8: Live/dead fluorescence image of microparticles coated with BMP-7 seeded with OB 6 cells on day 10. Microparticles are three-dimensional and therefore in order to capture all the cells attached throughout the surface of the particle, different views were considered starting from the periphery of the particle to its upper surface (a-d).
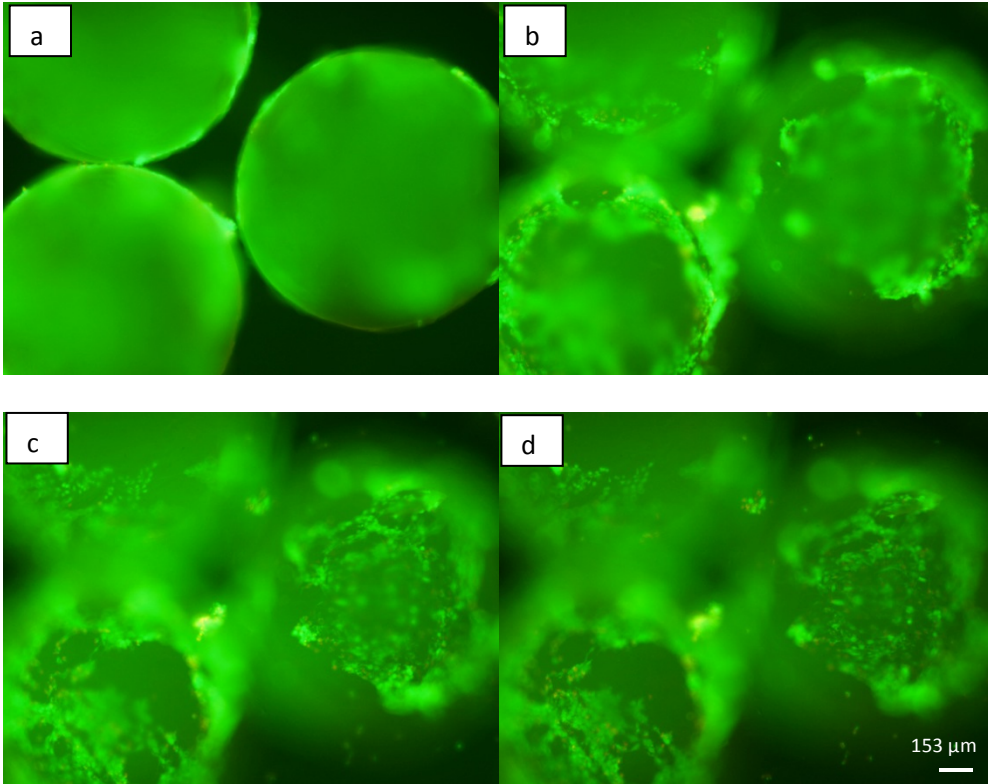
Figure 5.9: Live/dead fluorescence image of microparticles encapsulated with BMP-7 seeded with OB 6 cells on day 10. Microparticles are three-dimensional and therefore in order to capture all the cells attached throughout the surface of the particle, different views were considered starting from the periphery of the particle to its upper surface.

5.3.4 Quantification of DNA

Cell attachment and proliferation on the three dimensional surface of the microparticles was successfully demonstrated by DNA quantification experiment. The amount of DNA can be correlated to the number of cells, with direct proportionality between them. Figure 5.10 shows the amount of DNA obtained from all the cells present in the well, which include the cells attached to the well plate and microparticles. The amount of DNA followed a similar trend, increasing with time in all the four samples. The results of DNA

assay also show that the amount of DNA obtained from BMP-7 coated microparticles on day 5 and 10 was significantly different from all the other three samples ($p < 0.05$).

In another experiment, the microparticles were transferred to another well before performing the DNA assay. These experimental results will give us only the DNA amount corresponding to the cells attached to the surface of the microparticles. Figure 5.11 shows that the amount of DNA increased as the time period increased indicating proliferation on the surface of the microparticles for all the three groups. This demonstrates the capability of the chitosan surface with and without growth factors to support OB-6 cell proliferation. The data also shows a significant increase ($p < 0.05$) in the amount of DNA obtained from BMP-7 coated microparticles than that obtained from other two groups on day 5. However on day 10, a significant increase is observed in the amount of DNA obtained from BMP-7 encapsulated microparticles in comparison with normal microparticles without any growth factors ($p < 0.05$) and a significant increase is observed in BMP-7 coated microparticles in comparison with BMP-7 encapsulated microparticles ($p < 0.001$). This data confirms that bioactive BMP-7 being released from the microparticles improves cell proliferation.
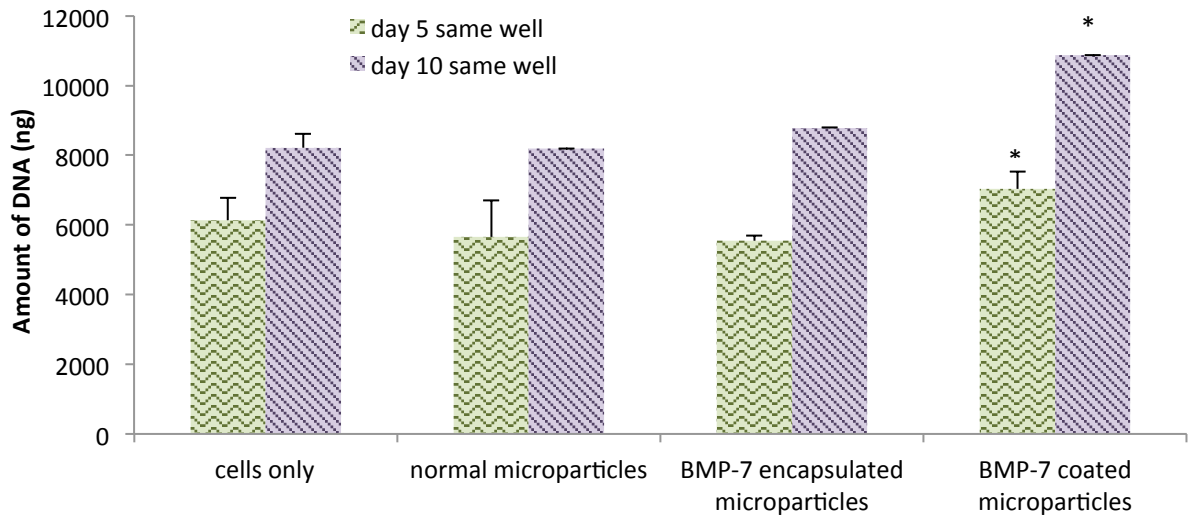
Figure 5.10: Amount of DNA obtained in the samples when the assay was performed in the well the cells were cultured for the respective time periods. This data gives us information regarding the number of cells attached and proliferating on the surface of the well plate as well as on the surface of the microparticle
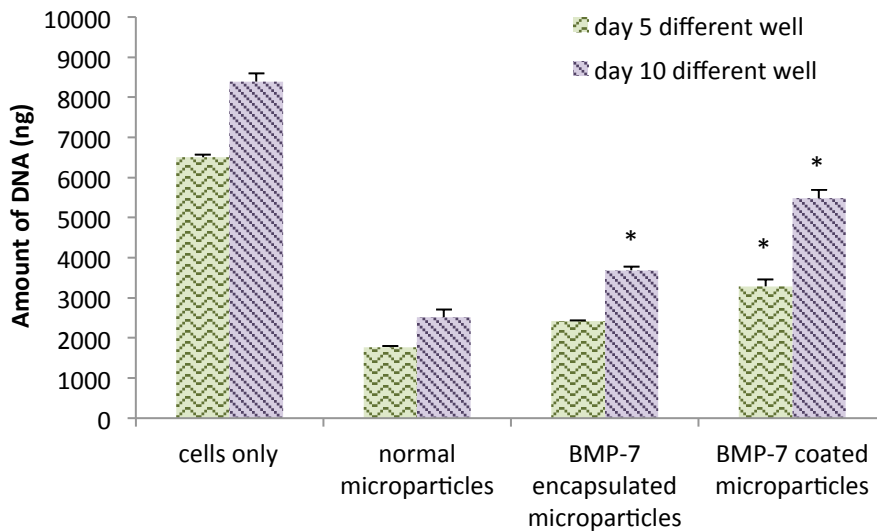
Figure 5.11: Amount of DNA obtained from the samples when the assay was done after transferring the microparticles to a different well on the respective time points. This data gives us an insight of the number of cells attached and proliferating on the surface of the microparticles only.

5.3.5 Real Time RT-PCR

Dlx5 gene: On day 5, a significant difference (p<0.001) is observed in the expression of Dlx5 expression when a pairwise comparison is done between all the four samples. mRNA levels were drastically up-regulated on day 5 for microparticles with BMP-7 encapsulated (8-fold) and BMP-7 coated microparticles (9-fold). On day 7, a significant difference (p<0.001) is observed between all the samples except for BMP-7 encapsulated and BMP-7 coated microparticles (p=0.292). Dlx5 expression levels for microparticles without growth factors remained at baseline levels for most of the time points. Figure 5.12a shows that there is significant increase in the expression of Dlx5 in BMP-7 coated and encapsulated microparticles in the early time points (day 5 and 7) when compared to microparticles without growth factors and cells only, which indicates effect of BMP-7 in inducing the expression of this gene. By day 10, the expression level in all the samples went down, and there was no significant difference (p=0.052) observed in the gene expression between cells adhered to BMP-7 encapsulated microparticles and cells adhered to the well plate.

Runx2 gene: SPSS two-way ANOVA pairwise comparison of the runx2 gene expression indicated that there is a significant difference (p<0.001) between all the four samples on day 5, 7 and 10. Posthoc Tukey's HSD also indicates a significant difference (p<0.001) in the expression of the gene when pairwise comparison is done. The posthoc multiple comparison between the three time points also indicates a significant increase (p<0.001) in the gene expression on day 10 in comparison with day 7 and a significant increase (p<0.001) on day 7 in comparison with day 5 (Figure 5.12b). A fold change of 7.5 in the runx 2 gene expression on day 10 for cells adhered to the microparticles in comparison

with the cells adhered to the surface of the well plate indicates the influence of chitosan microparticles on differentiation of the pre-osteoblasts. A fold change of 17 was observed for cells adhered to BMP-7 encapsulated surface indicating differentiation of pre-osteoblasts to mature osteoblasts under the influence of BMP-7.

Osx gene: Osterix is another transcription factor necessary for osteoblast differentiation. SPSS two way ANOVA indicated a significant difference ($p<0.001$) is observed in the expression of osx between all the samples when a pairwise analysis is conducted on day 5, 7 and 10. Posthoc Tukey's HSD also indicates a significant difference ($p<0.001$) in all the samples. A posthoc Tukey's HSD for the three time points also indicated a significant difference ($p<0.05$). From Fig. 12c we can observe a significant increase in the expression of osterix expression level on day 5 for BMP-7 encapsulated (25-fold) and coated microparticles (34-fold). As indicated in Figure 5.12c, on day 7 and 10, there is a decrease in the expression levels of osx for all the samples, but in comparison to cells only, there is almost 2-6 fold increase in its expression levels for all the types of microparticles.

OCN gene: Two-way ANOVA pairwise analysis indicated a significant difference ($p<0.001$) in the expression of OCN gene between all the samples on day 5, 7 and 10. There is also a significant difference ($p<0.001$) in the expression of the gene at the three different time points. A posthoc analysis confirms the significant difference ($p<0.001$) between the four samples and the three different time points. As shown in Figure 5.12d, OCN showed very low levels of expression at the early time point (day 5), but with time its expression increased. For microparticles without growth factors showed a maximum of 17-fold increase by day 10. For BMP-7 coated and encapsulated microparticles, there

is a significant increase in the expression of OCN, 27-fold and 35-fold respectively by day 7, indicating the influence of BMP-7 on OCN expression.

BSP gene: SPSS two-way pairwise ANOVA indicated a significant difference ($p<0.001$) in the expression on BSP gene between all the samples on day 5, 7 and 10. There is also a significant difference ($p<0.001$) observed in the expression when compared between the three time points. Figure 5.12e shows that BSP mRNA levels were almost to the baseline on day 5 and 7. However, on day 10 there was a significant increase observed in the expression levels of BSP in microparticles without growth factors (9-fold), BMP-7 encapsulated microparticles (54-fold) and BMP-7 coated microparticles (53-fold).

OPN gene: OPN shows a trend similar to OCN, with the up-regulation of the gene with time. Two-way pairwise ANOVA analysis indicated a significant difference ($p<0.001$) in the expression of the gene between all the four samples on day 5, 7 and 10. Post hoc Tukey's test indicated a significant difference ($p<0.001$) in the expression of genes in the different samples as well as a significant difference ($p<0.001$) at the three different time points. OPN mRNA levels were increased on day 7 in comparison with day 5 for BMP-7 encapsulated (7-fold) and BMP 7 coated microparticles (8-fold). Figure 5.12f indicates a slight decrease in the expression levels for microparticles only from 6-fold on day 5 to 3.6-fold on day 7. There is a significant increase observed in mRNA levels of OPN for BMP 7 coated microparticles on day 10 in comparison with day 7.
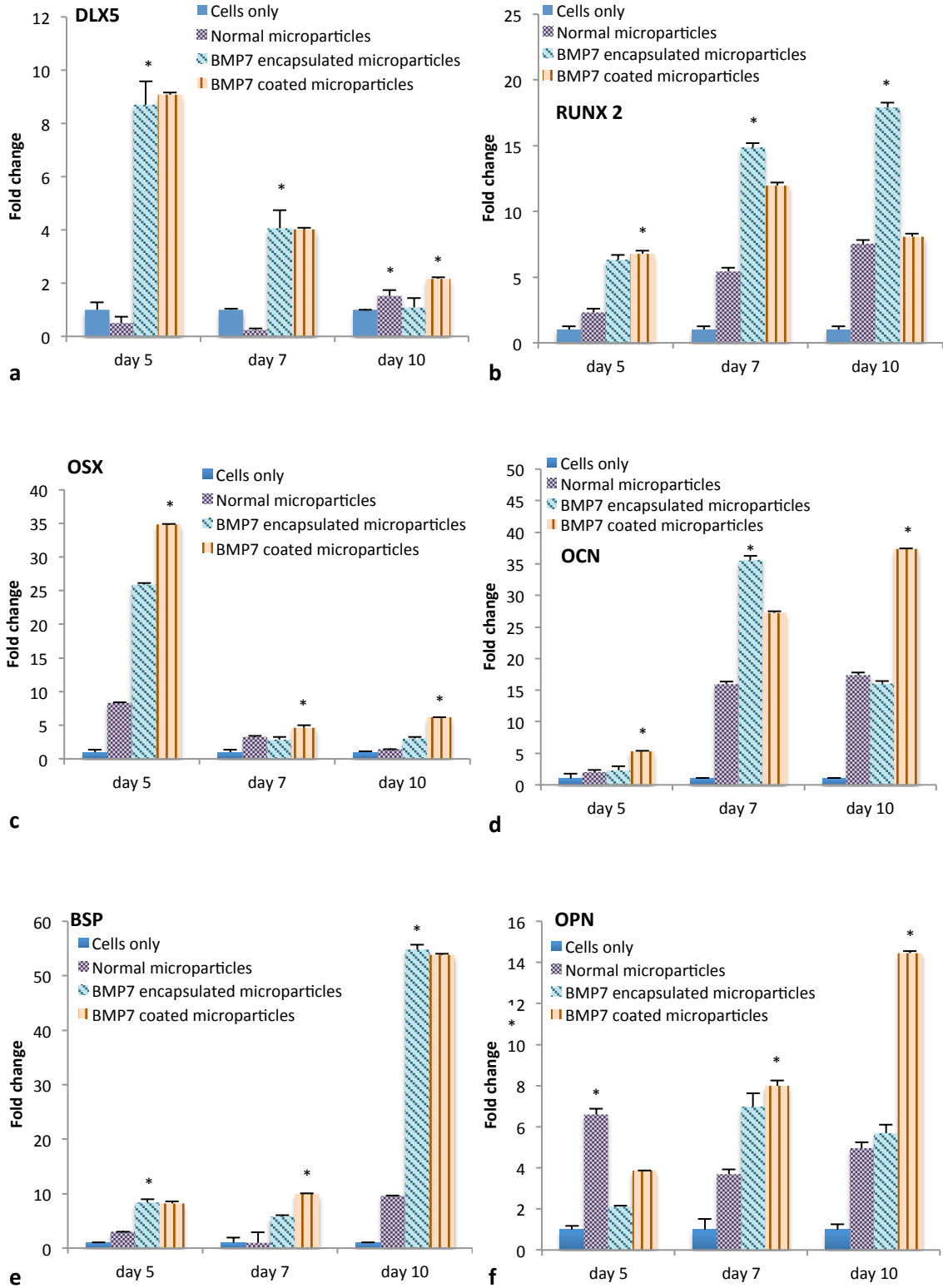
Figure 5.12: Fold change in the expression of the genes: a) dlx5, b) runx2, c) osx, d) OCN, e) BSP and f) OPN.

5.3.6 Von Kossa Assay

This staining procedure stains mineral deposits in black. On day 5, there is not much mineralization observed in either BMP 7 coated or encapsulated microparticles. However, by day 10 the assay shows increasing mineral deposition through the period of study both by BMP-7 encapsulated and BMP-7 coated microparticles, with substantial increase for BMP-7 coated microparticles (Figure 5.13). The mineral deposit was mainly localized in the area adjacent to the microparticles. This indicates differentiating osteoblasts. Mineralization was quantified by calculating the area of mineralization per image. The average area occupied by the mineral deposits is shown in Figure 5.14. One-way ANOVA was conducted using SPSS, and the analysis showed that there is a significant difference between the four different samples ($p < 0.001$). Tukey's post hoc multiple comparison analysis indicated that there is a significant difference ($p < 0.05$) between cells grown in well plates without microparticles and BMP-7 encapsulated ($p = 0.017$) and coated microparticles ($p < 0.001$). A significant increase ($p < 0.05$) in mineralization was observed in BMP-7 encapsulated microparticles in comparison with microparticles without any growth factors ($p = 0.017$). There is also a significant difference ($p < 0.05$) observed between BMP-7 encapsulated and BMP-7 coated microparticles ($p = 0.036$). Though this assay does not take into consideration the three dimensional nature of the microparticles or the mineral deposits, it identifies the presence of mineralization and demonstrates increasing deposits with time and so the assay gives satisfactory results.
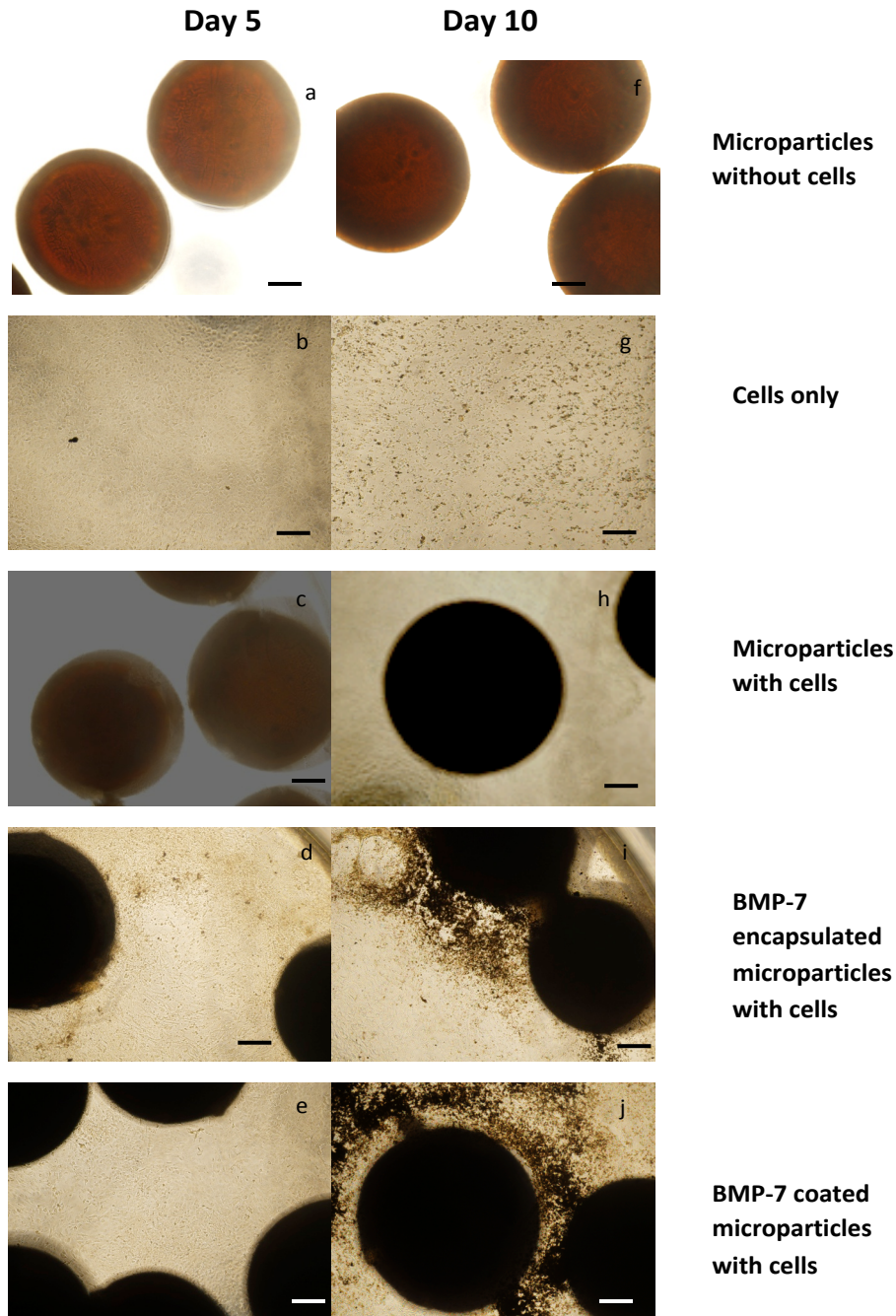
Figure 5.13: Von kossa assay (Scale bar = 153 μm).
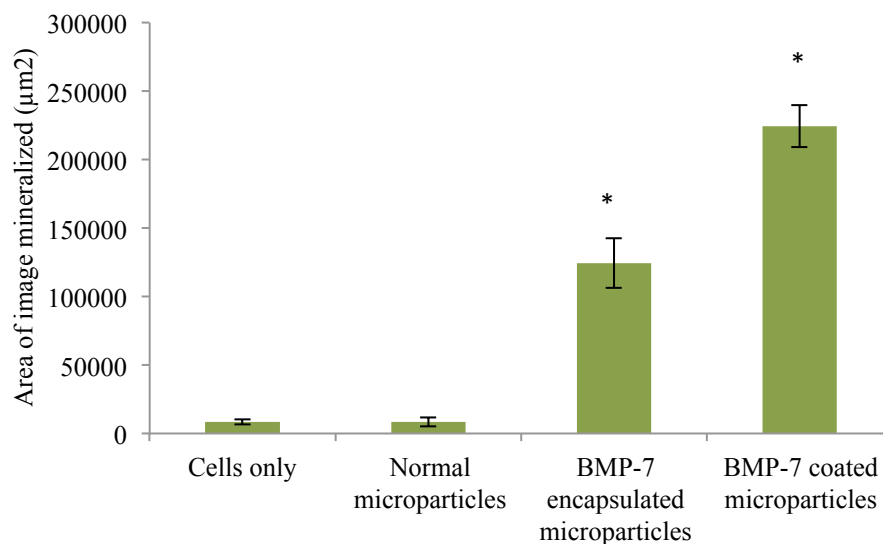
Figure 5.14: Area of the image occupied by the mineralized calcium deposits.

5.4. Discussion

This investigation of biocompatibility, osteoconductivity and osteoinductivity of chitosan microparticles for pre-osteoblasts indicate that chitosan-TPP surface of the microparticle supports pre-osteoblast adhesion, proliferation and differentiation [216-220] and bioactive BMP 7 is released from the microparticles [221].

This study indicates that chitosan-TPP microparticles and bioactive BMP-7 released from microparticles together contribute to the significant increase in the response from pre-osteoblasts. Incremental changes in cell proliferation were observed in BMP-7 coated and encapsulated microparticles in comparison with microparticles only on day 10 [222]. This result was confirmed by all the three tests – SEM analysis, live/dead cell assay and DNA assay and this can be attributed to the surface morphology of the microparticles and release of biologically active growth factor [223-225].

These microparticles were added to PBS to test the change in pH and it was found to be always in the range of 7.4-7.5, thus assuring that the osteoblasts are not affected in our experimental system. Moreover, chitosan is a polymer possessing osteoconductive characteristic [226,227], as shown in previous studies where its polymerization with TPP ameliorated cell adhesion [228]. Cells attached on the surface of the microparticle can be explained from the fact that osteoblasts are polarized. In the sense that part of the cell membrane in direct contact with the surface possesses many cytoplasmic processes that extend onto the surface. On day 5 cells appeared elongated which suggests dividing cells. Previous studies suggest that it is the pre-osteoblasts and not the mature osteoblasts that have the capability to actively divide [229]. Mature osteoblasts are found to attain more of the cuboidal morphology and are directly in contact with the surface [230], which is clearly seen in the SEM images on day 10 results for all the samples. The osteoblasts also elicited a distinct response to microparticles with and without BMP-7. This indicates the potential of chitosan-TPP microparticles to support cell adhesion and viable cell proliferation and the presence of BMP-7 further adds to the benefit of the cells [231,232]. The difference observed between BMP-7 encapsulated and coated microparticles can be attributed to the effect of concentration of BMP-7 on cell growth. Studies have shown that increased concentration of BMP-7 lead to increased cell proliferation [232].

Osteoblast-specific gene expression study also revealed the influence of chitosan-TPP microparticles and BMP-7 on osteoblasts. Murine pre-osteoblasts that were differentiated into osteoblastic lineage were evaluated with respect to the effect of the microparticles itself as well as the combination of microparticles and BMP-7. The effect of chitosan-TPP microparticle itself is revealed distinctly in the expression of Runx2 (7.5-fold), OCN

(17.3-fold), OPN (6.6-fold) and BSP (9.6-fold). This observation explains the influence of the microparticles surface morphology and chemistry on osteoblast differentiation and mineralization. Previous studies have also demonstrated its beneficial effect on osteoblast differentiation *in vitro* and *in vivo* [233-235]. Additional influence of BMP-7 on pre-osteoblast differentiation was observed in the expression of runx2 (17-fold), dlx5 (14-fold), osx (25-fold), OCN (36-fold) and BSP (55-fold). BMP-7 signaling is known to regulate processes in bone formation. Runx2 and osx are needed for osteoblast differentiation and also plays an important role in proper function of mature osteoblasts, including the synthesis of bone matrix [236]. Expression levels are low in undifferentiated mesenchymal cells. BMP-7 induces Runx 2 and osx expression in mesenchymal progenitor cells, which induces osteoblastic differentiation [237]. Runx2 is not a direct target of BMP signaling, Dlx5 is activated by BMPs, which in turn induce expression of Runx2 in osteoprogenitor cells [238,239].

A significant increase in mineralization was also found in BMP-7 encapsulated and coated microparticles, which can be attributed to significant increase in the expression of OCN, OPN, and BSP in these samples. These genes are usually regarded as late markers for osteoblast differentiation and play an important role in hard tissue regeneration [240-243].

Thus from the *in vitro* data obtained, it can be concluded that chitosan microparticles prepared by coacervation method are ideal osseointegration materials by itself and the BMP-7 being released from the microparticles retains its bioactivity and further enhances the functionality of the microparticles as bone substitute materials. The microparticles surface with growth factor aided in greater osteoblast proliferation and differentiation by

increasing osteoblast specific gene expression. The present data however lacks *in vivo* data, which will eventually prove the osseointegration capability of the system.

Chapter 6

The Influence of Antibiotics Released from Chitosan Microparticles on Osteoblasts and *Staphylococcus epidermidis*

In this chapter, the experiments conducted address hypothesis IV. Cefazolin and vancomycin are incorporated into the microparticles by encapsulation and coating. Two different concentrations of each drug are used and the release kinetics is studied. The drugs along with growth factor BMP-7 are also incorporated in the microparticles to study the release kinetics and bioactivity. Influence of drugs and growth factor on pre-osteoblasts is also studied.

6.1 Materials

Chitosan (85% deacetylated), sodium tripolyphosphate (TPP), acetic acid, PBS, tryptic soy agar and broth were purchased from Sigma Chemicals, bone morphogenetic protein 7 (BMP-7) was purchased from Peprotech and BMP-7 ELISA kit was supplied by R & D

systems, live/dead cytotoxicity/viability assay and α-MEM (Invitrogen), vancomycin hydrochloride and cefazolin sodium salt were purchased from MP Biomedicals.

6.2 Methods

6.2.1 Fabrication and Characterization of Chitosan Microparticles Incorporated with Antibiotics and Growth Factors

6.2.1.1 Fabrication of Microparticles

Microparticles were prepared by coacervation method using 2% chitosan and 50% tri-polyphosphate (TPP). The microparticles were cross-linked overnight and then were air-dried.

6.2.1.2 Fourier Transform Infrared Spectroscopy Analysis of Various Samples

Microparticles prepared using chitosan and TPP was analyzed using Varian Excalibur Series FTIR with microscopy to determine the presence drugs: vancomycin and cefazolin. The microscope, UMA 600 was used to detect the drugs in these samples. A micro-ATR with Germanium crystal was used to do this. The transmittance data was collected and plotted for identifying the peaks.

6.2.2 Release Study *In vitro*

6.2.2.1 Release Study of only Drug from the Microparticles

Two different amounts of each drug were incorporated into the microparticles (Table 6.1). These concentrations were determined based on the minimum inhibitory

concentration (MIC) of each for *Staphylococcus* strain. These drugs are incorporated into the microparticles by two methods – encapsulation and coating. It was ensured that 20 mg of the microparticles that will be used for release kinetics has the same amount of drug encapsulated and coated onto them. Microparticles were suspended in 2 ml of PBS and samples were collected at pre-determined time points.

To quantify the amount of drug released, ultra-violet (UV) spectroscopy was used. A standard graph was plotted between known concentrations of the drug and absorbance at 280 nm for both vancomycin and cefazolin. Absorbance of the release samples collected at certain time points was determined and extrapolated on the standard graph to determine the concentration of the drug. Cumulative release graph was plotted to determine the total amount of drug released at the end of 2 weeks period. Encapsulation efficiency and loading efficiency of the each sample was also determined.

6.2.2.2 Dual Release Study of Growth Factor and the Antibiotics from Microparticles

20 mg of BMP-7 encapsulated microparticles were added to 20 mg of cefazolin and vancomycin encapsulated microparticles respectively. These microparticles were then suspended in 2 ml of PBS buffer solution for release study at 37$^{\mathrm{o}}$C and samples were taken at pre-determined time intervals. Release of both the drug and the growth factor was determined.

To quantify the drugs, UV spectroscopy was used and to determine BMP-7, enzyme-linked immunosorbant assay (ELISA) was used. The protocol mentioned in the BMP-7 ELISA kit was followed to quantify the BMP-7 amounts in the release samples. A standard graph was obtained from known drug concentrations by determining its

absorbance at 450 nm with wavelength correction at 540 nm. Unknown concentration in the samples was determined by using the standard graph.

6.2.3 Bioactivity of the Released Antibiotics

The released drugs were tested for ability to inhibit the growth of *S.epidermidis* (strain was kindly given to us by Dr. Robert Blumenthal, Department of Microbiology and Immunology, The University of Toledo), usually associated with infected orthopedic wounds. The ability of the released drug to inhibit bacterial growth was determined by turbidity test. To grow *S. epidermidis*, bacterial stock previously stored and frozen at -$70^{o}C$ was resuscitated on solid medium (Tryptic Soy Agar, Sigma Aldrich). Two colonies were selected and cultured overnight in 10 ml tryptic soy liquid medium in two separate conical flasks in shaking water bath at $37^{o}C$. After overnight incubation, a second transfer was made to fresh tryptic soy medium (1:10 dilution) and was grown to attain an $OD_{600\,nm} = 0.05$ for *S.epidermidis* (SPECTROstar Omega, USA). In the meantime, 100 μl of drug solution obtained for the release study at each time point were added to a 96-well plate (n=3). As soon as an OD of 0.1 was obtained, 100 μl of the bacterial suspension was added to the wells and OD readings were taken at pre-determined time intervals for a period of 24 h. The growth curves plotted were compared against the growth of the control that had only the bacterial culture in PBS.

Bacterial inhibition (%) = absorbance (Ic-Is)/(Ic)*100, where Ic and Is are the absorbances of control solution containing tryptic soy broth and bacterial culture without drug and bacterial culture solution with drug release sample, respectively at 600 nm after 24h [244].

6.2.4 Effect of the Drugs on Viability of Osteoblasts

Above certain concentrations, the antibiotics are harmful for the cells in the body. Therefore in order to determine the amount of drug harmful for the growth and proliferation of osteoblasts, a live-dead assay was performed. For this assay, two different concentrations of each drug was used – 50 μg/ml and 100 μg/ml of cefazolin and 500 μg/ml and 1000 μg/ml concentration of vancomycin. A combination of growth factor BMP-7 and each drug concentration was also used to determine the effect of the combination on the growth of osteoblasts. Osteoblasts growth in regular α-MEM medium was used as a control. A live dead cell assay was performed on day 1 and 3 by removing all the medium in the wells, washing it with PBS solution thoroughly and then adding 300 μl of D-PBS and 300 μl of live-dead assay solution containing calcein which stains the live healthy cells green and ethydium homodimer which stains the dead cells red. After 45 minutes, the plate was observed under fluorescence microscopy. For statistical analysis, each group had n=3 triplicates, and for live cell counting, 30 images were taken for each group and analyzed using ImageJ software.

6.2.5 Statistical Analyses

Triplicates of each sample were used in all the experiments. Two-way ANOVA was performed using SPSS to determine whether a statistical significant difference exists between the groups. Post-hoc Tukey's test was performed to determine statistical difference between the groups. A probability value of $p<0.05$ was used to determine significance, unless otherwise mentioned.

6.3 Results

6.3.1 FTIR Analysis

6.3.1.1 FTIR Analysis of Microparticles with Cefazolin

FTIR spectra of the drug, cefazolin only show a broad peak in the range from 3100-3500 cm^{-1}, and a sharp intense peak at 1759 cm^{-1} (which clearly shows presence of carbonyl group) and combining the two indications, we can confirm the presence of the carboxylic group in cefazolin (Figure 6.1a). The peaks at 1647 cm^{-1} and 1593 cm^{-1} indicated C=N stretching and the presence of amide. The peaks at 2939 and 2866 cm^{-1} indicates C-H stretching vibrations. The peak at 1666 cm^{-1} along with the broad peak in the 3200 cm^{-1} range indicates the presence of amide.

The double peaks at 3340 and 3271 cm^{-1} indicates the presence of primary amine with two N-H bonds formed due to complex formation between the COOH group of cefazolin and NH_2 group of chitosan. The proof of interaction between COOH group in cefazolin and NH_2 group in chitosan is also indicated by the fact that the strong peak at 1759 cm^{-1} in the drug disappears in the drug with microparticle samples (Figure 6.1b). The amide and C=N functional groups appear to have a shift in their wavenumber to 1666 cm^{-1} and 1585 cm^{-1} respectively indicating interaction between cefazolin and chitosan microparticles [245]. The P-O stretching is distinctly shown at the almost the same wavenumber, 1184 cm^{-1} which indicates no interaction of drug with TPP [246] (Figure 6.1c).
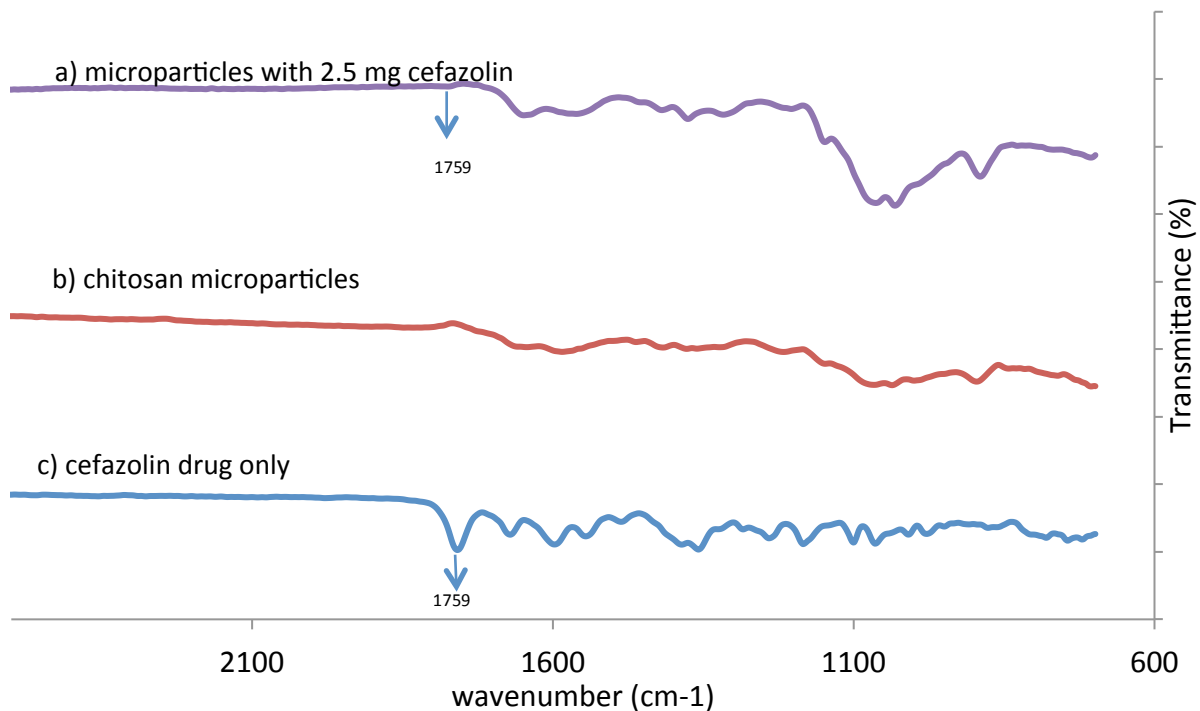
Figure 6.1: FTIR spectra of (a) chitosan microparticles with 2.5 mg cefazolin (b) chitosan-TPP microparticles without drug (c) cefazolin drug only

6.3.1.2 FTIR Analysis of Microparticles with Vancomycin

FTIR spectrum of the vancomycin drug alone indicates a broad peak range from 3600 to 2900 cm^{-1} indicates the presence of OH groups and NH groups [247,248]. The presence of a peak at 1643 cm^{-1} shows that it is an amide group. The crowded spectra from 500-1500 cm^{-1} is due to the skeletal vibrations of C-O, C-N, C-C bonds in the vancomycin structure Figure 6.2a. The presence of a peak 1222 cm^{-1} indicates the presence of an aromatic ester.

The FTIR spectrum of microparticles with vancomycin shows one distinct peak, which indicates primary amine while the broad peak indicates the weak OH group. The peak at 1643 cm^{-1} together with the broad peak range in 3000 cm^{-1} region supports the presence of amide (Figure 6.2b). The presence of a new peak in this sample at 1230 cm^{-1} indicates

the presence of an aromatic ester, thus showing that there is an interaction between the chitosan microparticles and vancomycin (Figure 6.2c).
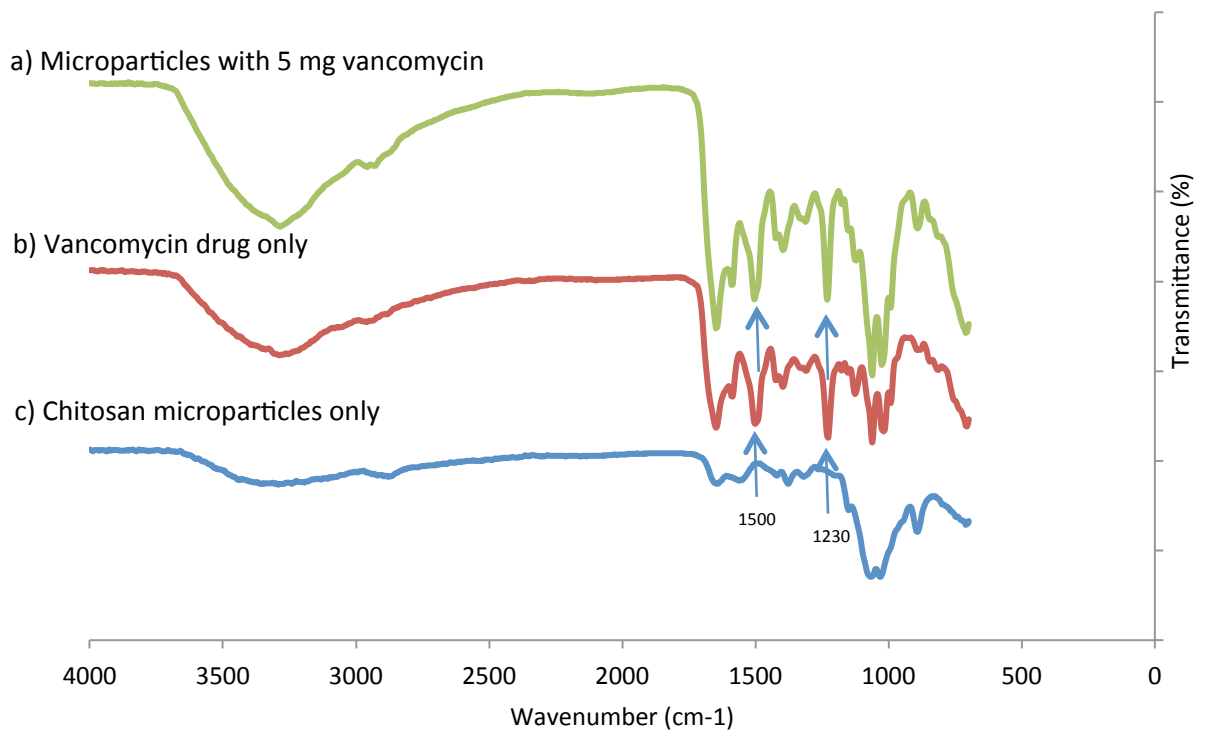
Figure 6.2: FTIR spectra of (a) chitosan-TPP microparticles with 5 mg drug incorporated (b) vancomycin drug only (c) chitosan-TPP microparticles only.

6.3.2 Release Kinetics

6.3.2.1 Cumulative Release of Vancomycin and Cefazolin

The microparticles with vancomycin and cefazolin encapsulated into it exhibited high encapsulation efficiencies, indicating that most of the drug added to the microparticles was incorporated (Table 6.1). In case of microparticles with drugs coated, since we added the drugs to the particles after their preparation and then allowed the drug to be

completely incorporated, encapsulation efficiency of 100% was considered for calculations.

The release of vancomycin and cefazolin was analyzed by UV spectrophotometry and the results obtained are represented in Figure 6.3 From all the release profiles, we can observe that when the drug is encapsulated, the release is much controlled and nearly just 50% of the drug encapsulated is released in 2 weeks time period, whereas in microparticles with drug coated onto it, approximately 95% release was observed in the same time period. In microparticles coated with either vancomycin or cefazolin, nearly more than 50% was released by day 1, which indicates burst release of the adsorbed drug. In contrast, microparticles with drug encapsulated into it showed minimal burst release, with only 10% cumulative release by day 1. Two different concentrations used for the two drugs (Figure 6.3 a,b and Figure 6.3 c,d), showed similar release profile, indicating that an increase in the amount of drug incorporated into the microparticles, increases the release amount proportionally. Statistical analysis performed using SPSS indicated $p<0.01$ for cumulative release amounts at different time intervals, which means that vancomycin and cefazolin release decreases significantly in drug encapsulated microparticles in comparison with drug coated microparticles till day 14.

After studying the release profiles (Figure 6.3 a,b,c,d), microparticles with 3 mg vancomycin and cefazolin with 2.5 mg encapsulated into it were considered for the BMP-7 dual release study and *in vitro* antibacterial test. This was done so because we wanted vancomycin release above 8 μg/ml at each time point over the two-week time period. Similarly for cefazolin dual release study, microparticle with 2.5 mg of cefazolin was

considered, since we wanted a release of above 4 µg/ml at each time point. These groups also show least burst release and longest release period.

Table 6.1: Encapsulation efficiency of various drug samples used in the experiments

Group	Amount of vancomycin added to 20 mg microparticles (mg)	Encapsulation efficiency (%)
Vancomycin 8mg/ml	3.05	98.4
Vancomycin 16 mg/ml	5.11	97.8
Cefazolin 4 mg/ml	1.53	98.2
Cefazolin 8 mg/ml	2.53	98.6
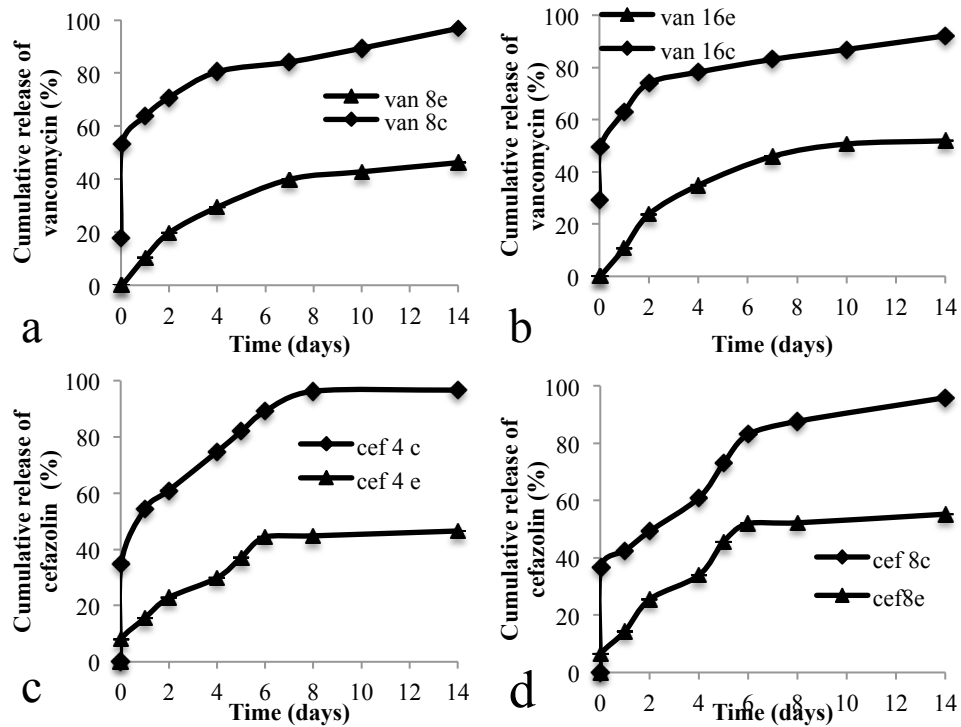
Figure 6.3: Cumulative release profile of the drugs from microparticles containing (a) 3 mg vancomycin (b) 5 mg vancomycin (c) 1.5 mg cefazolin (d) 2.5 mg cefazolin, encapsulated and coated onto it. These microparticles were immersed in PBS buffer of pH 7.4 at 37°C and samples were collected at pre-determined time intervals. Each data point is mean $\pm$ standard deviation (n=3)

6.3.2.2 Dual Release of BMP-7 and the Antibiotics
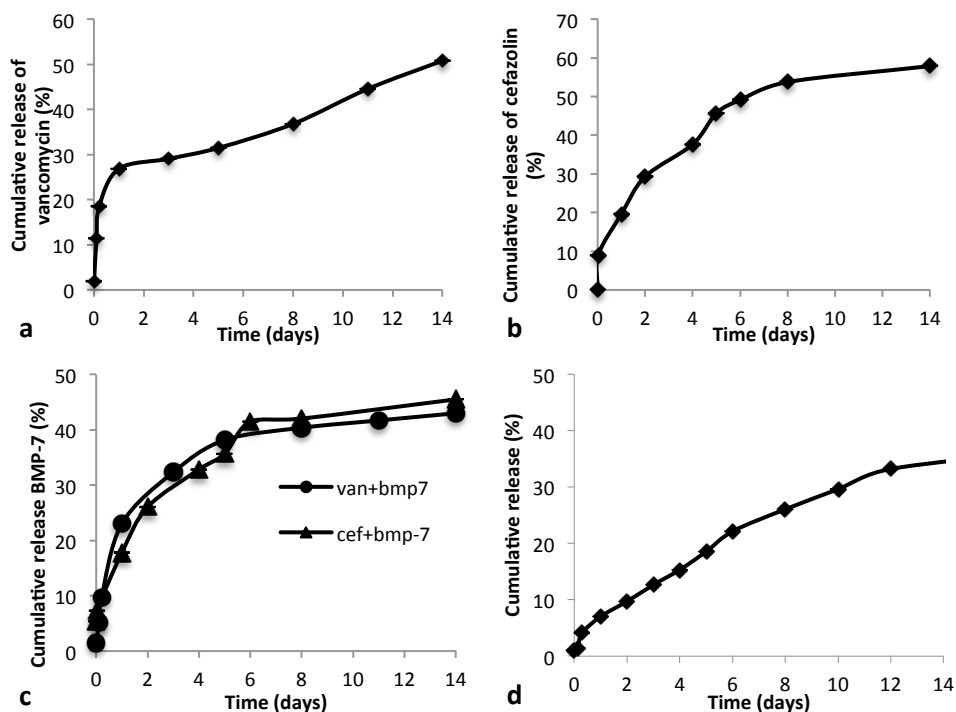
Figure 6.4: Cumulative release profiles of (a) 3 mg vancomycin (b) 2.5 mg cefazolin (c) BMP-7 encapsulated in the microparticles (d) BMP-7 release profile in the absence of drugs. Each data point is mean $\pm$ standard deviation (n=3)

The release profile of vancomycin in presence of BMP-7 was similar to the individual drug release profile. In the presence and absence of BMP-7, the cumulative release amount for the 3 mg vancomycin release study was 50.79% and 51.89% respectively, which indicates that the presence of BMP-7 does not affect the stability or release amounts of vancomycin (Figure 6.4a). A similar observation was made for cefazolin release as well, with a cumulative release percent of 57.87% and 55.25% in the presence and absence of BMP-7 respectively (Figure 6.4b). Statistically, there was no significant difference ($p > 0.01$) observed between the cumulative release amounts at the various time

points, when a comparison is made between the drug release in the presence and absence of BMP-7.

BMP-7 cumulative release was determined from the above release samples and the release profile was similar in the presence of vancomycin and cefazolin. Also when these profiles are compared with BMP-7 release only, a similar result was observed, with the cumulative release percentage being 45.49%, 42.99%, and 36.45% in presence of cefazolin, vancomycin (Figure 6.4c) and BMP-7 itself (Figure 6.4d) respectively, which indicates that the presence of drugs have no effect on the stability of BMP-7.

6.3.3 Biocompatibility Tests *In vitro*

On day 1, a post hoc Tukey's HSD analysis indicated a significant difference ($p<0.001$) in the proliferation of pre-osteoblasts (OB-6) grown in plain media (control) and that with growth factor BMP-7, indicating that on day 1 itself, BMP-7 has an influence on the cells growth and proliferation (Figure 6.5). In the antibiotics containing samples, a significant difference ($p<0.001$) was observed between controls and that containing BMP-7 and vancomycin (1000 µg/ml). In comparison with BMP-7 containing media, there was a significant difference ($p<0.001$) observed between all the other samples except media containing BMP-7+cefazolin (100 µg/ml) (Figure 6.5a), and BMP-7 + vancomycin (1000 µg/ml) (Figure 6.5b). This shows that higher concentrations of drugs are tolerable by the pre-osteoblasts in the early time period (day 1). In medium containing cefazolin (50 µg/ml) and vancomycin (500 µg/ml) only, a significant decrease ($p<0.05$) is observed in comparison with medium containing BMP-7 and cefazolin (100 µg/ml). In medium containing BMP-7 and cefazolin (100 µg/ml), a significant increase ($p<0.05$) in

proliferation was observed in comparison with media containing BMP-7 and vancomycin (500 µg/ml).

On day 3 however, media containing vancomycin (1000 µg/ml) showed significant decrease in the cell proliferation in comparison with all the samples except media containing 500 µg/ml of vancomycin and a combination of vancomycin (1000 µg/ml) and BMP-7. These results indicate that higher concentration of vancomycin (1000 µg/ml) inhibits pre-osteoblasts cell proliferation. Media containing 500 µg/ml vancomycin showed significant decrease ($p < 0.05$) in cell proliferation in comparison with media containing BMP-7 and cefazolin (100 µg/ml and 50 µg/ml). A significant increase ($p < 0.05$) was also observed in proliferation in media containing BMP-7 and cefazolin (100 µg/ml and 50 µg/ml) over media containing BMP-7 and vancomycin (1000 µg/ml). These results show that 50 µg/ml and 100 µg/ml cefazolin concentrations in presence and absence of BMP-7 increases cell proliferation.
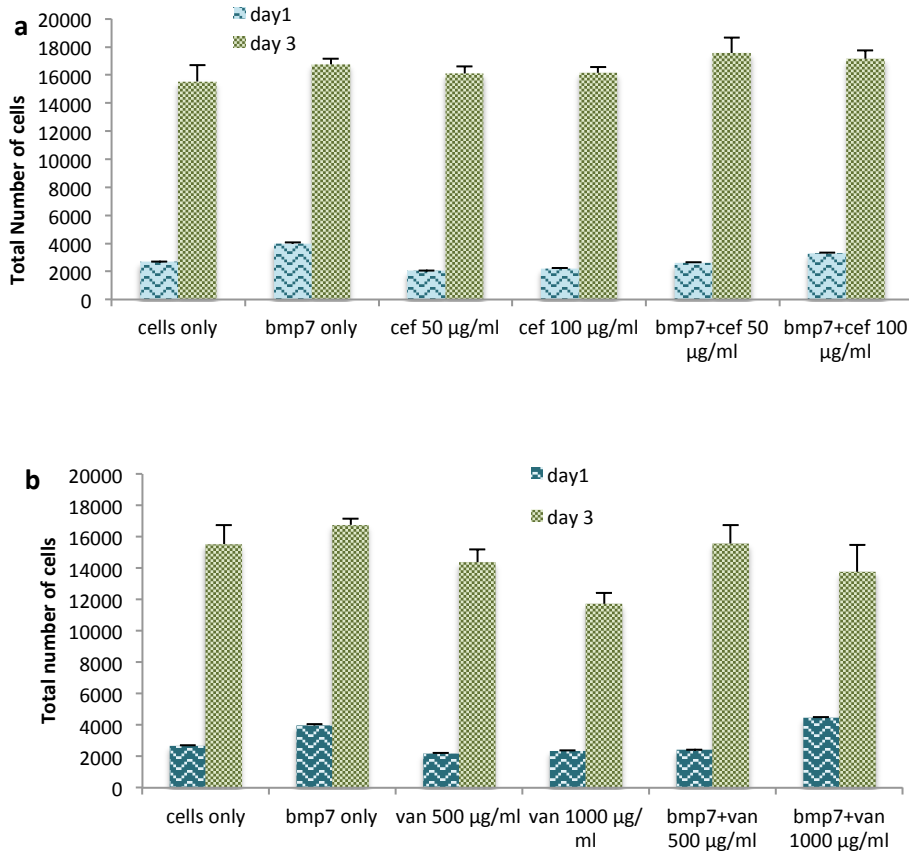
Figure 6.5: Effect of a) cefazolin b) vancomycin and growth factor on viability and proliferation of pre-osteoblasts OB-6 (n=10). OB-6 cells were exposed to 100 μl of the respective drug concentrations for a period of 24 h and 72 h.

6.3.4 Bacterial Activity *In vitro*

6.3.4.1 Effect of Vancomycin on Staphylococcus epidermidis

The data from the liquid bacterial culture (*S.epidermidis* data as shown in Figure 6.6, demonstrated that the antibacterial function of vancomycin lasted for almost the complete 2 weeks, except at day 3 and 5, when partial inhibition of bacterial growth was observed (14.37% and 34.89% inhibition respectively). Average inhibition of 85% was observed for the release samples at other time points, suggesting vancomycin has a good

antibacterial activity on *S. epidermidis*. There was a significant difference ($p<0.05$) in the OD_{600} at 24 h between the prior mentioned release samples and the control, which consists of media with 100 µl of PBS. It can be understood that the release concentrations between 16-30 µg/ml is not adequate to completely inhibit their growth. These results also indicated that encapsulation of vancomycin in chitosan-TPP microparticles not only controlled the release rate and prolonged its release duration, but also retains its antibacterial activity.
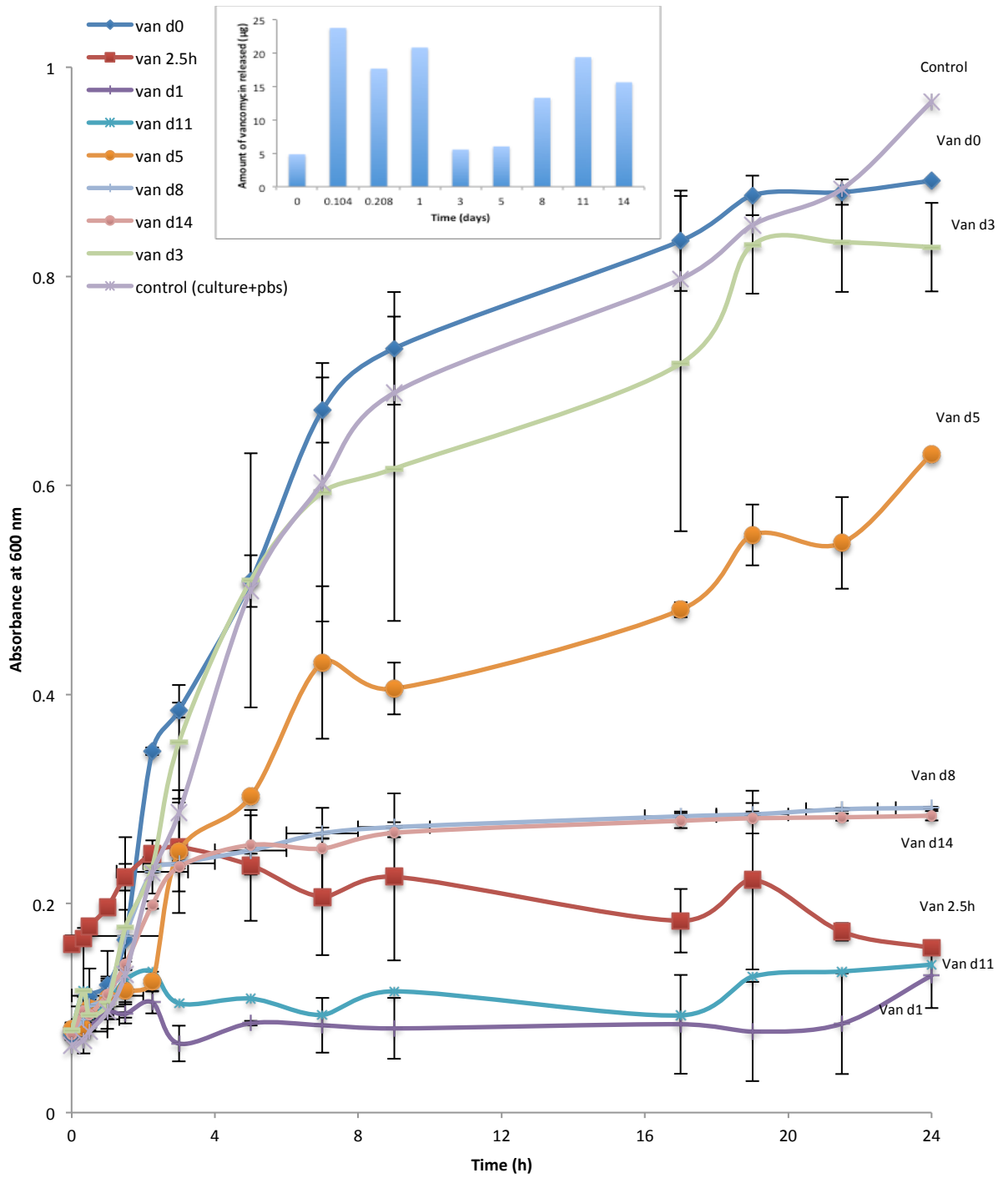
Figure 6.6: Growth curve of *Staphylococcus epidermidis* in presence of vancomycin release samples collected at various time points (n=3).

6.3.4.2 Effect of Cefazolin on Staphylococcus epidermidis

The amount of cefazolin released at the time points mentioned in Figure 6.7 is the difference in the drug released between the two time points. This is because the method of sample collection for drug release was to collect the entire PBS in the vial and replace it with fresh amount of PBS. This approach for bacterial study is comparable with what happens *in vivo,* as the drug released on day 1, would have dispersed from the defect site in some period of time.

Antibacterial study demonstrated that the cefazolin released from the microparticles can inhibit the growth of S. epidermidis completely during the study period. An average inhibition rate of 94% was observed for the release samples till day 5 and later an average inhibition rate of 72% was observed. The later inhibition rate corresponds to a cefazolin concentration of around 20 µg/ml.

The release profile of vancomycin from coated microparticles is similar to that of cefazolin (Figure 6.7), but the amount of vancomycin encapsulated is higher than cefazolin. This decision was based on the MIC of cefazolin (1 mg/L) and vancomycin (8-16 µg/ml).
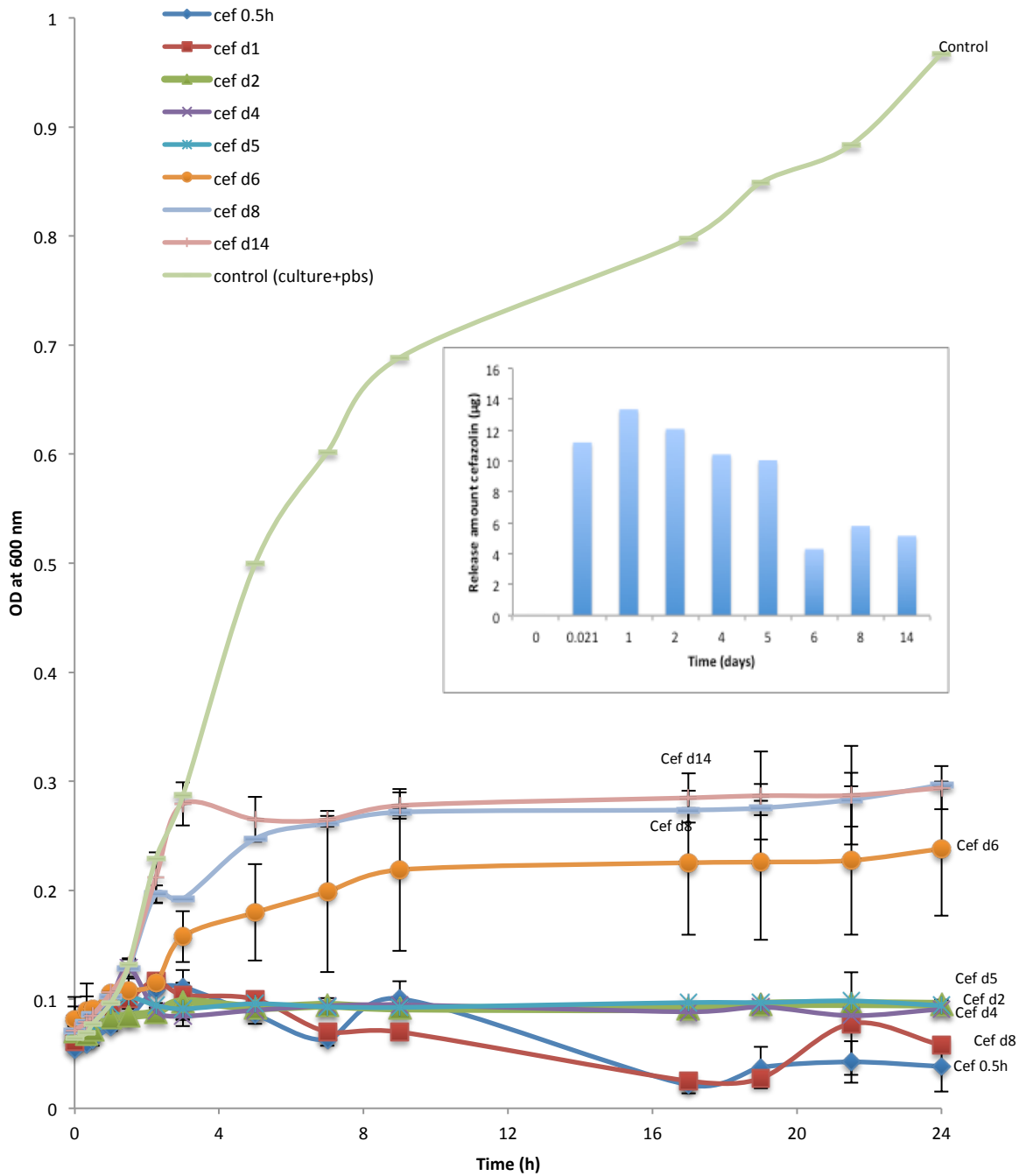
Figure 6.7: Growth curve of *Staphylococcus epidermidis* plotted over a period of 24h in presence of cefazolin release samples collected at various time points (n=3).

6.4 Discussion

The main objective of this study was to incorporate vancomycin and cefazolin into chitosan-TPP microparticles along with growth factor BMP-7, to release them in controlled manner, and to retain the antibacterial activity. The main justification of the antibiotics we chose was to address the most commonly used antibiotics in clinical practice today, delivered either systemically or locally. Our lab has been involved in developing novel chitosan based scaffolds capable of delivering growth factors for bone regeneration. Since chitosan-TPP microparticles were prepared using coacervation procedure, it was easy to entrap hydrophilic small molecules of vancomycin and cefazolin into the microparticles by both the processes (encapsulation and coating procedure). High encapsulation efficiencies (Table 6.1) were obtained in this study in comparison with other studies where water-in-oil-in water (w/o/w) double emulsion procedures were used, wherein it is difficult to achieve high encapsulation efficiency since the drug has high solubility in the external phase and it is easy for majority of the drug to diffuse to the external phase during emulsion and solvent evaporation process [249]. The drugs were incorporated in two ways- encapsulation and coating (adsorption) to determine their influence on the release profiles of both the drugs. We observed a similar trend in all the release studies-cefazolin, vancomycin and BMP-7; when these molecules were encapsulated, an average release of about 50% was observed by the end of 2 weeks and minimum burst initial burst release (15-20%) was observed. In contrast, when these molecules are coated onto the microparticles (by the process of adsorption), we observed a burst initial release of about 50% by day 1 and by the end of 2 weeks period nearly 95% of the adsorbed protein was released. This huge difference in the

release patterns can be attributed to the larger travel distance for the encapsulated drug to diffuse out of the microparticle, resulting in lower burst release during the early stages of release study. Also, since the viscosity of the chitosan solution is high, it reduced the diffusion of drug to the outer surface as a result least amount of drug was found on or near the surface of the microparticle, in contrast to the drug coated microparticles, where most of the drug was incorporated near to the outer surface, resulting in the burst release [250].

In order to eradicate infection in bone and joints, it is essential to maintain antibiotics at the therapeutic concentration at the implantation site for an extended period of time. Parenteral administration of antibiotics is unsuccessful in the treatment of bone infections because of the insufficient local penetration of systemic administration. Traditionally, osteomyelitis has been treated with parenteral antibiotics for a period of 4-6 weeks after surgery. The high doses of systemic antibiotics above the minimum inhibitory concentration required at fracture site cause systemic toxicity [251,252]. Studies have shown that more than 80% of vancomycin is excreted unchanged in urine within 24 h after administration and cefazolin's half-life is found to be approximately 4 h after IV injection [253]. Even after an intra-articular (IA) injection, half-life of the delivered vancomycin was just over three hours, and the therapeutic level was maintained for 24 h in the joint serum [254]. Therefore, it can be advocated that local antibiotic administration continuously and in a controlled fashion from a biodegradable scaffold will avoid risk of systemic toxicity and act as a prophylaxis measure against bone infections during the surgery. But it has also been found that high concentration of drugs inhibits the bone healing activity [255]. Our day 3 experiment of osteoblasts proliferation

in presence of antibiotics and BMP-7 suggests that cefazolin concentration of 50 µg/ml and 100 µg/ml did not significantly change the cell number in comparison with controls and also the presence of BMP-7 improved cell proliferation. This result indicates that cefazolin concentrations used are not toxic to osteoblasts and they also do not inhibit the activity of BMP-7. Our results are in agreement with other studies, which showed that at a concentration of 200 µg/ml cefazolin, they start to become toxic to osteoblasts, decreasing the cell number by >75% [256,257]. Figure 6.5 also indicates an increase in the cell proliferation in cefazolin concentration of 50 µg/ml and 100 µg/ml and BMP-7 in comparison with BMP-7 containing wells. This indicates that cefazolin itself improves osteoblast viability and proliferation. This observation is also in support with another study, which observed an increase in the ALP activity in presence of cephalosporins [258,259]. On the other hand, vancomycin concentration of 1000 µg/ml was found to be toxic to OB-6 cell line, even in presence of BMP-7, which indicates its toxicity [260]. Although others reported positive effects of vancomycin on osteoblasts until 2000 µg/ml [261], our observation clearly indicates a significant decrease (p<0.001) in cell number in comparison with controls. Vancomycin belongs to glycopeptide family of drugs and cefazolin belongs to cephalosporin family and have indicated that there is a difference in with regards to their effect on cell viability and osteogenic potential.

Antibiotic loaded microparticles, antibiotics coated spacers and antibiotic coated implants may reduce infection, but they do little to improve bone regeneration, therefore, we studied the dual release of the drugs and growth factor to simultaneously promote bone growth and prevent infection. The cell proliferation experiment along with the release study supports our results that the released BMP-7 is active and unaffected by the

presence of drugs. Also, the drug release profiles in the presence of BMP-7 were similar to drug release alone, suggesting that no interaction occurred between drugs and growth factor. Since both the growth factors and drugs were encapsulated into the microparticles, controlled release was observed, with about 50% cumulative release over the period of 2 weeks. Almost steady amount of drug is released over this period of time, minimizing peak/trough fluctuations, while maximizing the amount of time the drug concentrations remain at therapeutic levels. The justification for our choice of drug concentration to be incorporated were influenced from the osteoblasts viability experiment, where we concluded that cefazolin concentration less than 100 μg/ml supported osteoblasts proliferation and vancomycin concentration less than 500 μg/ml would be beneficial for their growth. The concentration of drugs incorporated into the microparticles were chosen such that the release concentration at any time point did not exceed those limits and in our release study we found that for drug encapsulated microparticles, the maximum release was 70 μg/ml and 120 μg/ml of cefazolin and vancomycin respectively.

The antimicrobial experiment demonstrated the biological function of vancomycin and cefazolin released from the chitosan-TPP microparticles for over a period of 2 weeks. In both the experiments, only about 50% of the total encapsulated drug is released and in that period, it was observed that cefazolin could inhibit bacterial growth to a greater extent (~85%) at lower concentrations in comparison with vancomycin (~80%). Minimum inhibitory concentration for vancomycin was found to be around 24 μg/ml, which is in agreement with other studies [262]. While the chitosan-TPP microparticles

along with BMP-7 encapsulated may promote bone tissue regeneration, the vancomycin and cefazolin encapsulated in the scaffold will protect the tissue from microbial invasion.

This work has shown the capability of the chitosan-TPP microparticles to deliver bioactive and stable drugs in a controlled fashion over a prolonged period of time. The study also demonstrated that the amount of drugs incorporated should be optimized in order to inhibit bacterial growth and at the same time not negatively influence osteoblasts proliferation and activity.

Chapter 7

Influence of Chitosan Microparticles in Healing Critical Sized Defects in Rat Femur

7.1 Material

Chitosan (85% deacetylated), sodium tripolyphosphate (TPP), acetic acid, and PBS were purchased from Sigma Chemicals, bone morphogenetic protein 7 (BMP-7) was purchased from Peprotech, 10% formalin and decalcification solution, Cal-Ex 11 was obtained from Fisher Scientific.

7.2. Methods

7.2.1 Fabrication of Chitosan Microparticles

Microparticles were prepared by coacervation method. In this method, 2% chitosan was prepared by dissolving in acetic acid (1% v/v) at room temperature. The mixture was passed through a nylon mesh to remove insoluble substances. This mixture was then added drop wise to 50% sodium tri-polyphosphate (TPP) solution kept on ice-bath. The

microparticles were allowed to cross-link overnight and then were air-dried. BMP-7 was dissolved in water to an appropriate concentration and was added to the chitosan solution to encapsulate the growth factor. In order to coat the microparticles with BMP-7, the same amount was added to 7 mg of microparticles.

7.2.2 Surgical Procedure

Three different groups of microparticles were tested to observe their effect on bone regeneration. Chitosan microparticles without any growth factors, BMP-7 encapsulated microparticles and BMP-7 coated microparticles were used. Prior to the surgery, they were packed in 1 ml syringes along with very small amount of saline. These microparticles were sterilized using gamma radiation for 5 minutes at 1358.5 rads.

Inbred male Lewis rats, 8 weeks old, weighing between 240-290 g, were used as experimental animals. The protocol was approved by The University of Toledo Institutional Animal Care and Use Committee (IACUC, Approval no: 105818) and national guidelines for care and use of laboratory animals was followed.

Surgery was performed under general inhalation anesthesia containing isofluorane and oxygen that was induced using a constant volume ventilator. Initially to anesthetize the animal, a dosage rate of 3% was used and later during the surgery a rate of 1.5% was used. In order to minimize the postoperative pain, animals were given subcutaneous buprenorphine (0.5 mg/kg body weight) just prior to the surgery and to reduce the postoperative infection risk, antibiotic penicillin G procaine (40,000 U/kg) was injected intramuscularly 12-24 h before surgery. The surgical site was shaved and disinfected first with 70% isopropyl alcohol followed by solutions of benedine and betadine. A lateral

approach was used to expose the right femoral diaphysis. After the exposure of the mid shaft region of the femur, a 4-5 mm hole was drilled through one of the cortex using orthopedic microdrill. Low rotational drill speeds were used to make a hole through one of the posterior cortex to reach the bone marrow, until the marrow came through the defect site and constant physiological saline irrigation was used to remove any bone debris formed during drilling. The microparticles prepared prior to surgery were then injected into the defect site. Defects without any filling were used as controls to compare the natural bone formation versus scaffold induced bone formation. After injecting the material, the soft tissues and skin was closed layer-by-layer using absorbable suture.

Each type of microparticle was implanted in 10 animals. Thus for 4 groups (including control) and two time points, a total of 80 animals were used in this study. At 6 and 12 weeks postoperation, rats were anesthetized using over dose of kedamine (80 mg/kg) and xylazine (10 mg/kg). After anesthetizing the animals, they were subjected to cardiac perfusion with saline, followed by a 10% formalin flush. Later, the femur was harvested for evaluation and drop-fixed in 10% formalin. Fixative volume was around 20 times that of tissue on a weight per volume.

7.2.3 Methods of Evaluation of Regenerated Bone

7.2.3.1 Histological Procedures

After keeping the tissue in 10% formalin for 24 h, the tissues were transferred to 70% ethyl alcohol and later were put in decalcifying solution containing 7.4% formaldehyde, 10.6% formic acid and less than 1% methyl alcohol for 5-7 days, before sectioning the tissue. Samples were embedded in liquid paraffin and cut into 5 μm thick sections and

fixed on microscopy slides for further analysis. The sections were stained with hematoxylin and eosin (H&E) and observed using a Leica DMLB microscope (Leica Microsystems, IL). For H&E staining, the slides were treated with xylene for 1 minute followed by a series of dehydration in 100%, 95% and 70% ethanol for 5 min each. After dehydration, they were treated in hematoxylin stain for 3 minutes. The stained samples were rinsed in water. This was followed by acid alcohol and ammonia treatment, followed by 70% ethanol treatment for 2 minutes. Next the slides were dipped in eosin stain for 15 seconds, followed by 95% and 100% ethanol treatment. Finally the slides were treated with xylene for 5 minutes and then the slides were dried thoroughly before viewing under Olympus light microscope.

7.2.3.2 μ-CT Analysis

Samples were firmly positioned in the sample holder using low-density foam. In order to obtain highest contrast between the specimen and the surrounding medium, air was used as the scanning medium for all the samples. The fixed scaffolds were scanned with a high-resolution μ-CT scanner (μCT 35, Scanco Medical AG) at 70 kVp. Beam hardening of the X-ray was reduced by placing a beam-flattening filter in the X-ray path to narrow the energy spectrum. Signal-to-noise ratio (SNR) and scanning time had to be optimized to obtain good voxel information; therefore a tube current of 114 μA was used with an integration time of 100 ms per projection. The tradeoff between voxel size and scan time was also carefully considered in order to analyze the newly formed bone in rat and an isotropic voxel size of 12 μm was used for scanning all the bones. Region of interest (ROI) exceeding defect boundaries was used for scanning purposes (includes newly formed bone as well as old bone) and is approximately 20% of bone length.

The standard method of quantitatively describing bone architecture is the calculation of morphometric indices. Measurements such as bone volume fraction, specific bone surface, porosity of new bone, thickness of new bone fragments, spacing between newly formed bone fragments and number of new bone fragments were calculated using a preprogrammed algorithm to determine trabecular bone morphometry. But prior to computing the values of each of these outcome measures, a Gaussian filter (sigma=0.8, support=1.0) was applied for noise reduction. The basic morphometric indices like bone volume (BV), and tissue volume (TV) are derived from simple voxel counting method, while bone surface (BS), which is another basic measure, is conventionally computed using a marching-cube algorithm. 3D calculations for thickness and spacing were determined by sphere fitting method, where for thickness measurements, spheres are fitted into the object and for separation; the spheres are fitted to the background. Another index - porosity, was used to characterize the redundancy of trabecular connections. In order to determine all the above-mentioned parameters, contours were manually drawn carefully around the newly formed bone based on the visible threshold difference between the old and the new bone for all the groups. This threshold was carefully determined based on visual inspection of tomograms of regular cortical bone. Voxels above the threshold value of 289 and below 1000 were collected and the segmented bone was reconstructed for measurements.

7.2.3.3 Multiphoton Second Harmonic Generation

Multiphoton second harmonic generation (SHG) imaging is based on the process of frequency doubling by which two near-infrared photons are converted into a single photon with exactly twice as much energy as the input photons. SHG signals arise due to

interaction with anisotropic molecules, which in biological imaging, is most often present in collagen. Collagen being an important part of new bone formation can be analyzed using this technique. We used Leica TCS SP5 laser scanning confocal microscopy (Leica Microsystems, Bannockburn, IL) equipped with a Ti-sapphire tunable multi-photon laser (Coherent, Santa Clara, CA). SHG for collagen was optimally imaged using 860 nm excitation (MP laser) for maximum efficiency and emission collection was in the range of 425-435 nm with a peak emission generated at 430 nm. H&E stained slides were used for imaging. The images obtained were analyzed using ImageJ 1.48j version software (NIH). During this analysis, collagen images were thresholded to precisely match the collagen outline and converted to binary image for measurement. Three collagen attributes were acquired: total collagen area, collagen bundled area and collagen bundled area/total collagen area. Following an initial blind coded evaluation of 35 images, it was determined that an area of 3500 μm^2 was the minimum criterion for a collagen collection to be considered a collagen bundle. Accordingly, in each image, collagen bundle area with an area of atleast 3500 μm^2 was summed to determine collagen bundled area of the entire image. The collagen bundle area was divided by the total collagen area to determine the relative amount of collagen bundling. For each group, n=15 images were processed.

7.2.4 Statistical Analysis

All statistical analyses were performed using SPSS software (IBM Corporation, Somers, NY, USA). A student T-test was applied for comparison of the groups at different implantation periods. Significant differences between the groups were determined using ANOVA's Tukey's Honest Significant Difference (HSD) test. The relationship between

various parameters determined in this study was calculated by Pearson's regression coefficient. Results were considered significantly different if p<0.05, unless otherwise mentioned.

7.3. Results

7.3.1 Characterization of the Microparticles

Chitosan-TPP microparticles displayed a round and groovy surface morphology. The size of the microparticles obtained for a batch had less variation (Fig. 1b) and had an average diameter of 700 μm. The microparticles obtained by this method of cross-linking were found to have an internal less dense structure, which is advantageous in terms of growth factor delivery and degradation process. In order to incorporate BMP-7 into the microparticles, below room temperatures were employed to ensure structural and functional integrity of BMP-7.

7.3.2 Clinical Observations

All the 80 rats, which were operated exhibited good health and showed no complications throughout the study period. At the end of the postoperative time periods, i.e. 6 and 12 weeks, all the 80 femurs were harvested and no visual signs of visual adverse tissue responses or inflammatory response were observed. In some of the animals, we could observe that some microparticles had dispersed into the nearby muscle tissue, but for almost all the groups, there were a good number of animals, which had the microparticles at the defect site (Figure 7.1).
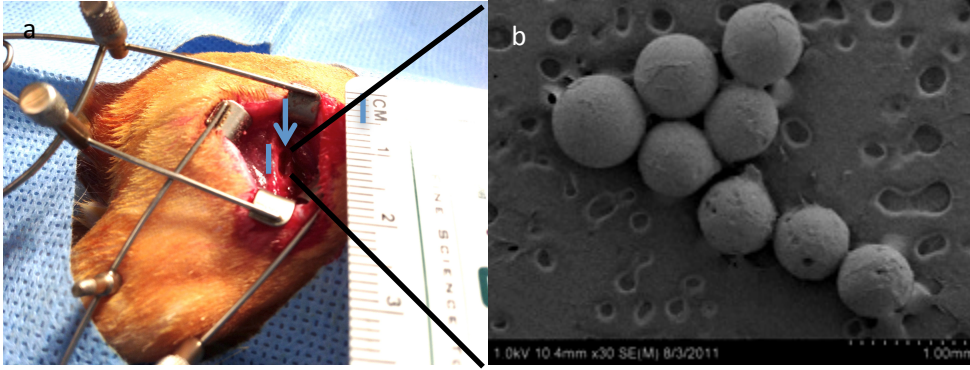
Figure 7.1: (a) The surgical procedure showing a 4-5 mm defect in diaphysial region of femur, which was implanted with chitosan-TPP microparticles (b) SEM image of chitosan-TPP microparticles.

7.3.3 Histology Observations

7.3.3.1. Controls

At 6 weeks, in controls, a number of marrow filled cavities were observed around which new bone was being formed (Figure 7.2a,b). Lining those cavities, we could observe active cuboidal osteoblasts forming new bone. In some of the spaces, multinucleated giant osteoclasts were also observed, suggesting active remodeling. Fibrous connective tissue/granulation tissue was also observed along the edges of the newly formed bone, which would later be mineralized to form woven bone. Lacunae were observed which had osteocytes. These cells can be seen very randomly arranged and in higher population suggesting that the Figure 7.2a,b indicates the newly formed woven bone, which still needs remodeling. Figure 7.2a also suggests intramembranous healing process, where a primary ossification center in first formed by the mesenchymal stem cells in the bone marrow, which later start secreting osteoid and are so differentiated into osteoblasts, which start laying down the woven form of bone, indicated in figure 7.2b by the small

circular woven structure in the center of the marrow cavity. Figure 7.2b also shows newly formed osteocytes, lying side by side, in the newly formed bone region, which will gradually be separated as more bone forms and as remodeling occurs.

At 12 weeks, the number of marrow cavities and their size had dramatically reduced (Figure 7.2c). We could still observe fibrous connective tissue/granulation tissue with fibroblasts, indicating active healing process. At the edges along the woven bone, we can observe active osteoblasts laying down bone (Figure 7.2d). Well-developed blood vessels can be seen in the newly formed bone region. Osteoclasts were also observed in the small marrow cavities remodeling the bone.
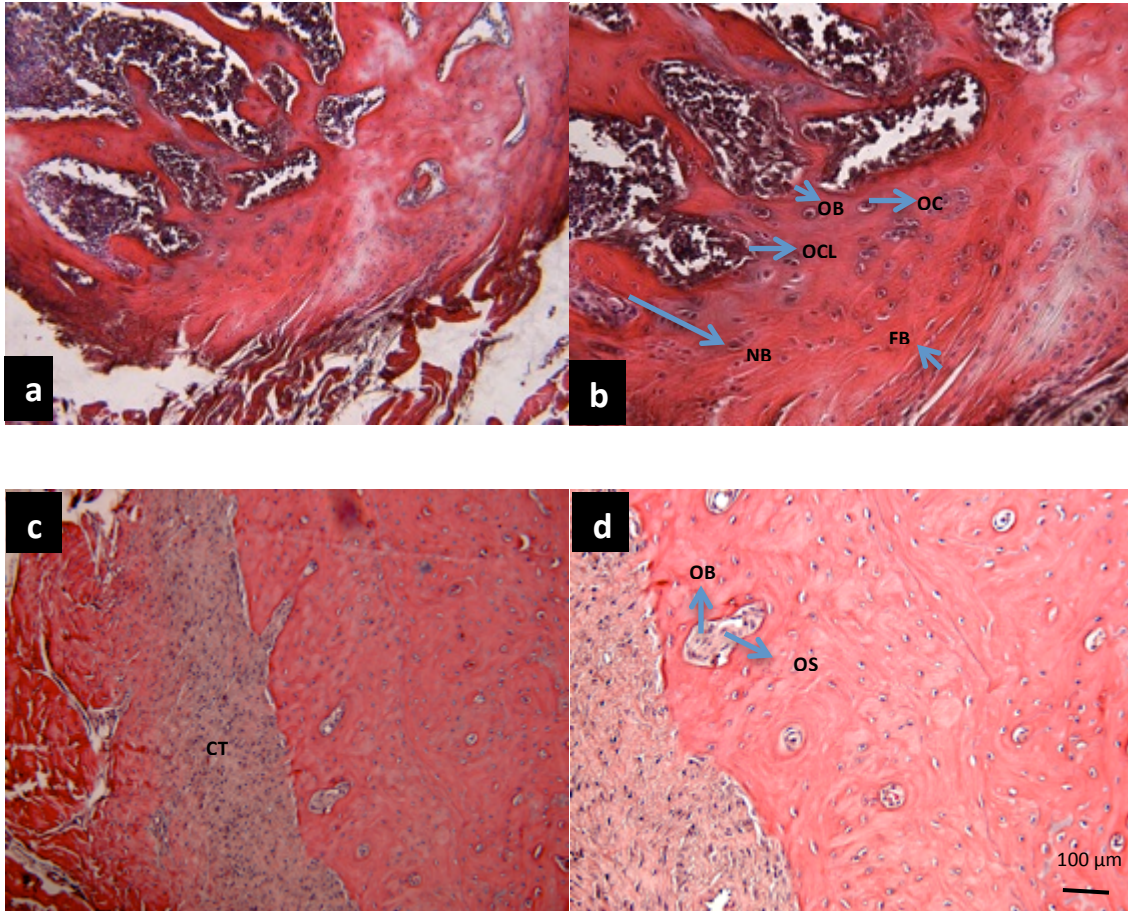
Figure 7.2: Microscopic images of transverse sections (H&E) of rat femur, where a defect was created but was not implanted with any material (controls). The defect site indicates formation of granulation tissue and new woven bone formation a,b) at 6 weeks post-implantation - 10X and 20X magnification respectively c,d) at 12 weeks post-implantation - 10X and 20X magnification respectively. CT, connective tissue; FB, fibroblasts; NB, new bone; OB, osteoblasts; OC, osteocytes; OCL, osteoclasts; OS, osteoid (Scale bar represents 100 µm).

7.3.3.2 Microparticles without Growth Factor

At 6 weeks, the microparticles appeared intact with no degradation. Inflammatory response was found confined only to the region around the microparticles. Newly formed bone tissue was found in close proximity, around and in between microparticles. Active cuboidal osteoblasts were found on the uneven surfaces of the newly forming bone. Blood vessels were formed in the new bone region. Fibrous tissue was found confined to the tissue- microparticle interface, which is consistent with postoperative changes (Figure 7.3a,b). Loose granular-filamentous structure, containing collagen fibrils and fibroblasts is also found in-between microparticles. The morphological appearance of the newly formed bone was similar to the control and no necrotic tissue was observed indicating biocompatibility of the microparticles.

At 12 weeks, the microparticles were still found to be intact, with lesser inflammatory response found around its perimeter (Figure 7.3c,d). Fibrous tissue was confined to the implant-tissue interface. Overall thickness of the newly formed woven bone adjacent to the microparticle appeared to have increased at 12 weeks postoperatively. Blood vessel infiltration was also observed in newly formed bone region.
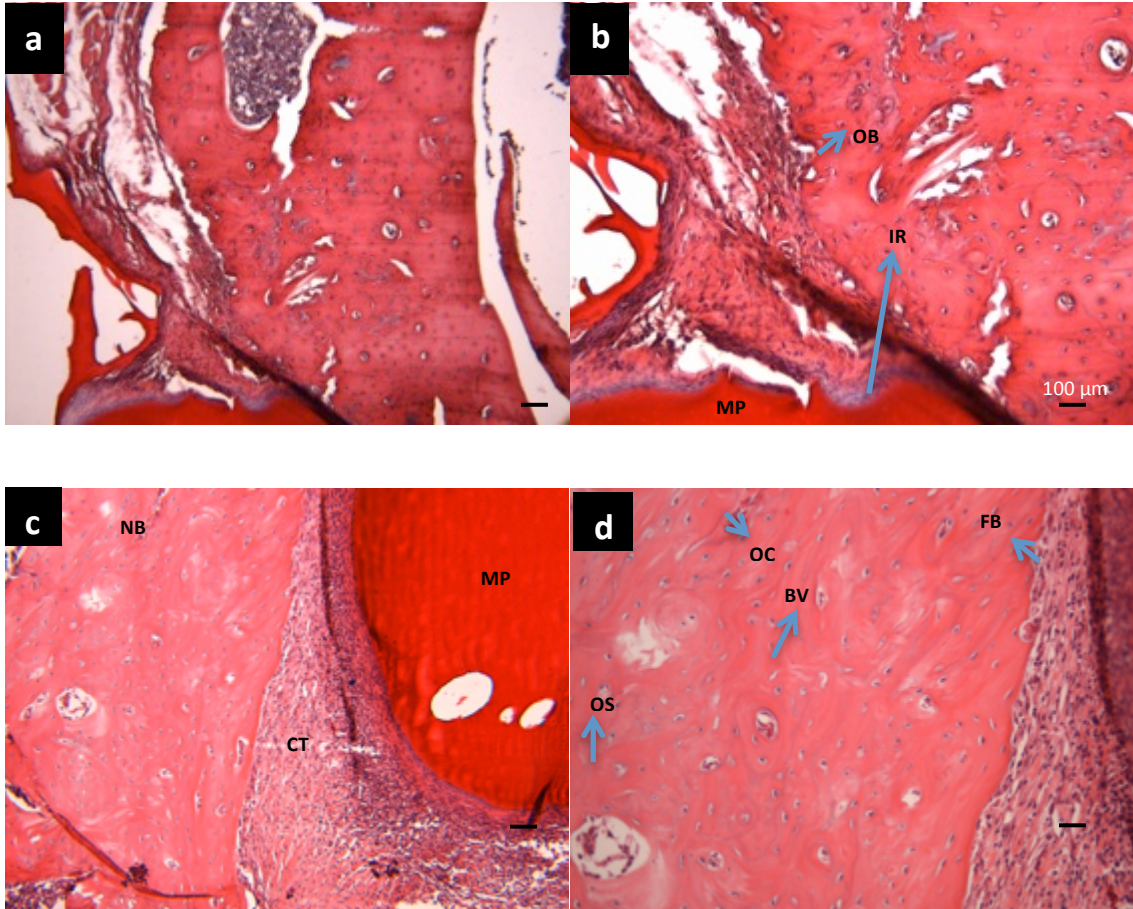
Figure 7.3: Microscopic images of transverse sections (H&E) of rat femur, where a defect was created and implanted with chitosan-TPP microparticles. The defect site indicates formation of granulation tissue and new woven bone formation, with very little inflammatory response around the implanted biomaterial a,b) at 6 weeks post-implantation - 10X and 20X magnification respectively c,d) at 12 weeks post-implantation - 10X and 20X magnification respectively. CT, connective tissue; FB, fibroblasts; MP, microparticle; NB, new bone; OB, osteoblasts; OC, osteocytes; OCL, osteoclasts; OS, osteoid; IR, inflammatory response; BV, blood vessel (Scale bar represents 100 µm).

7.3.3.3 BMP-7 Coated Microparticles

H&E staining images for 6 weeks indicated that microparticles were intact with no degradation (Figure 7.4a,b). Inflammatory response was found surrounding the microparticles. By carefully viewing all the related images, we found that the imflammatory response in BMP-7 coated microparticles was more in comparsion with microparticles without growth factor. There were huge marrow-filled cavities around which new bone was forming. In the marrow cavity itself, at 6 weeks we could see osteoid being laid down by the differentiated osteoblasts. There were osteoblasts that lined the newly forming bone from the endochondral side as well as periosteal side laying the bone.

At 12 weeks, we could observe that the microparticle had started to degrade. We could observe foreign body response around the microparticle and fibrous tissue was also observed associated with the microparticle. The inflammatory cells were also found small gaps between the microparticles. From figure 7.4c,d, we could notice that the new bone was forming adhered to the microparticle and there was new blood vessel growth in that region. The newly formed bone around the microparticle appeared tighter without interposition of fibrous tissue. Also, in close proximity from the degraded microparticle, we could observe a number of comparatively larger regions of woven bone formation.
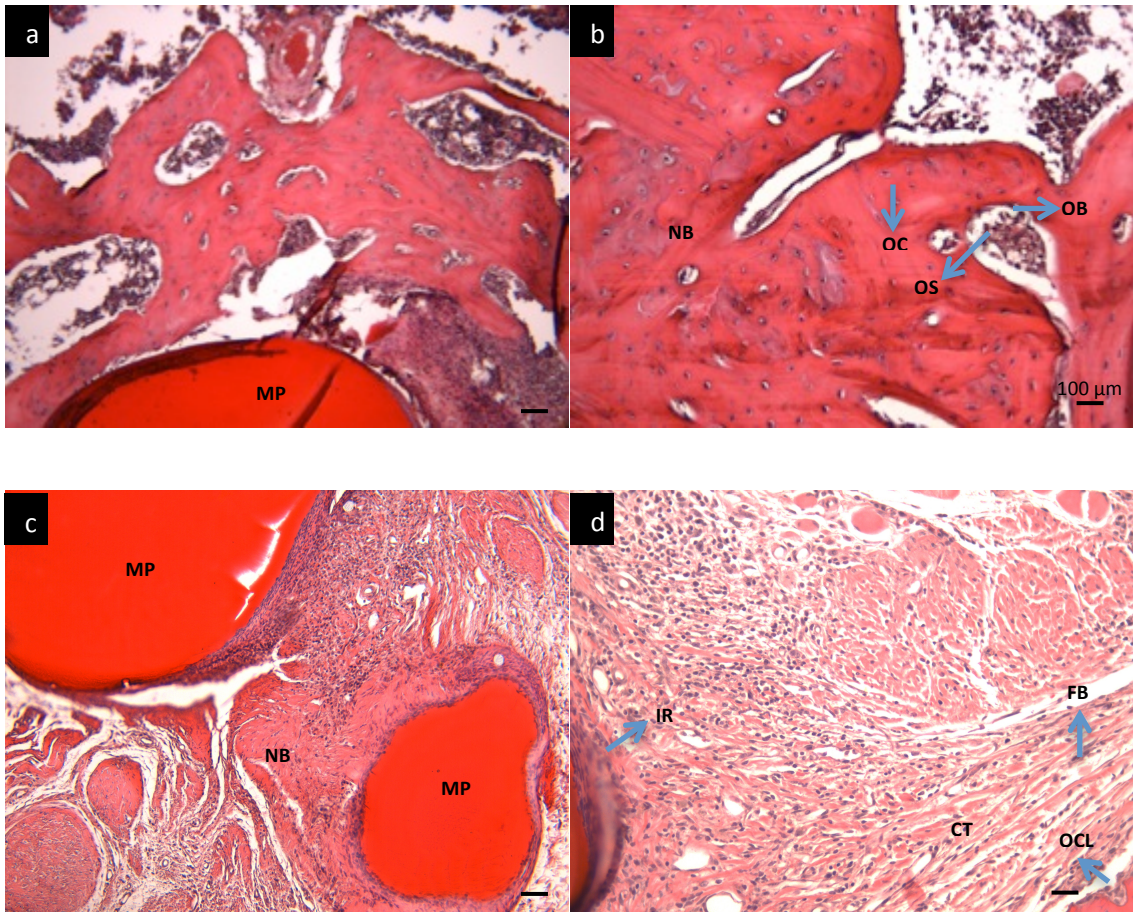
Figure 7.4: Microscopic images of transverse sections (H&E) of rat femur, where a defect was created and implanted with BMP-7 coated chitosan-TPP microparticles. The defect site indicates formation of granulation tissue and new woven bone formation in close proximity to the microparticles a,b) at 6 weeks post-implantation - 10X and 20X magnification respectively c,d) at 12 weeks post-implantation - 10X and 20X magnification respectively, where the left (10X) image indicates degraded microparticle. CT, connective tissue; FB, fibroblasts; MP, microparticle; NB, new bone; OB, osteoblasts; OCL, osteoclasts; OS, osteoid; IR, inflammatory response (Scale bar represents 100 μm).

7.3.3.4 BMP-7 Encapsulated Microparticles

6 weeks results indicates inflammatory response around the microparticle (Figure 7.5a,b). Similar to the BMP-7 coated microparticles; the inflammatory response was greater in comparison to microparticles without growth factor. We can also observe the formation of fibrous tissue at the interface of tissue and microaprticles. But near the surface of the newly forming bone, we could observe active osteoblasts. In some regions adjacent to the microparticle, we could observe bone tissue development. The marrow cavities appeared to be smaller in comparison with microparticles and lot of woven bone growth was observed at the defect site. Other morphometric features were common for all the groups.

12 weeks microscopic images indicated that there was foreign body response seen around the microparticle. Figure 7.5c,d indicate that the inflammatory cells, were penetrating the microparticle at 12 weeks. Similar to other groups, we could observe active osteoblasts laying down bone on the newly formed uneven woven bone surface. Osteocytes were randomly arranged in the new woven bone indicating that remodeling is going on. Blood vessels growth was observed in the newly formed bone region as well as the fibrous tissue region.
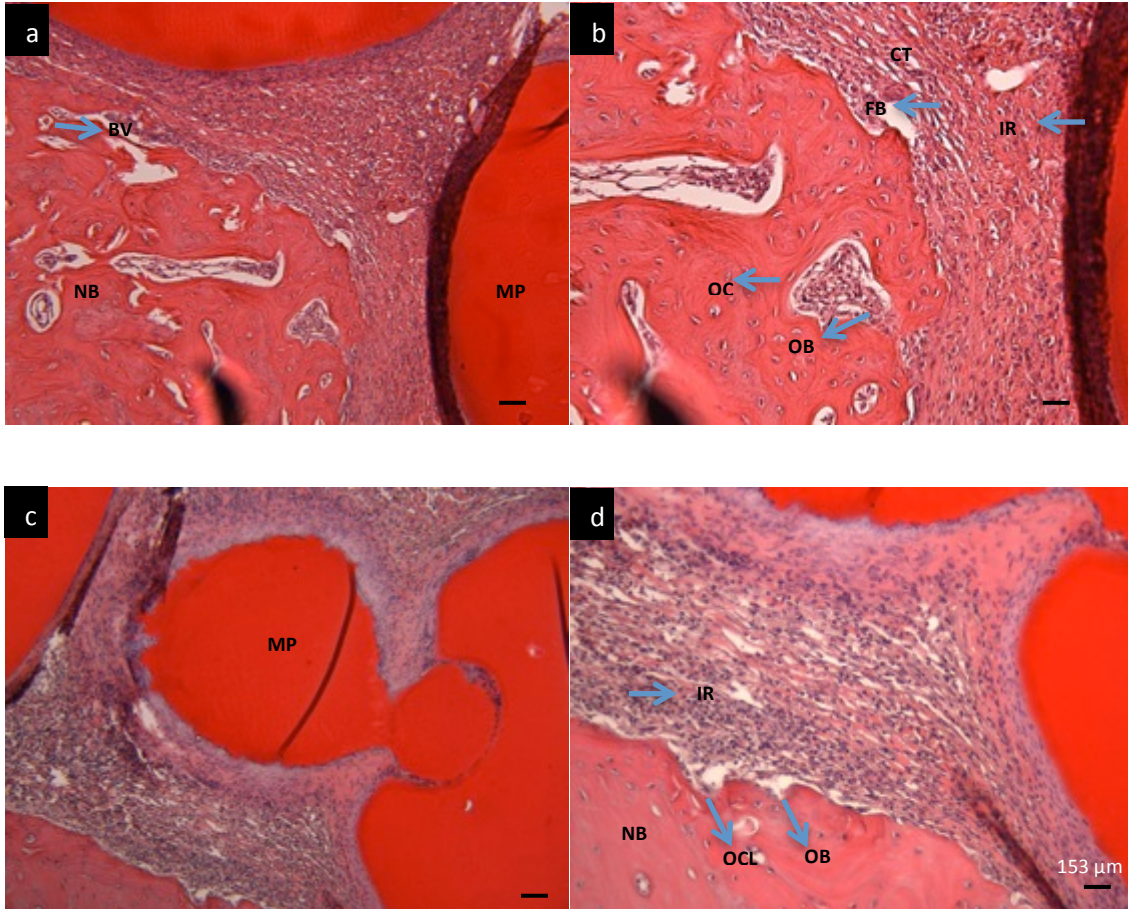
Figure 7.5: Microscopic images of transverse sections (H&E) of rat femur, where a defect was created and implanted with BMP-7 encapsulated chitosan-TPP microparticles. The defect site indicates formation of granulation tissue and new woven bone formation in close proximity to the microparticles a,b) BMP-7 encapsulated chitosan-TPP microparticles at 6 weeks post-implantation - 10X and 20X magnification respectively c,d) BMP-7 encapsulated chitosan-TPP microparticles at 12 weeks post-implantation - 10X and 20X magnification respectively. CT, connective tissue; FB, fibroblasts; MP, microparticle; NB, new bone; OB, osteoblasts; OC, osteocytes; OCL, osteoclasts; OS, osteoid; IR, inflammatory response; BV, blood vessel (Scale bar represents 100 μm).

7.3.4 µ-CT Analysis

7.3.4.1 Bone Volume Fraction

At 6 weeks, bone volume fraction (BV/TV) in controls with defect (n=10) averaged 0.58±0.08, for microparticles without growth factor (n=10) it averaged 0.42±0.07, for BMP-7 coated microparticles (n=10), the average is 0.38±0.10 and for BMP-7 encapsulated microparticles (n=10), the average is 0.37±0.08. Statistical analysis indicated a significant increase (p<0.001) in the BV/TV ratio in controls, in comparison with microparticles containing groups (with and without growth factors), also no significant difference is found in BMP-7 present and absent microparticles (Figure 7.6a).

At 12 weeks, BV/TV ratio for controls (n=10) is 0.58±0.05 and showed no significant increase (p>0.05) from 6 weeks. For other groups-microparticles without growth factor (n=10), the ratio is 0.51±0.08, BMP-7 coated microparticles (n=10), it is -0.48±0.06 and for BMP-7 encapsulated microparticles, it is 0.46±0.08 and these values indicate that BV/TV significantly increased in comparison with 6 weeks. There is also a significant increase (p<0.05) observed between the controls and the microparticles containing groups, but no significant difference was observed between microparticles and BMP-7 containing microparticles. The ratio of BV/TV was found to be 0.998 for controls with no defect (Figure 7.6b).

7.3.4.2 Porosity of Newly formed Bone (mm^{-3})

At 6 weeks, a significant difference (p<0.001) was observed in the porosity between the controls and microparticles containing groups (Figure 7.6c). The controls (n=10) averaged 85.88±20.73, the microparticles (n=10) average 204.92±69.25, BMP-7 coated

microparticles average to 203.31±79.78 and BMP-7 encapsulated average to 194.85±65.58. There was no significant difference observed between microparticles and BMP-7 containing microparticles.

At 12 weeks, there was a significant decrease ($p < 0.001$) in porosity in comparison with its values at 6 weeks. Also, there was a significant difference ($p < 0.05$) observed between the controls (n=10), which showed an average of 30.90±13.25 and the microparticles containing groups-where microparticles indicated an average of 50.19±19.84, BMP-7 coated microparticles have an average of 54.30±28.05 and BMP-7 encapsulated microparticles had an average of 54.43±24.11. There was no significant difference observed between the BMP-7 containing microparticles and microparticles without any growth factors (Figure 7.6d).

7.3.4.3 Bone Surface Density (mm^{-1})

At 6 weeks, BS/BV ratio for controls (n=10) averaged 15.81±2.51 and this was significantly less ($p < 0.001$) than the microparticles containing groups, where microparticles (n=10) showed an average of 21.54±2.29, BMP-7 coated averaged (n=10) 23.47±5.33 and BMP-7 encapsulated (n=10) averaged 24.46±8.12. Statistical analysis indicated that there is no significant difference ($p > 0.05$) between microparticles and BMP-7 containing microparticles (Figure 7.6e).

However, at 12 weeks, there is no significant difference observed between the four groups, but in comparison with 6 weeks there is a significant decrease ($p < 0.05$) in the bone surface density (Figure 7.6f), with controls showing an average of 12.15±1.69, microparticles with an average of 11.79±1.97, BMP-7 coated microparticles indicating

about 12.75$\pm$1.64 and BMP-7 encapsulated microparticles showing an average BS/BV ratio of 12.21$\pm$1.62.

7.3.4.4 Newly formed Bone Fragments Analysis

Number of newly formed bone fragments (1/mm) at 6 weeks was averaged to be 7.52$\pm$0.51 for controls (n=10), 6.41$\pm$2.43 in microparticles group (n=10), 6.53$\pm$2.90 in BMP-7 coated microparticles (n=10) and 4.89$\pm$3.14 in BMP-7 encapsulated microparticles (n=10) (Figure 7.6g). But a decrease in bone fragments was observed at 12 weeks, controls showed an average of 5.71$\pm$0.49, microparticles averaged 6.21$\pm$1.62, BMP-7 coated microparticles averaged 5.01$\pm$2.32 and -7 encapsulated microparticles had an average of 5.59$\pm$2.29 trabecular number. At 6 and 12 weeks there was no significant difference observed in the trabecular number (mm^{-1}) between controls (n=10) and microparticles containing groups (n=10), although there was a significant decrease ($p<0.001$) observed in the trabecular number from 6 weeks to 12 weeks in controls (Figure 7.6h).

Newly formed bone fragment thickness (mm) comparison indicated a significant difference ($p<0.001$) between controls and microparticle groups at 6 weeks (Figure 7.6i). Controls (n=10) averaged 0.12$\pm$0.01, whereas microparticles (n=10) had an average of 0.10$\pm$0.01, BMP-7 coated microparticles (n=10) had an average of 0.1$\pm$0.01 and BMP-7 encapsulated microparticles (n=10) had an average of 0.1$\pm$0.005. There is no significant difference observed between microparticles and BMP-7 containing microparticles. At 12 weeks also, a significant difference ($p<0.05$) was observed between controls and microparticles containing groups. Controls had an average of 0.19$\pm$0.02; while microparticles averaged to 0.17$\pm$0.02, BMP-7 coated microparticles averaged to

0.16 ± 0.02 and BMP-7 encapsulated microparticles averaged to 0.16 ± 0.02. There was no significant difference observed between microparticles and BMP-7 containing microparticles (Figure 7.6j).

Spacing between newly formed bone fragments (mm) analysis at 6 weeks indicated that controls (n=10) had an average spacing of 0.14 ± 0.03, while microparticles (n=10) had an average of 0.25 ± 0.18, BMP-7 coated microparticles (n=10) averaged to 0.28 ± 0.26 and BMP-7 encapsulated microparticles (n=10) had an average spacing of 0.44 ± 0.31. There was a significant difference ($p<0.001$) observed between controls and BMP-7 encapsulated microparticles (Figure 7.6k). At 12 weeks, the controls had an average spacing of 0.16 ± 0.04, microparticles averaged 0.25 ± 0.2, BMP-7 coated microparticles had an average of 0.43 ± 0.35 and BMP-7 coated microparticles had an average of 0.34 ± 0.3. There was a significant difference ($p<0.05$) observed between controls and BMP-7 coated and encapsulated microparticles (Figure 7.6l). There was no significant difference observed between BMP-7 containing microparticles and only the microparticles and also there was no significant increase in trabecular spacing observed between 6 and 12 weeks.

Figure 7.6 and Figure 7.7 are the three dimensional representation of the bone region scanned using micro-CT at 6 and 12 weeks repectively. These images indicate that due to the periosteal activity, a layer of bone has been formed at the periphery, but beneath that layer, there is still a lot of bone healing that needs to occur to bring back the original form. Figure 7.6c, 7.6e, 7.7e and 7.7g, we can clearly observe that microparticle is present at the defect site and new bone is being formed around it.

6 weeks

12 weeks

a

b

c

d

e

f
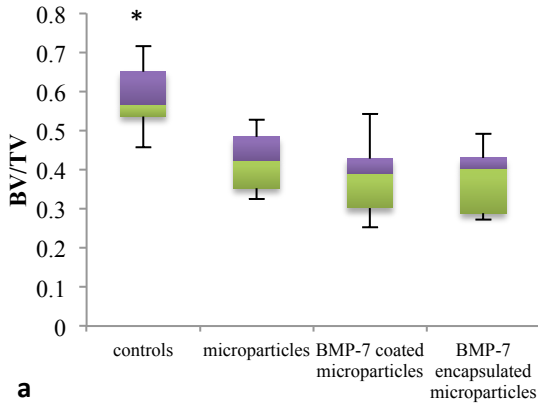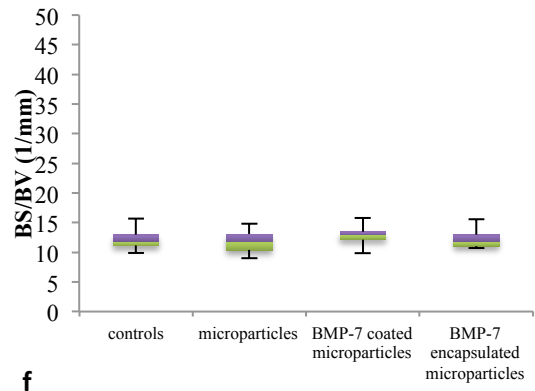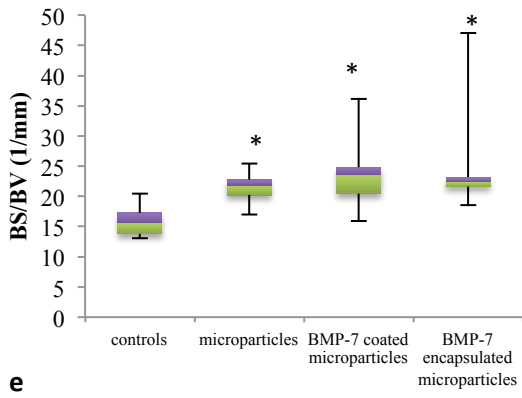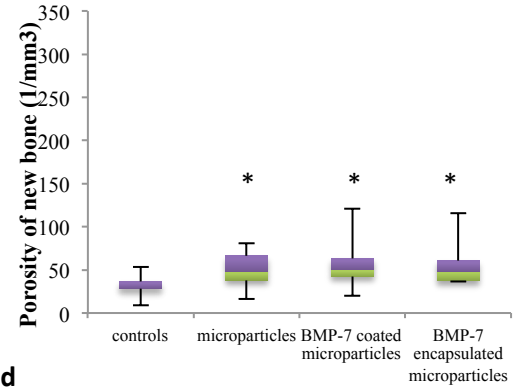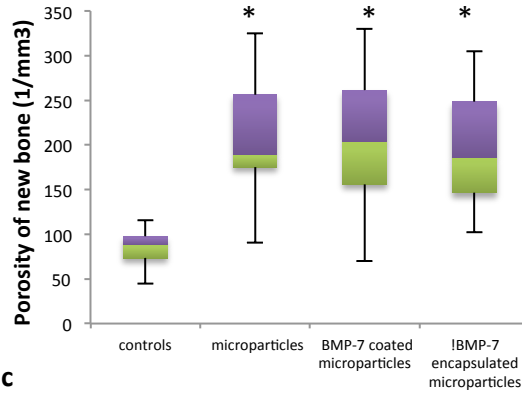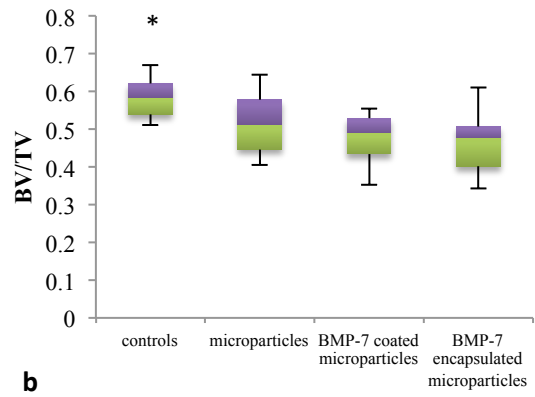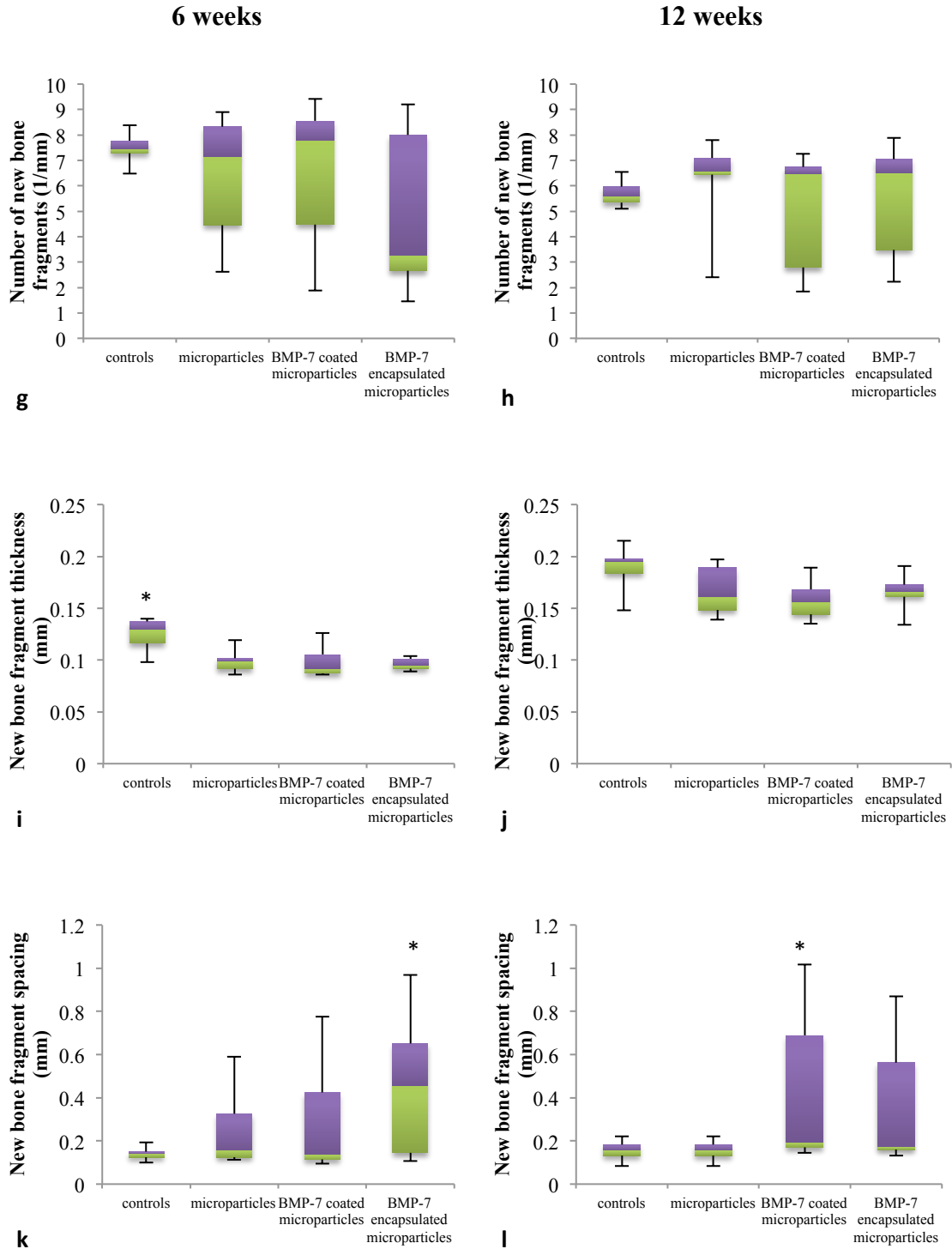
Figure 7.6: Box plot representation of a,b) Bone volume fraction (BV/TV); c,d) Porosity of new bone; e,f) Bone surface density (BS/BV); g,h) Number of new bone fragments; i,j) New bone fragment thickness; k,l) New bone fragment spacing measured in the newly formed bone region by microcomputed tomography at 6 and 12 weeks (n=10).
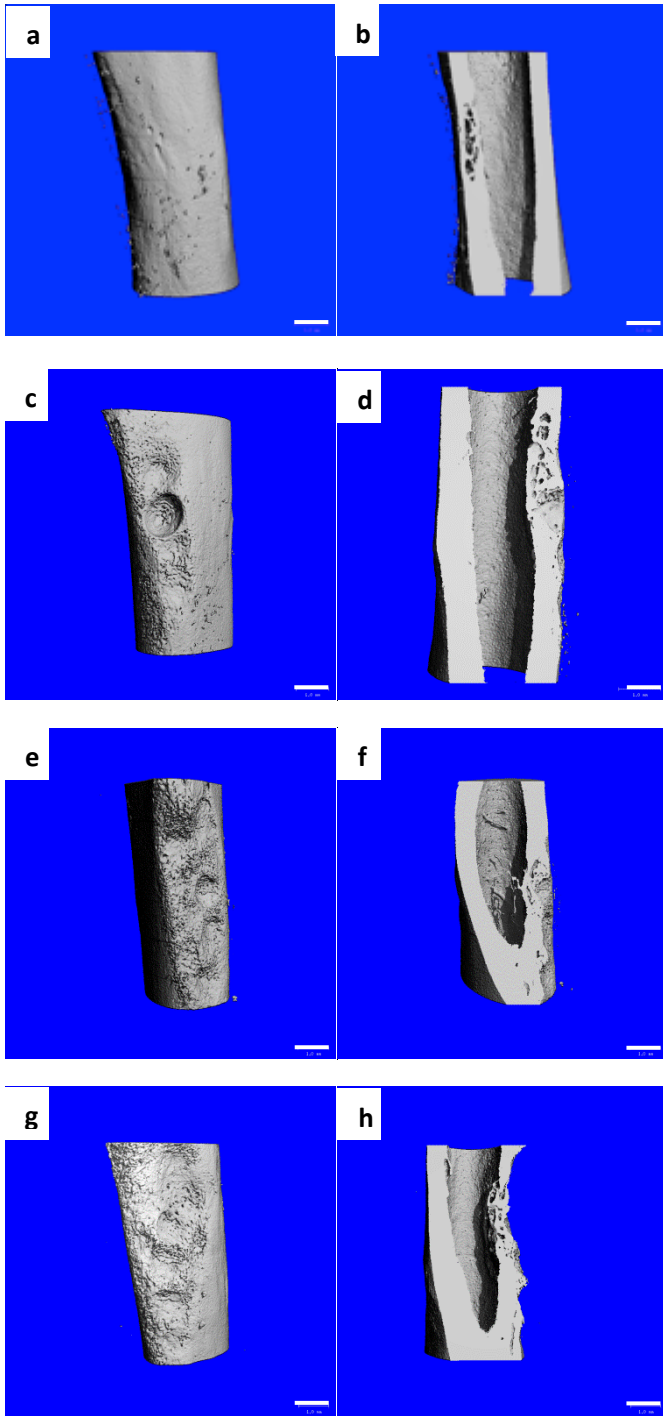
Figure 7.7: Representative week 6 post-surgery micro-CT images of femurs for controls (a,b) and treated groups- microparticles (c,d); BMP-7 coated microparticles (e,f); BMP-7 encapsulated microparticles (g,h). Scale bar = 1 mm
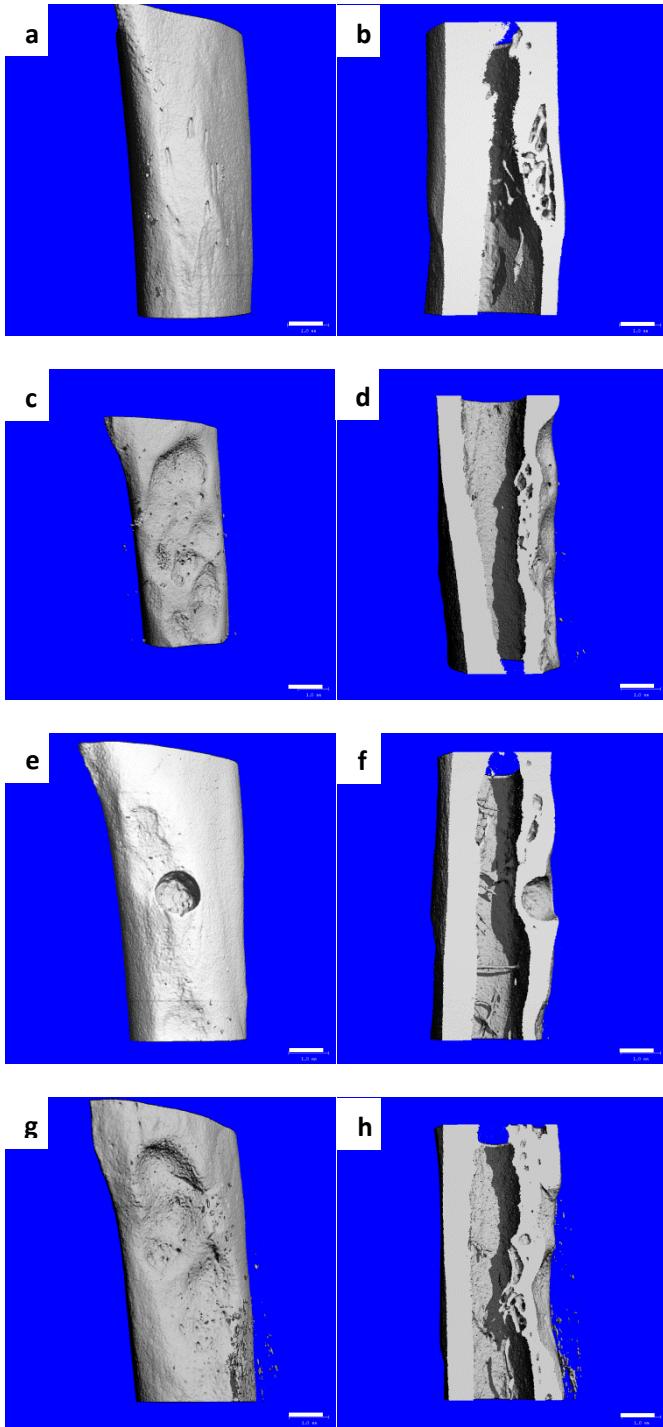
Figure 7.8: Representative week 12 post-surgery micro-CT images of femurs for controls (a,b) and treated groups- microparticles (c,d); BMP-7 coated microparticles (e,f); BMP-7 encapsulated microparticles (g,h). Scale bar = 1 mm.

7.3.5 Multiphoton Second Harmonic Generation

The bundled collagen fibrils constitute fibrils running parallel to each other. The newly formed region of bone constituted single fibrils, which have very small diameter, small bundled fibrils, with comparatively bigger diameter, and the thick bundled fibrils, with different dimensions, which may represent various stages of extracellular collagen organization. The fibrils organized into discrete bundled showed well-defined orientation. At 6 and 12 weeks, the images were analyzed using ImageJ and the regions in an image with an area greater than 3500 μm^2 (determined based on negative controls, data not mentioned here) were summed up to get the total bundled collagen area. Total collagen area was also determined in an image.

Figure 7.9a, 7.10a, 7.11a, and 7.12a are the bright field view of the new bone region analyzed and Figure 7.9b, 7.10b, 7.11b, 7.12b are the corresponding multiphoton confocal microscopy images respectively at 6 weeks post-surgery. The bundled collagen regions were analyzed (n=15) using ImageJ software. At 6 weeks, average percent of bundled collagen is around 25.35 ± 5.36 for controls, 42.58 ± 13.00 for microparticles without growth factors, 41.63 ± 10.55 for BMP-7 coated microparticles and 49.91 ± 18.09 for BMP-7 encapsulated microparticles. It is observed that there is a significant difference in percentage of bundled collagen (p<0.005) between controls and microparticles containing groups (Figure 7.13a). However, no significant difference was observed between microparticles containing BMP-7 and without BMP-7.

Similarly, at 12 weeks post-surgery, Figure 7.9c, 7.10c, 7.11c, and 7.12c are the bright field view of the new bone region analyzed and Figure 7.9d, 7.10d, 7.11d, 7.12d are the corresponding multiphoton confocal microscopy images respectively. At 12 weeks,

percent of bundled collagen averaged to 13.45$\pm$6.79 for controls, for microparticles, the average is 38.09$\pm$16.13, for BMP-7 coated microparticles, it averaged 49.06$\pm$17.15 and for BMP-7 encapsulated microparticles, the average is 32.50$\pm$15.06. These results indicated a significant difference ($p<0.05$) between controls and microparticles containing groups (Figure 7.13b). There was no significant difference observed in the percentage of bundled collagen between the BMP-7 present and absent groups. Also there was no significant decrease observed in the percent of bundled collagen between 6 and 12 weeks.
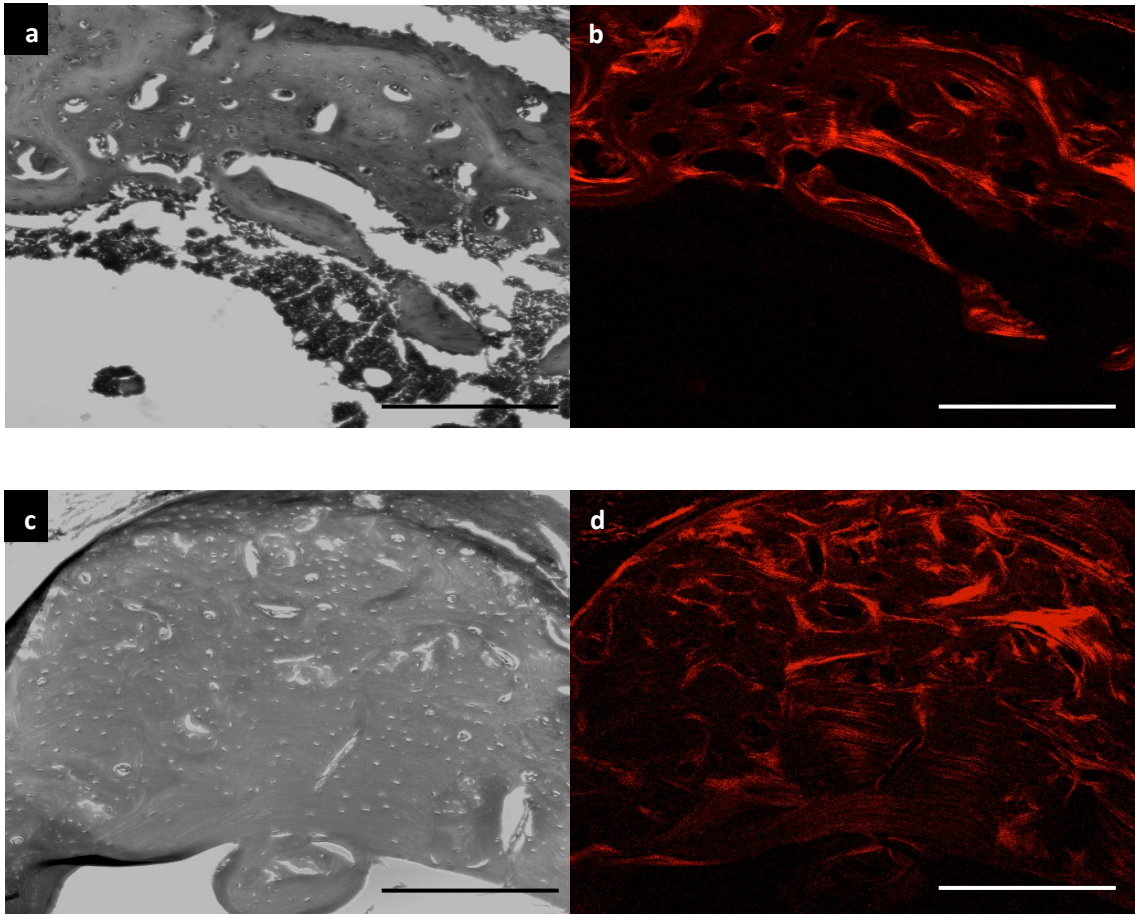
Figure 7.9: Representative histological section (H&E) of controls as observed under multiphoton confocal microscopy at a,b) 6 weeks - bright field view and the corresponding view of collagen fibers in the newly formed bone region (ROI) respectively c,d) 12 weeks - bright field view and the corresponding view of collagen fibers in the newly formed bone region respectively (Scale bar represents 250 µm).
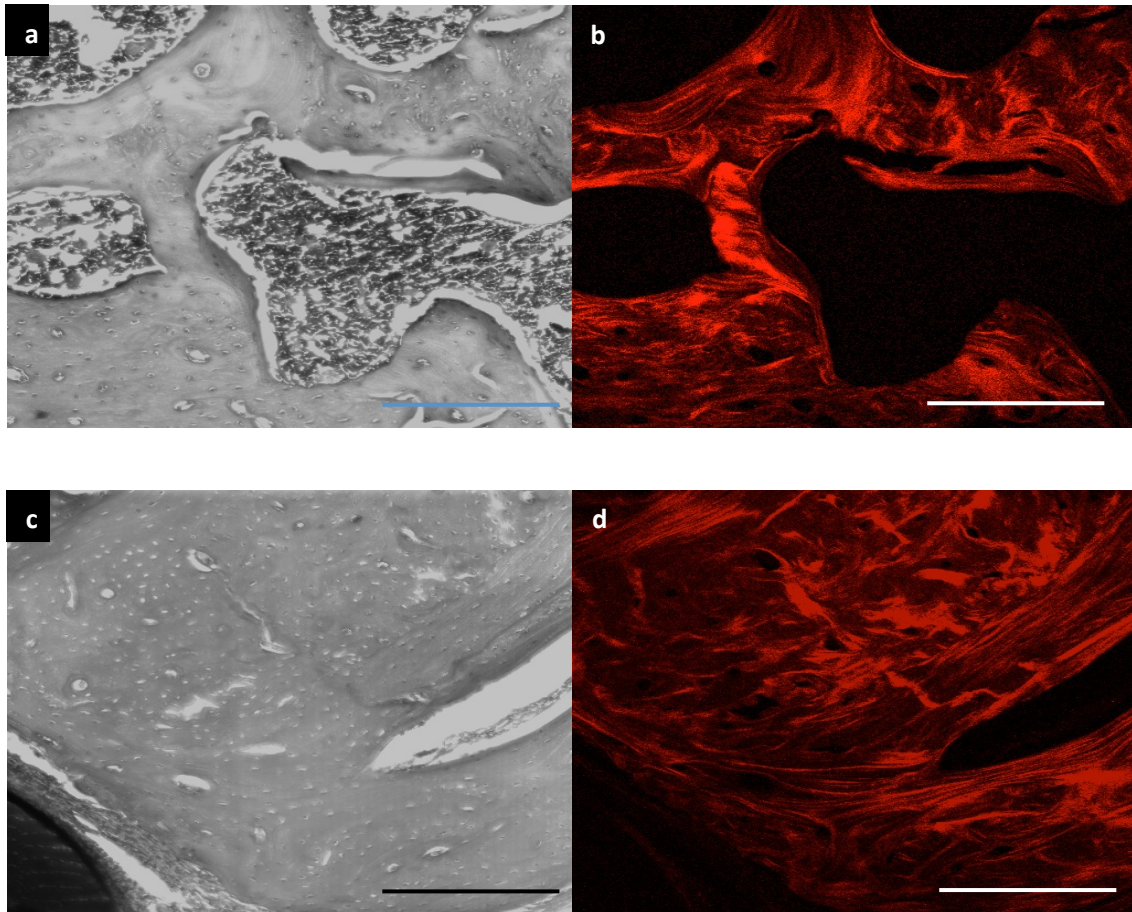
Figure 7.10: Representative histological section of chitosan-TPP microparticles without growth factors as observed under multiphoton confocal microscopy at a,b) 6 weeks - bright field view and the corresponding view of collagen fibers in the newly formed bone region (ROI) respectively c,d) 12 weeks - bright field view and the corresponding view of collagen fibers in the newly formed bone region respectively (Scale bar represents 250 μm).
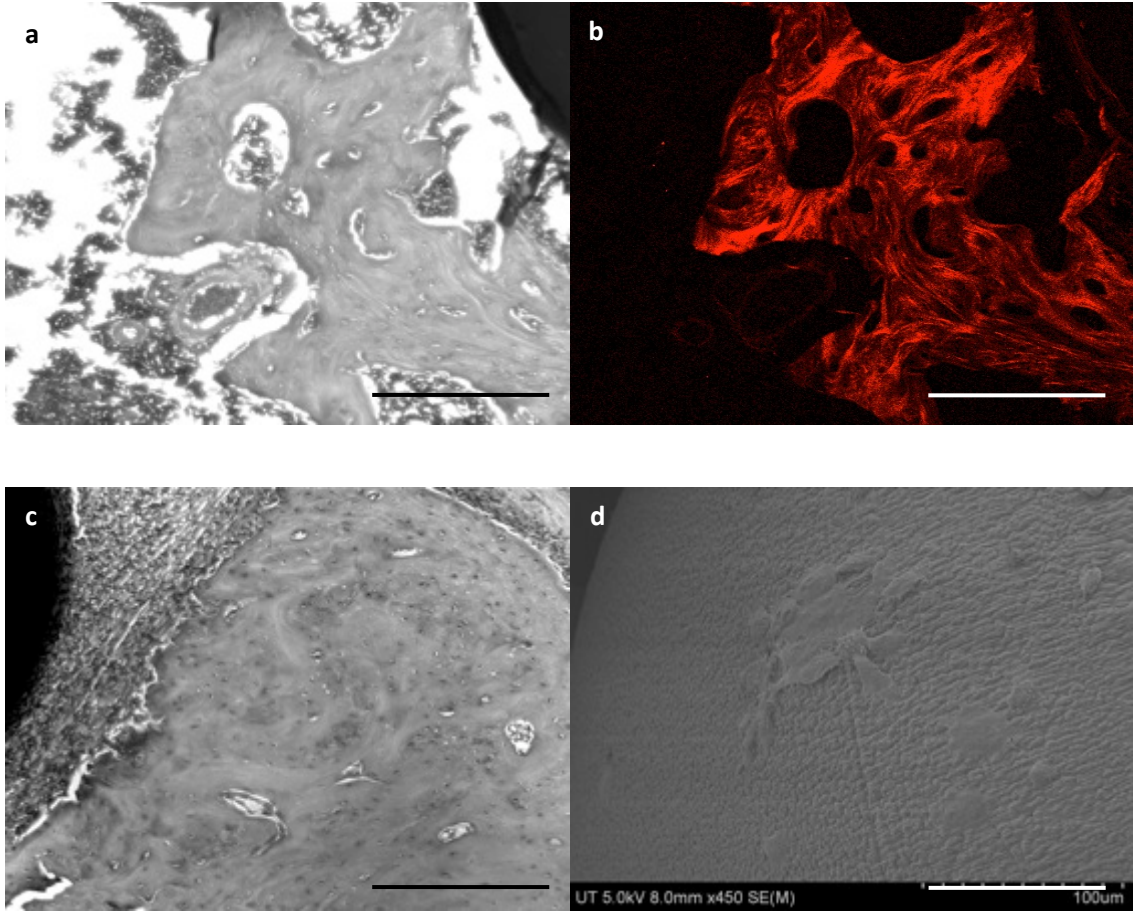
Figure 7.11: Representative histological section of BMP-7 coated chitosan-TPP microparticles as observed under multiphoton confocal microscopy at a,b) 6 weeks - bright field view and the corresponding view of collagen fibers in the newly formed bone region (ROI) respectively c,d) 12 weeks - bright field view and the corresponding view of collagen fibers in the newly formed bone region respectively (Scale bar represents 250 µm).
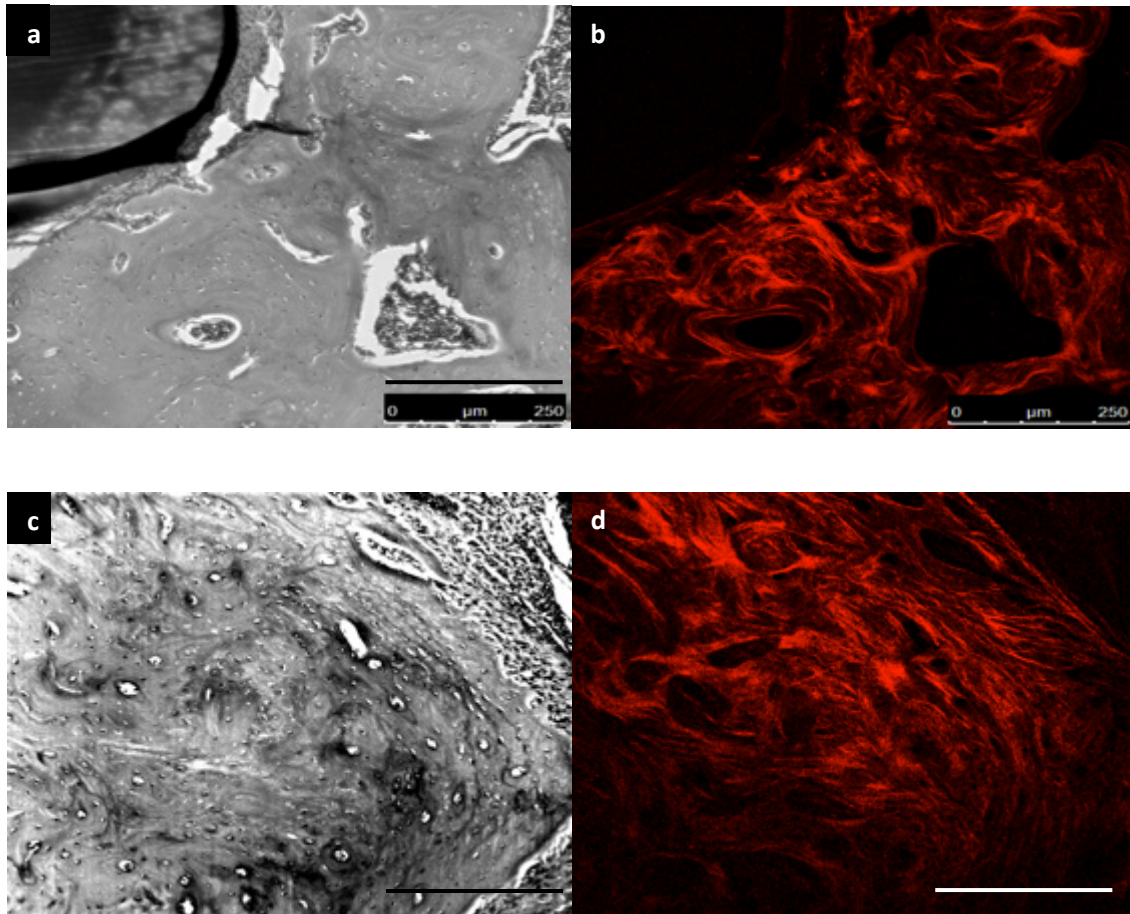
Figure 7.12: Representative histological section of BMP-7 encapsulated chitosan-TPP microparticles as observed under multiphoton confocal microscopy at a,b) 6 weeks - bright field view and the corresponding view of collagen fibers in the newly formed bone region (ROI) respectively c,d) 12 weeks - bright field view and the corresponding view of collagen fibers in the newly formed bone region respectively (Scale bar represents 250 μm).
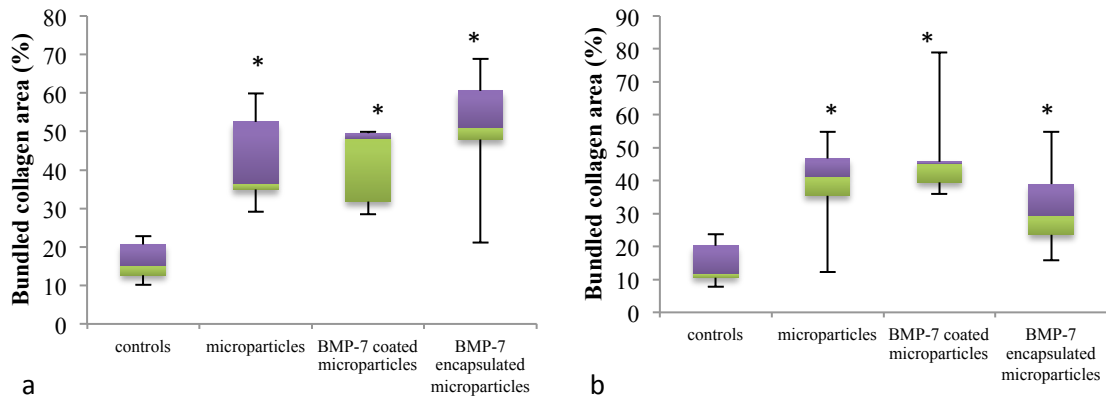
Figure 7.13: Box plot representation of bundled collagen formed in the new bone region (ROI) obtained by analyzing the confocal multiphoton microscopy images (n=15) using Image J software at a) 6 weeks b) 12 weeks.

7.4 Discussions

The objective of this study was to examine the events in the bone repair at 6 and 12 weeks following application of chitosan-TPP and chitosan-TPP-BMP-7 scaffolds in femoral defect in skeletally mature rats.

A critically sized femoral defect model can serve as a robust test bed for tissue-engineered bone regeneration scaffold even in small animals such as rats [263]. As per our observation of the animals during the study, we could observe that the rats were using their injured leg to move and climb up the cage. μ-CT and histology data suggests that bone formation was observed around and adhered to the microparticles. No degradation in microparticles was observed till 6 weeks, and 12 weeks, indicating that the microparticles are not brittle and have desirable mechanical properties.

Histology analysis was carried out to provide biologic insight to the various cellular events occuring during the complex healing process. Control defects in our study healed

in a sequence which closely resembled natural fracture healing process, starting with clot formation, inflammatory response, followed by marrow derived stromal cell migration, vascularization, granulation tissue formation followed by bone formation by intramembranous and endochondral processes. Woven type of bone is formed during this process, which will be later remodeled. Even after 12 weeks post-surgery, we can observe soft cartilaginous callus formed around the newly formed bone in controls, which indicates that the bone healing process is still an ongoing process.

Chitosan can be considered a polysaccharide that structurally mimics the proteoglycan macromolecules of the extracellular matrix, and therefore can exert similar morphogenetic funtions, as experimental evidence points out. Examination of new bone formed under the guidance of microparticles suggested that new mineralized tissue was actively produced by osteoblasts and remodeled by osteoclasts, by the process of intramembranous and endochondral ossification. Studies have shown that following implantation of biomaterial, host reactions include blood-material interaction, provisional matrix formation, acute inflammatory response, chronic inflammatory response, granulation tissue development, and foreign body reaction followed by fibrous capsule formation [264,265]. The observations in our study were similar, wherein at 6 weeks, we could observe minor inflammatory response around the microparticles, and bone tissue growing in close proximity to the microparticles. Previous studies have shown that chitosan demonstrates chemotactic potential *in vitro* and *in vivo* [266-268]. There are many studies, which showed minimal inflammatory response of chitosan [269,270], but there also exists many studies which show that chitosan could lead to high degree of inflammatory infiltrates [271,272] and that reaction could last for long periods [273]. But

in our case, for chitosan-TPP and chitosan-TPP-BMP-7 microparticles fabricated by coacervation technique, we observed minor inflammatory response at week 6, which reduced by 12 weeks period. We observed that the granulation tissue is separated from the biomaterial by the cellular components of foreign body reaction where one or two layer of monocytes, macrophages and foreign body giant cells were present. These cells are mainly responsible for phagocytosis and degradation of the microparticles, which we started to observe by week 12. Fibrous tissue was observed around particles, which was similar to observations from other studies [274]. The migration of cells is an important aspect of the stimulatory influence for tissue reconstruction. Chitosan seems to induce attractive effects on undifferentiated and mature fibroblasts and also undifferentiated mesenchymal elements to build up microvessels. There is a noticeable difference in the inflammatory response observed between microparticles and BMP-7 coated and encapsulated microparticles. This observation can be the reason for the prsence of inflammatory cells in gaps in the particles in BMP-7 coated and encapsulated, which can lead to their early degradation. The possible explanation for this observation is that maybe due to the BMP-7 released from the microparticles, cells migrate quicker to scaffold and induce scaffold degradation [275].

μ-CT uses X-ray attenuation data acquired at multiple viewing angles to reconstruct a 3D representation of a specimen that characterizes the spatial distribution of material density. Therefore, quantitative analysis data for newly formed bone obtained by this method is more accurate. Bone volume fraction (BV/TV) results indicate that the ratio is significantly high in controls at 6 and 12 weeks, where natural healing is observed in healthy bone. The relatively less mineralized bone fraction in microparticles containing

groups can be attributed to the fact that the defect site were partially occupied by the microparticles, which did not degrade in our study period. But, when we consider the two time points in the study, a significant increase ($P<0.05$) in BV/TV is observed in microparticles containing groups, while that was not the case in controls. This can be understood by the definition of bone volume fraction, which is a ratio of bone volume and tissue volume. When individually these parameters were analyzed, we observed that in controls, there was a simultaneous increase in bone volume and tissue volume, which did not change the ratio, but in case of microparticles containing groups, there was twice an increase in bone volume in comparison with tissue volume between the two time points, therefore accounting for the significant difference. The fact that BV/TV ratio does not significantly change in controls confirms that the defect was critically sized for rats and is consistent with previous studies [276-278]. No significant difference is observed between microparticles and BMP-7 containing microparticles, which can be explained by three reasons: (i) the quantity of BMP-7 incorporated was not sufficient to observe significant difference in bone growth. Even though our *in vitro* studies have demonstrated that the BMP-7 being released from the microparticles is stable and bioactive, *in vivo* conditions are completely different, and results cannot be predicted definitely. Previous *in vitro* studies have also shown that femtomolar and nanogram range of BMP have shown mitogenic and osteogenic effects, however macroscopic quantities of bone *in vivo* are induced only by milligram quantity of purified BMP or microgram range of rhBMP. In addition, threshlold levels also differ between species. A study reported that the use of 1.4 µg BMP-2 in rat segmental defect in femur did not result in union, whereas a dose of 11 µg was sufficient to complete union. In rabbits, 3.13 µg of BMP-7 was insufficient to

heal segmental ulnar. These data suggest that the threshold of dose for *in vivo* bone induction is several magnitudes greater than that for cell response *in vitro*. (ii) the formation of fibrous capsule around the microparticles prevents the release of growth factor. Studies have shown that activated inflammatory cells (monocytes, macrophages) produce pro-fibrinogenic factors, which enhance fibrogenesis by fibroblasts [279]. Therefore the macrophages adhered to the microparticle can secrete proteins that modulate fibrosis and in turn, fibrous capsule develops around the biomaterial (iii) the inflammatory cells (macrophages) that adhere and spread over the material surface release mediators of degradation such as reactive oxygen intermediates (ROIs, oxygen free radicals), degrading enzymes and acids into the zone between cell membrane and biomaterial surface [280]. Biomaterial surface is therefore susceptible to high concentrations of these degradative agents (pH as low as 4.0), which may have degraded the releasing protein.

The new bone fragments thickness was averaged to be between 170-210 μm in controls and 140-190 μm for microparticles treated groups. These values were higher than those reported by Wronski et al. [281,282]. TRI plate model was used to determine these values in both the cases and therefore discrepancy in the results can be due to difference in the calculation algorithm or the difference in the chosen threshold value. The number of new bone fragments was found to be about ~5 mm^{-1} at the end of 12 weeks, which coincided with previously obtained results [282].

Of the different parameters tested in this study, bone surface density and porosity density were found to be important parameters, which were significantly higher in microparticles containing groups in comparison with controls. Comparative analysis of microCT results

show that BS/BV and porosity of new bone show good Pearson's correlation coefficient value of r=0.59 (p<0.001). Positive correlation factor indicates that more the surface area per bone volume, greater is the porosity. The presence of microparticles (with and without BMP-7) leads to increased BS/BV and porosity at 6 weeks, but with time, the porosity decreased, as observed at 12 weeks. By definition, connectivity density is a topologic measure counting the number of objects, the number of marrow cavity surrounded by bone and the number of connections that must be broken to split the structure into two parts. This supports the fact that the newly formed bone is more interconnected and porous in comparison with controls.

To further analyze the new bone, we determined the collagen fibrils formed in the new bone. This type of study is first of its kind to use confocal multiphoton second harmonic generation microscopy to determine the collagen fibril thickness and area in the newly formed bone and compare it between the scaffold-containing groups and controls. The capacity of the bone to resist mechanical forces and fractures depends on both the quantity of bone as well as on its quality. The quantity is in part evaluated by bone mineral density, which confers strength and stiffness to the tissue [283], whereas the quality in part is contributed by collagen phase, which confers ductility, playing a greater role in affecting the postyield properties of bone and overall toughness of the tissue [284,285]. A study revealed that there is a 35% decrease in strength, 30% decrease in modulus and 50% decrease in toughness of collagen network with age, that results in failure of whole bone [286]. Of the various structural and composition properties, collagen fibril diameter has been regarded as the most important factor related to biomechanical strength of the tissue [287]. Our study revealed that microparticles

containing femur defects showed significant increase in the percent of well-defined and organized bundled collagen area in the newly formed bone, in comparison with controls at both time points, which suggests the presence of microparticles, influences the mechanism of collagen fibrils formation. While it is evident that local microenvironment can influence fibril aggregation, it is also known that cells are responsible for molding tissue into specific configurations, by close spatial contact. Studies have shown that proteoglycans consisting of core protein and glycosaminoglycans (GAGs) have been implicated as regulators of collagen fibril I structure in different tissues [288]. Though the information on precise role and mechanism by which the GAGs regulate collagen structure is limited, it can be explained that the presence of chitosan (containing structure similar to GAG) may be a considered a cell-mediated modulary tool, which influence mesenchymal elements, as already documented for GAGs. These differences in fibril diameter have biomechanical implications. As we know, bone is mainly composed of type I collagen with type III and V modulating the fibril diameter [289]. Type I fibrils has larger diameter than type III collagen [290,291]. Therefore, it may be postulated that new bone formed in the presence of microparticles (with and without BMP-7) has larger amount of type I collagen in comparison with controls.

Chapter 8

Conclusions

In conclusion, although there have been studies with chitosan microparticles, majority of the studies used conditions that are not suitable for the growth factor encapsulation. We prepared particles in ideal conditions, by not using any organic solvents for particle preparations and also employing low temperatures during microparticle encapsulation, thus ensuring the structural and functional stability of the growth factors. The particles obtained were in the size range of 500-700 μm, balancing the effect of maximum release of encapsulated growth factor and bone filling material requirement. Preparation of microparticles at lower temperatures also ensured increased encapsulation efficiency and release when compared to the release at higher temperatures. The method used is also a cost effective procedure as it avoided the use of chemicals like oil, hexane, acetone and use of other equipment necessary for particles preparation. The cell study proves that the microparticles help in enhancing the proliferation and differentiation ability of the cells. The difference in the IGF-1 incorporated particles and normal particles shows that the

IGF-1 being releases in biologically active and helps in the cell multiplication. Thus the prepared microparticles may allow for a wider range of application for *in vivo* bone regeneration and other regeneration of tissue applications.

An improved response of pre-osteoblasts was observed due to the chitosan-TPP microparticles and BMP-7 released from these microparticles. Significant increase in cell attachment and proliferation was observed on the surface of the microparticles with BMP-7 indicating the influence of BMP-7. Differentiation of the pre-osteoblasts to osteoblasts was demonstrated by the significant up-regulation in the expression of transcription factors – runx 2 and osx as well as late osteoblast markers – OCN, OPN and BSP, which lead to increased mineralization. Therefore, it is postulated that *in vivo*, these materials may be able to act as a better and more reliable bone substitute material thus improving osseointegration response.

Results of *in vitro* release and antibacterial experiment suggest that the fabricated chitosan microparticles containing cefazolin and vancomycin are capable of effectively delivering the drug in a controlled fashion over a period of time. The study over the two-week time period indicated that cefazolin released can completely inhibit the growth (~85%) of *S. epidermidis*. Vancomycin was also found to be an effective against S. epidermidis at higher concentrations (MIC - 24 µg/ml). The microparticles with drug and BMP-7 encapsulated into it showed a better-controlled profile over the coated microparticles, where burst initial phase was observed. It is also extremely important to take into consideration the concentration of drugs being incorporated into the microparticles as it has a significant influence on osteoblasts cytotoxicity. 50 µg/ml and 100 µg/ml of cefazolin were found to positively influence cell number and viability of

osteoblasts. In the complete duration of our release study of cefazolin, the concentration of cefazolin remained <70 µg/ml. On the other hand, in case of vancomycin 1000 µg/ml was found to significantly reduce cell number, indicating its toxicity for osteoblasts. Therefore, we chose the amount of vancomycin to be incorporated such that the release concentration is always less than 120 µg/ml during the two weeks period. Therefore, the scaffold system we developed can be used as an effective dual delivery system for drugs and growth factors for various complex tissue-engineering applications.

In vivo study provides evidence that biocompatible, biodegradable and biomechanically stable chitosan scaffold can be developed by cross-linking with TPP at low temperatures, using minimum organic solvents, which accelerates better, and healthy bone formation. This was illustrated by histology, which indicated healthy bone growth adhered to the periphery of the microparticles. Influence of BMP-7 was noticed in histology, where we could observe inflammatory cells in gaps between the microparticles by 12 weeks. This can be attributed to faster migration of cells towards BMP-7 containing microparticles. Micro-computed tomography analysis was used to quantify 3D bone growth and mineralization. Bone surface density and connectivity density were found to be significantly difference (p<0.05) for microparticles containing groups, which suggests higher connectivity and also higher in the newly formed bone. Confocal multiphoton second harmonic generation microscopy was employed to visualized collagen formation in the newly formed bone. We observed a significant improvement in the formation of well-defined and organized bundled collagen in microparticles containing groups, from which we understand that the collagen fibril diameter is higher. Chitosan possessing structural similarities with GAGs, have been shown to influence collagen fibril structure,

thereby resulting in higher bundled collagen area. Further studies need be done to determine the mechanical properties of the healed bone, which can support the collagen experiment results.

As a conclusion to this work, we can state that though the *in vitro* studies have demonstrated that chitosan microparticles with growth factor BMP-7 result in enhanced osteoblasts proliferation and differentiation, *in vivo* studies showed that the BMP-7 is either insufficient or is not being released or is degraded by the inflammatory cells/fibrotic tissue formed surrounding the bone. The chitosan microparticles started to show signs of degradation at around 12 weeks, especially in BMP-7 containing microparticles, which can be due to the release before inflammatory cells crowded the region. The presence of chitosan microparticles did show an increased bundled collagen formation, which suggests that the new bone is more ductile, but mechanical tests should be conducted before concluding. Therefore, future studies must focus on increasing the concentration of BMPs to determine its effect on bone volume and modifying the surface of the microparticles to minimize the tissue response.

Chapter 9

Business Plan

9.1 Executive Summary

The gold standard to treating bone injuries/fractures is to use bone obtained from another part of the body. This type of treatment is associated with limited supply, can undergo unpredictable resorption, and leads to immense donor site pain and morbidity. Bone graft substitutes currently used (like methyl methacrylate, poly-lactic acid) leads to marked inflammatory response and fibrous capsule formation around the implant, resulting in possible infection, loosening and exposure of implant. Also, these materials neither fail to integrate with naturally remodeling bone nor can grow in the patient, making it a poor bone graft substitute. Therefore, there is an unmet need in the regenerative medicine market to repair and regenerate bone. This unmet need can be satisfied by OsseoCHI bone graft substitute.

OsseoCHI microparticles are synthetic, osteoconductive, resorbable chitosan-tripolyphosphate (TPP) based bone substitutes, which can replace autogenous bone. OsseoCHI eliminates the need for autologous bone harvesting, thus reducing patient morbidity. OsseoCHI microparticles will be manufactured in a clean-room environment from biocompatible, radiopaque material, chitosan. Chitosan is a linear polysaccharide composed of randomly distributed β- (1-4) linked D-glucosamine (deacetylated unit) and N-acetyl-D-glucosamine (acetylated unit). This chemical composition is similar to glycosaminoglycan units in the extra cellular matrix of bone, which play a very important role in regulating growth factors and other factors involved in bone formation. Chitosan salts formed by mixing chitosan with an organic acid (such as acetic acid or lactic acid) render it a positive charge leading to interactions with negatively charged cells (like osteoblasts) leading to bone healing when injected at defect site. The protonated chitosan is broken down in the body by lysozyme to glucosamine, which is biocompatible and can be further degraded to carbon dioxide. Chitosan also has natural antibacterial property, which is advantageous to treat infection. FDA has already approved chitosan for use in bandages and other hemostatic agents in United States and Europe. *In vivo* rodent studies have shown that chitosan-TPP microparticles show significant increase in connectivity density and collagen formation in comparison with controls, which indicate that the newly formed bone in presence of microparticles is more stable. OsseoCHI is therefore ideal for many bone void filler applications.

The initial target market for the proposed device consists of orthopedic/neuro surgeons dealing with tibial and craniofacial fractures respectively. Buyers will be hospitals, orthopedic and neurosurgeons. Early adopters will be those surgeons who are extending

their practice with InFuse, an emerging bone morphogenetic protein (BMP) related product. However, the target market includes those currently using more conventional autografts, allografts and non-biological synthetic bone graft substitutes.

The competitive advantages of OsseoCHI are i) it is user-friendly and easy to use ii) due to its appropriate size, it remains at the defect site during the healing process iii) it is injectable and therefore is easy to handle iv) it releases biologic in a controlled fashion, limiting the concentration to safe margin range, eliminating any side effects v) the scaffold itself is osteoconductive and by using the bone marrow of the patient along with the graft, it can be made osteogenic as well.

The bone graft substitutes market is forecasted to reach $3.3 billion globally and $2.2 billion in the US by 2017. Bone graft substitutes are divided into three major markets i) synthetic bone graft substitutes ii) demineralized bone matrix (DBM) iii) bone morphogenetic protein (BMP). Synthetic bone graft substitutes are currently used in about 25% of bone grafting procedures performed annually in United States.

First year sales are expected to be approximately 50,000 units, yielding to $14 million in net sales. An initial investment of $3 million will be utilized to conduct pre-clinical studies to prove the technology for FDA approval for human clinical trials. Later for Phase IIb/III human clinical trials, $40 million will be required over the period of four years. Break-even will be obtained in third year when nearly 133203 units are sold and positive cash flow will be generated. Revenues from sales will ramp up the market share to an expected 25% by the end of 5 years.

9.2 The Industry, Company, Product

9.2.1 Opportunity Rational

There are four main reasons why OsseoCHI has excellent business potential, they are listed below:

- **Increasing Old Age Population**

A major percent of the patient population is made up of the baby boomers and unlike the aging population of previous generations; they practice an active lifestyle that leads to a number of injuries. Till date, always the numbers of young children have outnumbered the elderly population; however in about five years from now, the elderly population will outnumber the children younger than five years old [292]. One of the major chronic conditions reported by aging population is arthritis; it is a fact that one in every five adults suffer from it [293]. The major cause of the increased arthritis rates found amongst patients is obesity; about 54% of adults who suffer from arthritis are obese [294]. Osteoporosis and trauma are the other major reasons for joint replacement. Treatment for arthritis depends on the type of arthritis, its location, severity and the medical condition of the patient. Therefore the treatment procedure can vary from medication, joint injections to surgical operation being the last resort.

- **Improvement in Material and Technology**

With the availability of a variety of bone grafts and substitutes in the market and improving surgical techniques, physicians now have a greater flexibility to treat their patients thereby allowing for higher success. In order to increase their range of expertise,

surgeons are ready to adapt to new technologies. One of the advanced techniques is minimally invasive surgery (MIS), which has been gaining lot of popularity as it allows for smaller incision and faster healing. These add to reduced expenditure by minimizing inpatient stay time and leads to early patient recovery. MIS also opens up a growing younger demography to orthopedic surgeries. It has been found that despite autografts being the gold standard, surgeons prefer machined bone products (allografts) for use in spinal fusion as they help avoid second surgery that causes morbidity in more than 25% of the patient population and also adds to the cost aspect.

- **Increasing Healthcare Expenses**

Musculoskeletal disorders are the most widespread human health issue, with knee and hip replacements costing around $42.3 billion within US in 2009 [295]. Surgical implantation of artificial biomaterials have allowed surgeons to ameliorate the lives of patients by reducing the pain and restoring function to the otherwise functionally compromised structure. Hip, knee, and spine are the body part being replaced most frequently.

Apart from the increased number of the replacement surgery, there has been a simultaneous and parallel increase in the revision surgery of hip and knee implants [296]. From the year 2000 through 2011, Food and Drug Administration (FDA) gave a premarket approval for more than 150 new high-risk medical devices and an additional 600 devices were cleared through the 510(k) process [296]. The public directly relates increased flooding of the market with new devices to the demand rate. In 2006, the sales of orthopedic implants and trauma products totaled $12.2 billion and by 2012, it has increased at a compound annual rate of $18.1 billion [296]. The total cost for hip and knee replacement surgery has increased to 10.2% annually since 2000 and this value

outpaces the overall U.S. healthcare expenditure growth of 8% [296]. In order to control the increasing expenses, government is restricting the reimbursements to the hospitals and this is expected to continue in the market. This puts a pressure on the hospitals to adapt technologies and procedures that will give them maximum profit margins.

- **Room for Innovative Products**

This leads to low barriers for entry in some niche markets like bone substitute market, cell based matrices etc. Despite the presence of around 40 product types in bone graft substitutes market, it has been found that there is a lot of room here for new designs and materials as scaffolds. But in order to gain market revenue and thereby increase market share, it is necessary to differentiate products and given the current economics, products can be differentiated based on cost as well as benefits these products have over the existing ones.

9.2.2 The Product

- **Features**

OsseoCHI is an injectable bone substitute material made from chitosan and sodium tri-polyphosphate that can be incorporated with BMP-7, which are released in a sustained fashion over a period of time (Figure 9.1). The product formula and delivery system are proprietary. The formula is unique and has been found to be effective in healing femoral bone defects in rodents. The material will act as a scaffold for the cells to adhere, proliferate and differentiate and build bone and with time, it will degrade, being completely replaced by natural bone [297-299]. The product can be used in as a bone filler material and also in a wide variety of bone grafting procedures such as spinal

fusions, craniofacial defects, acute and open tibial fractures (guided bone regeneration) or sinus lift and ridge augmentation (bone augmentation) needed for dental implants. Chitosan polysaccharide has structural similarities to glycosaminoglycan molecules in the extracellular matrix of bone, which are known to be involved in regulating growth factors which play a crucial role in bone healing mechanism and therefore chitosan can be considered an effective bone scaffold material. The material must be used in conjunction with a metallic external fixation device that is indicated for temporary stabilization of the bone.
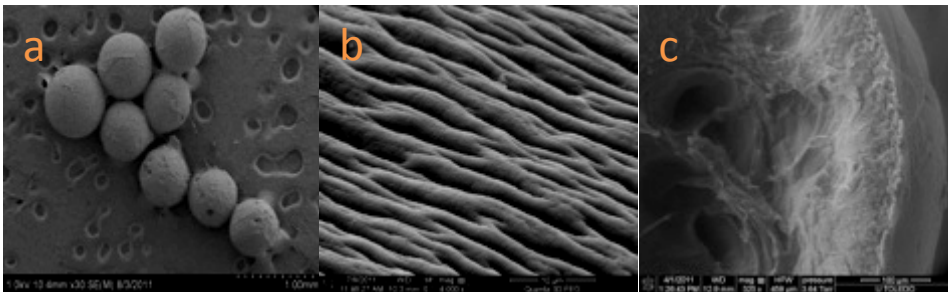
Figure 9.1: SEM images of a) microparticles b) Surface morphology of microparticles c) Cross section of microparticle shows the internal hollow structure.

OsseoCHI can be injected into the defect of the skeletal system and can also be combined with autogenous blood or bone marrow, which increases the biological activity at the defect site. Following placement of OsseoCHI into the bone void, it will act as a scaffold/bridge for bone cells to adhere, grow and differentiate leading to bone formation during the healing process and at the same time will be resorbed leading to complete replacement by natural bone.

OsseoCHI is biocompatible and safe. Biocompatibility is defined as a material's property to be compatible with a biological system and therefore depends primarily on material's chemical composition, its three-dimensional structure and its surface topography. OsseoCHI is made from chitosan, which is a linear polysaccharide with chemical and structural resemblance with GAG molecules in the extracellular matrix of bone and is therefore free of any cytotoxic effects, as indicated by histologic evidence at week 12 [300]. Also since it is completely synthetic, there is no risk of disease transmission as observed in allografts.

OsseoCHI facilitates bone-healing process due to its osteoconductive surface. Rough surface topography, and cationic characteristic of the microparticles mainly influence osteoconductivity. The microparticles are approximately in the size range from 500 μm - 700 μm. The spaces between the microparticles offer optimum environment for vascularization and bony infiltration.

Due to its synthetic manufacturing process, OsseoCHI shows reliable and standardized biomechanical properties. The elastic modulus of dried OsseoCHI averages ~77.72 MPa, which is similar to that of human cancellous bone (50 MPa).

OsseoCHI is ready to use off the shelf and therefore avoids morbidity, thereby lessening pain to patients and risk of complications from second surgical site as observed in autograft procedures. Also there is guaranteed availability of sufficient bone graft substitute and it also shortens OR time.

The advantages of this product in comparison to the other similar products available in the market include:

I.   The product is cost effective and very easy to scale up for manufacturers

II. Eliminates the need for an open surgery which leads to faster healing in patients

III. Better handling properties (as it is injectable) for surgeons

IV. Defect of any shape and size can be filled with this material and surgeon need not waste their OR/surgery time reshaping/resizing the product, thereby eliminating wastage of product and time. Also during the graft preparation time, the patient is under anesthesia.

V.   Drastically will reduces the risk of infection associated with open surgeries

- **Product Information**
  - OsseoCHI chitosan-TPP microparticles, sterile, have diameter in range of 500 μm - 700 μm
  - Two types of products:
    - Microparticles
    - Microparticles with growth factor BMP-7
  - Sterile-packaged in 1.0 cc volume
  - Microparticles will be supplied in injectable syringes

9.3 Market Research and Analysis

9.3.1 Market Size and Trends

Total bone graft and bone graft substitute market can be segmented into seven sectors as represented in Figure 9.2.
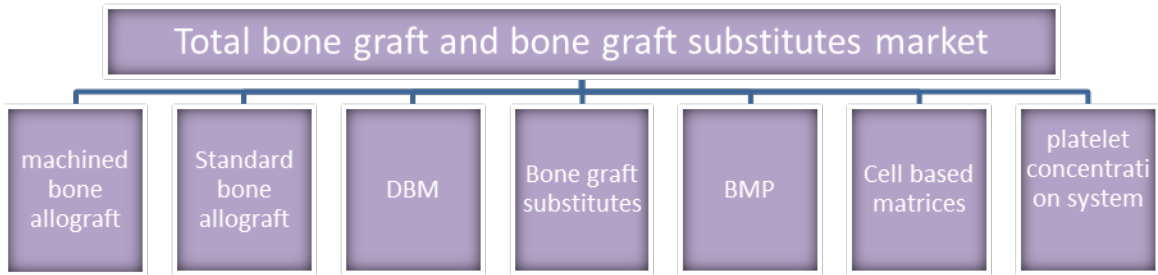
Figure 9.2: Total bone graft and bone graft substitutes market: Market Segmentation, United States, 2011 (Frost & Sullivan).

Total addressable market (TAM): This market includes bioresorbable fixation devices (pins, screws, tacks, suture anchors, and meniscal repair devices); allografts and bone replacement materials (base tissue, demineralized bone matrix, machined bone allografts, and synthetic bone grafts), and osteobiologics (autologous therapy/platelet concentrate systems, gene therapy, platelet-derived growth factors, recombinant human bone morphogenetic proteins, small molecule therapies, and stem cells). The combined U.S. market for orthopedic biomaterials for bone repair and regeneration is projected to reach an estimated value of $3.5 billion in the year 2017. For 2012, it is around $1.6 billion (Figure 9.3).

Served addressable market (SAM): $875 million - The portion of TAM that our product can fill.

Target market - $250 million –This segment our target market, which includes bone fillers and BMP segment for craniofacial and tibial defects.

As an example of the revenue potential for our product, one of the current two BMP containing bone graft substitutes earned $140 million just one year after approval for use in the spine, and currently generates annual revenue of at least $700 million.
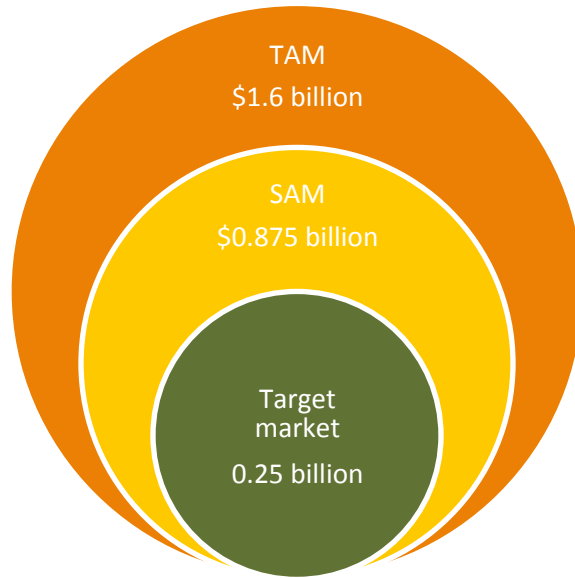
Figure 9.3: Total addressable market, served addressable market and target market for our product.
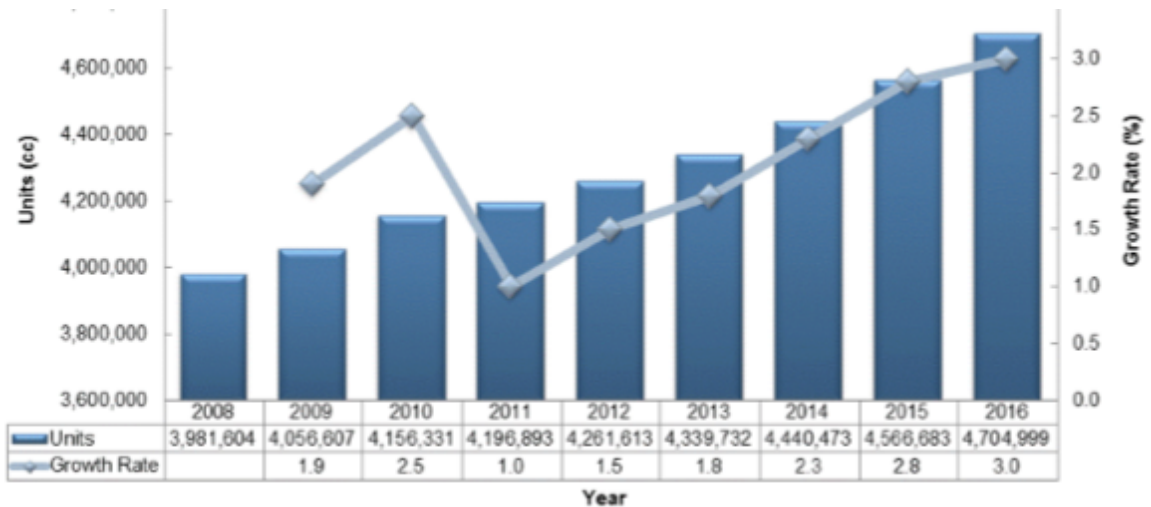
Figure 9.4: Total bone graft and bone graft substitutes market: Unit Forecast, United States, 2008-2016, CAGR = 2.3% (Frost & Sullivan)

An important point to note in figure 9.4 is that the number of units will rise steadily from 1 % to 3% from 2011 to 2016. This is due to the positive data that is being reported with the emergence of new technologies and products. As the population ages, there will be an increasing demand for improved quality of life as a result the number of orthopedic surgeries are bound to go up. Due to the weak economy, growth rates are modest but introduction of new products with better clinical data will result in increased market interest.

Year	2008	2009	2010	2011	2012	2013	2014	2015	2016
Revenue	1,698.5	1,679.0	1,665.0	1,633.0	1,598.9	1,591.0	1,596.2	1,622.5	1,655.5
Growth Rate		(1.1)	(0.8)	(1.9)	(2.1)	(0.5)	0.3	1.7	2.0
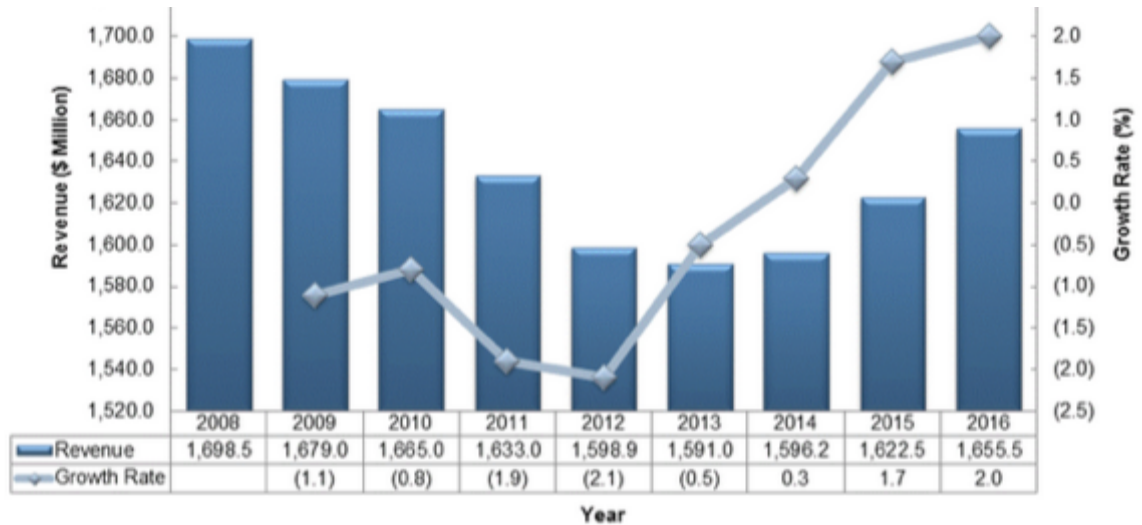
Figure 9.5: Total bone graft and bone graft substitutes market: Revenue Forecast, United States, 2008-2016, CAGR = 0.3% (Frost & Sullivan).

In figure 9.5, consider the overall growth as a factor of high-growth segments as well as the declining segments in the market. Due to the high cost of the BMP products, in this weak economic conditions, BMP segment is a declining market (Figure 9.6), which is pulling the overall bone graft and bone graft substitute market down as they hold the

largest share in the revenue in this market. But orthopedic surgeries such as spine and

joint reconstruction are on a rise and are creating a demand for bone graft products.

	2008	2009	2010	2011	2012	2013	2014	2015	2016
Revenue	850.0	800.0	750.0	675.0	594.0	534.6	481.1	442.6	407.2
Growth Rate		(5.9)	(6.3)	(10.0)	(12.0)	(10.0)	(10.0)	(8.0)	(8.0)
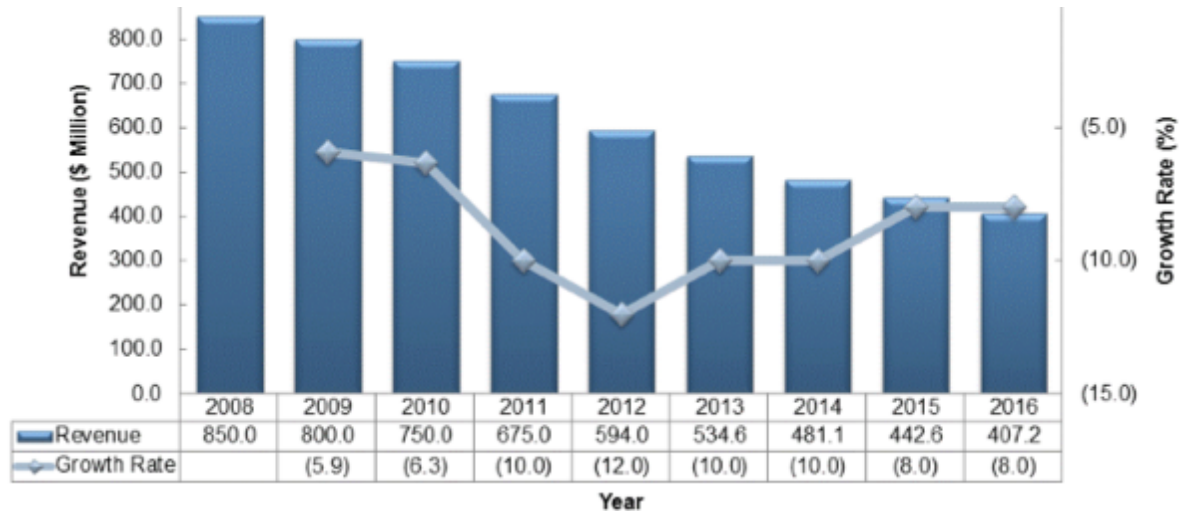
Figure 9.6: BMP segment: revenue forecast, United States, 2008-2016, CAGR = 9.6% (Frost & Sullivan)

Table 9.1: Current and future trends of market for bone graft and substitutes.

Measurement name	Measurement	Trend
Market stage (2011)	Mature	--
Market revenue (2011)	$1.633 B	Increasing
Average price per unit (2011)	$357.6	Increasing
Base year revenue growth rate	1.9%	Increasing
Compounded annual growth rate, 2011-2016	0.3%	Increasing
Customer price sensitivity (scale 1 to 10, low to high)	6	Stable
Degree of technical change (scale of 1 to 10, low to high)	7	Stable
Number of competitors (2011)	Over 40	Increasing
Number of companies that entered (2011)	0	Increasing
Average product development time (2011)	5 years	Stable

While the market size for bone repair grows, we anticipate that cost-effectiveness will continue to be a key driver at this level. There is direct evidence from interviewed surgeons, who report a disinclination to use Medtronic's InFuse^{TM} product because of

great cost to the patients with questionable benefits. Reimbursements for bone graft substitutes are moderate, but this is increasing. Nonetheless, current BMP-containing grafts cost more than quadruple the reimbursement, and therefore practitioners, and hospitals, are disinclined to purchase these grafts given their unclear advantage in the current formulation. With newer and more cost-effective methods for recombinant BMP production, cost of goods sold in the products will decrease for OsseoCHI making it more cost-effective and user-friendly graft substitute.

9.3.2 SWOT Analysis

Strengths

- Effective synthetic product

- Addressing an unmet need

- Simple storage and user interface

- Designed from platform technology allowing product development

- Reimbursement mechanism exists

- NIH credibility ($)

- Solid clinical and scientific leadership

Weakness

- Key component is a DNA biological

- Cash intensive biotechnology model

- Long development period

- Biologics increase cost of manufacturing

- Therapeutic products can involve potential liability

Opportunities

- Can expand the application/usage to spine, other orthopedic segments for market growth
- Appeal to several industry players for partnering
- Multi-billion dollar existing market
- Provide solution to current BMP risk
- Provide better bone graft substitute

Threats

- Negative publicity for InFuse
- DNA-based therapeutic
- Failure of industry-similar like OP-1
- Regulatory changes happening
- New unknown competitor products

9.3.3 Five Forces Analysis

Threats of Substitutes: The threat of substitutes for OsseoCHI product is medium as there are no products on the market, which use the same technology as ours, and patenting will protect of the product.

Threat of New Entrants: The threat of new entrants is medium for the product because there is unique formulation and manufacturing procedure used to make the product.

Therefore, it is extremely unlikely that a new product will be able to come in with respect to OsseoCHI and they would not get the benefit of first to market advantage.

Rivalry Among Existing Firms: The threat of rivalry among existing firms is medium. The bone graft substitute market is a competitive market, with a number of startups within the past couple of years. Given the demand in the orthopedic industry for better bone graft substitute, it indicates that the current products are not satisfactory and therefore effectively proved new products will be tried to determine their efficacy. Although, initially, we would be focusing on bone graft product without growth factor BMP 7, when it comes to BMP based products, there are only two main products available in the market and therefore will be able to overcome the competition.

Bargaining Power of Suppliers: The bargaining power of suppliers is low. The commercially purchased products will be chitosan and tri-polyphosphate for making the microparticles initially. There are multiple suppliers for each of these ingredients.

Bargaining Power of Buyers: The bargaining power of buyers will be medium for OsseoCHI. Initially, we plan on licensing the product, which will help in lean operations while maintaining enough profit margins to stay in business.

Osteo-Solutions plans on targeting a niche market, the minimally invasive, injectable spine and tibial fusion surgery industry.

Table 9.2: Five-Force Model to determine the attractiveness of market segment

Competitive forces	Threat to industry profitability		
	Low	Medium	High
Threat for substitutes		X	
Threat for new entrants		X	
Rivalry among existing firms		X	
Bargaining power of suppliers	X		
Bargaining power of buyers		X	

9.3.4 Customer Segment

The end users of this product would be the orthopedic surgeons performing spine surgeries. But in most of the cases, it will be the hospitals, who are the payers. There is a committee in the hospital called the value analysis committee (VAC) who based on the practitioners suggestion and hospital's budget will either agree or disagree to get the product to its shelf. Due to the decreased reimbursements from Medicare, Medicaid and other insurance firms, and increasing hospital expenditure, the VAC nowadays are very critical on making a decision of when to approve a product. Therefore the target customers for our product would be the surgeons and the hospitals. The key factors that are considered before choosing a particular product in this segment are contract

agreements, product efficacy (clinical and economic benefits), pricing, brand awareness, distribution network and service by the provider.

9.3.5 Competitors

In the BMPs segment, there are just two main competitors- Medtronic's (INFUSE) and Stryker (OP-1). BMPs are very expensive compared to the other bone graft materials available in the market. Though initially, the use of BMP has been approved for only one type of spinal fusion procedure – the anterior lumbar interbody fusion (ALIF), its off-label use continues to grow rapidly. Reports state that 85% of BMP use is off-label, mostly in spine region. Medtronic's INFUSE which consists of rhBMP-2 on an adsorbable collagen carrier has been associated with many adverse events like cervical swelling leading to complications. It is currently undergoing a review and results are expected this year. Stryker's OP-1 consists of rhBMP-7 and bovine collagen and was approved as an alternative to autograft in long bone non-unions where autograft is unfeasible. Clearly, when it comes to the revenue sector, Medtronic's has majority of the market share covering nearly 80% (Figure 9.7). This technology is still taking shape and there are several questions regarding the clinical efficacy that needs to be answered. And given the current practice, which relies on using low-cost autografts and allografts, surgeons will be reluctant to pick the prohibitively expensive BMP product.

Table 9.3: Bone morphogenetic protein segment market engineering measurements (Frost & Sullivan)

Measurement name	Measurement	Trend
Segment stage (2011)	Growth	--
Segment revenue (2011)	$675.0 M	Increasing
Average price per unit (2011)	$870.0	Increasing
Base year revenue growth rate	10.0 %	Increasing
Compounded annual growth rate, 2011-2016	9.6 %	Increasing
Customer price sensitivity (scale 1 to 10, low to high)	8	Increasing
Degree of technical change (scale of 1 to 10, low to high)	7	Increasing
Number of competitors	2	Stable
Brand loyalty (scale of 1 to 10, low to high)	7	Decreasing
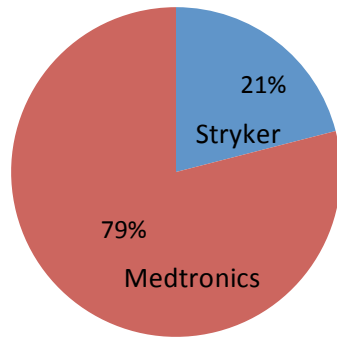
Figure 9.7: Bone morphogenetic segment: market share by revenue, United States, 2011.

9.4 Marketing Plan

9.4.1 Marketing

Marketing will be performed in conjunction with manufacturer or industry partner. The main emphasis of marketing will be on efficacy and safety of OsseoCHI for bone regeneration.

Sales representatives hired by the distribution company will primarily do advertising. Another effective way to promote our product will be through journal publications, meeting presentations, which are relatively inexpensive and advertising in medical journals, which cost somewhere in between $ 1,000 - $1,600.

9.4.2 Price and Margins

The direct manufacturing cost of 1 cc of the product (OsseoCHI) is expected to be $30. It is expected that 1 cc of OsseoCHI will be sold for $330, which is competitive in this current biological bone graft substitute market. We estimate approximately 50000 units

will be sold as a current market size, number of procedures statistics and given that many procedures will require multiple vials. The profit margin is expected to be approximately $200, with approximately $30/unit going to manufacturing when streamlined and $70/unit for distribution.

9.4.3 Distribution

If we move along through private or public financing without an industry partner, the initial plan is to distribute through third-party medical supply routes, where existing sales and distribution are in place. In case, we can license our product to an industry, we will use their distribution system to get into the market.

9.5 Design and Development

Initially, the focus will be on developing microparticles without growth factors to capture the niche market, and once the product has attained popularity, we will start focusing on BMP-7 incorporated microparticles. Customer feedback will be given utmost importance and the design will be perfected to maximize its selling in the market.

9.6 Manufacturing and Operations

The test OsseoCHI used for pre-clinical and early clinical trials will be manufactured in Toledo, Ohio. The facility will be in accordance with FDA guidelines for cGMP. The University of Toledo offers tremendous help to local startups, especially those from the research at the university and therefore, it will help cut down a lot of costs associated with renting space and operations in the initial stages of the startup. As clinical trials progress, a third party cGMP manufacturer will be contacted for packaging the implant.

Alternative sources of cheaper sources of components will also be evaluated as we go along.

9.7 Management Team and Organizational Structure

Venkata P. Mantripragada, Chief Technical Officer. Venkata Mantripragada has a bachelor's degree in Biotechnology and doctoral degree in biomedical engineering. Venkata has experience working in pharmaceutical quality control. She has also extensive experience as a researcher in plant tissue regeneration. Throughout the duration of her Ph.D. study, she has designed and prototyped three dimensional biodegradable and biocompatible bone graft substitute, OsseoCHI.

A. Champa Jayasuriya, Primary Mentor/Vice President. Jayasuriya currently holds the position of an Associate Professor at The University of Toledo. She received her master's degree in polymer science and technology and her Ph.D. degree in material science and engineering from Shizuoko University in Japan. Since past nine years, she has been actively involved in bone tissue engineering and regenerative medicine.

Stephen Callaway, Business Mentor. Callaway serves as an Assistant Professor of Management at The University of Toledo. He received his Ph.D. in Business Administration from Temple University and his primary fields of instruction and research include entrepreneurship and strategy development.

9.8 Financial Plan

Successful completion of the proposed project, with associated publications, presentations and advertisements will provide momentum for financing options (industry

or private sector equity financing) for product commercialization. A technology that has entered clinical stage is more likely to attract industry or private partnership because the regulatory risk has been minimized and also the time to return on-investment has become more acceptable. The most significant hurdle to overcome in obtaining human clinical data is the safety data that will be needed to fulfill the requirements for allowance of an IND from FDA allowing human testing. Financing for pre-clinical safety will require $3.0 million investment before moving to clinical testing. Risks associated with this regulatory pathway is that either the implant will not obtain good safety profile or too many additional tests will need to be conducted which will lead to depletion of capital. Further, we have already conducted extensive experimentation on rodents and histological and micro-CT data have indicated that OsseoCHI has shown no evidence of severe toxicity and therefore we are positive that OsseoCHI will act as a good scaffold for bone regeneration. Also the BMP-7 based scaffold have shown to locally deliver the growth factor and the proposed magnitude of concentration is lower than currently being used for commercial products.

As in any new device development, commercialization is expected to be delayed beyond Phase I/IIa clinical trials for approximately an additional 4 years. During the additional four years, the company will need new financing to complete Phase IIb and Phase III clinical trials and to finalize manufacturing processes. This is expected to cost an additional $40 million.

Table 9.4 Pro forma income statements over five-year period

Pro forma income statement, Years 1-5

	Year1	Year2	Year3	Year4	Year5
Net sales	$14000000	$34000000	$60000000	$160000000	$250000000
COGS	$11000000	$19000000	$30000000	$100000000	$155000000
Gross profit	$3000000	$15000000	$30000000	$60000000	$95000000
Advertising	$6000	$6000	$6000	$6000	$6000
Wages	$100000	$100000	$100000	$100000	$100000
Other	$4000	$4000	$4000	$4000	$4000
EBT	$2890000	$14890000	$29890000	$59890000	$94890000
Income tax	$90000	$90000	$90000	$90000	$90000
Net profit	$2800000	$14800000	$29800000	$59800000	$94800000

Break-even analysis

With variable cost/unit of $130, selling price/unit of $330, and fixed costs adding up to $44 million, break-even point will be reached in third year, when approximately 133203 units will be sold.

9.9 Critical Risks and Assumptions

9.9.1. Regulatory Approval

The US Food and Drug Administration (FDA) classifies most bone graft substitutes as Class II devices which are required to undergo a 510 (K) approval process (Figure 9.8). And this would be the case for our type 1 product- only microparticles, which has to prove that it is just as effective as one of the products already being used in the market. But for our type 2 products, which include BMP-7, it needs to undergo an approval process through PMA process with higher standards of clinical trials to prove its effectiveness. We may also choose to get our product approved under Humanitarian

Device Exemption (HDE), under which we will be approved to treat fewer than 4000 patients.
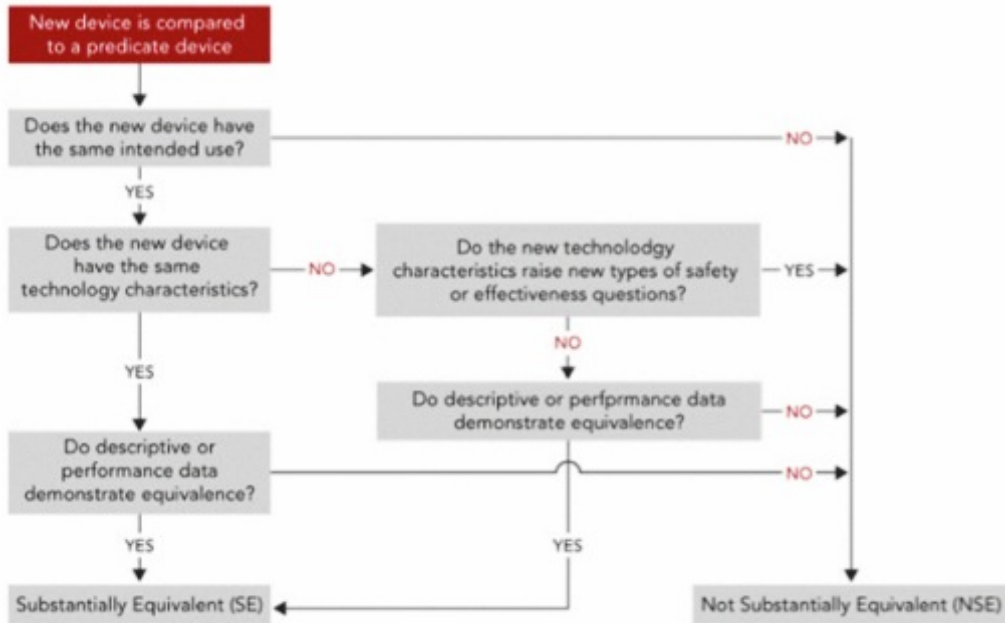
Figure 9.8: 510 (K) approval process.

9.9.2 IP Rights

We are working currently with the patent's office at The University of Toledo to submit a patent to protect the invention described in this project.

9.9.3 Raw Materials Supplies

We need to first tie up with manufacturers who can supply chitosan and tri-polyphosphate in bulk. For BMP7, there are very few companies (Pfizer) who manufacture it in bulk as it is an expensive procedure and we need to tie up with them.

References

1. Desai BM: Osteobiologics. *Am J Orthop* 2007;36:8-11.

2. US Centers for Disease Control and Prevention: http://www.cdc.gov/ncidod/dhqp/tissueTransplantsFAQ.html#d

3. Toolan BC: Current concepts review: Orthobiologics. *Foot Ankle Int* 2006;27:561-566.

4. Mantripragada VP, Lecka-Czernik B, Ebraheim NA, Jayasuriya AC. An overview of recent advances in designing orthopedic and craniofacial implants. J Biomed Mater Res A. 2013; 101: 3349-64.

5. De Long WG, Einhorn TA, Koval K, et al: Current concepts review: Bone grafts and bone graft substitutes in orthopaedic trauma surgery. *J Bone Joint Surg AM* 2007;89:649-658.

6. El-Ghannam A, Cunningham Jr L, Pienkowski D, Hart A. Bone engineering of the rabbit ulna. J Oral Maxillofac Surg. 2007; 65: 1495–502.

7. Liu XH, Ma PX. Polymeric scaffolds for bone tissue engineering. Ann Biomed Eng. 2004; 32: 477–86.

8. Li Z, Ramay HR, Hauch KD, Xiao D, Zhang M. Chitosan/alginate hybrid scaffolds for bone tissue engineering. Biomaterials. 2005; 26: 3919–28.

9. Lee JY, Nam SH, Im SY, Park YJ, Lee YM, Seol YJ. Enhanced bone formation by controlled growth factor delivery from chitosan based biomaterials. J Control Rel. 2002; 78: 187–97.

10. Taichman RS. Blood and bone: Two tissues whose fates are intertwined to create the hematopoietic stem cell niche. Blood. 2005; 105 :2631 –2639.

11. Eriksen EF, Axelrod DW, Melsen F. Bone Histomorphometry, New York, Raven Press,1994. pp1–12.

12. Clarke B. Normal bone anatomy and physiology. Clin J Am Soc Nephrol. 2008; 3: 131-139.

13. Pittenger MF, Mackay AM, Beck SC, Jaiswal RK, Douglas R, Mosca JD, Moorman MA, Simonetti DW, Craig S, Marshak DR. Multilineage potential of adult human mesenchymal stem cells. Science. 1990; 284 :143 –147.

14. Teitelbaum SL, Ross FP. Genetic regulation of osteoclast development and function. Nat Rev Genet. 2003; 4: 638 –649.

15. Kobayashi S, Takahashi HE, Ito A, Saito N, Nawata M, Horiuchi H, Ohta H, Ito A, Iorio R, Yamamoto N, Takaoka K. Trabecular minimodeling in human iliac bone. Bone. 2003; 32 :163 –169.

16. Parfitt AM. Targeted and nontargeted bone remodeling: Relationship to basic multicellular unit origination and progression. Bone. 2002; 30: 5 –7.

17. Roodman GD. Cell biology of the osteoclast. Exp Hematol. 1999; 27: 1229 –1241.

18. Boyle WJ, Simonet WS, Lacey DL. Osteoclast differentiation and activation. Nature. 2003; 423 :337 –342.

19. Blair HC, Athanasou NA. Recent advances in osteoclast biology and pathological bone resorption. Histol Histopathol. 2004; 19: 189 –199.

20. Silver IA, Murrills RJ, Etherington DJ. Microelectrode studies on the acid microenvironment beneath adherent macrophages and osteoclasts. Exp Cell Res. 1988; 175: 266 –276.

21. Delaisse JM, Andersen TL, Engsig MT, Henriksen K, Troen T, Blavier L. Matrix metalloproteinases (MMP) and cathepsin K contribute di=fferently to osteoclast activities. Microsc Res Tech. 2003; 61: 504 –513.

22. Reddy SV. Regulatory mechanisms operative in osteoclasts. Crit Rev Eukaryot Gene Expr. 2004; 14: 255 –270.

23. Hock JM, Centrella M, Canalis E. Insulin-like growth factor I (IGF-I) has independent effects on bone matrix formation and cell replication. Endocrinology. 2004; 122: 254 –260.

24. Locklin RM, Oreffo RO, Triffitt JT. Effects of TGFbeta and bFGF on the differentiation of human bone marrow stromal fibroblasts. Cell Biol Int. 1999; 23: 185 –194.

25. Smit TH, Burger EH, Huyghe JM. Is BMU-coupling a strain-regulated phenomenon? A finite element analysis. J Bone Miner Res. 2002; 15: 301 –307.

26. Logan CY, Nusse R. The Wnt signaling pathway in development and disease. Annu Rev Cell Dev Biol. 2004; 20: 781 –810.

27. Anderson HC. Matrix vesicles and calcification. Curr Rheumatol Rep. 2003; 5: 222 –226.

28. Burger EH, Klein-Nuland J, Smit TH. Strain-derived canalicular fluid flow regulates osteoclast activity in a remodeling osteon: A proposal. J Biomech. 2003; 36: 1452 –1459.

29. Bonewald LF. Establishment and characterization of an osteocyte-like cell line, MLO-Y4. J Bone Miner Metab. 1999; 17: 61 –65.

30. Rubin CT, Lanyon LE. Osteoregulatory nature of mechanical stimuli: Function as a determinant for adaptive bone remodeling. J Orthop Res. 1987; 5: 300 –310.

31. Jorgensen NR, Teilmann SC, Henriksen Z, Civitelli R, Sorensen OH, Steinberg TH. Activation of L-type calcium channels is required for gap junction-mediated intercellular calcium signaling in osteoblastic cells. J Biol Chem. 2003; 278: 4082 –4086.

32. Dobnig H, Turner RT. Evidence that intermittent treatment with parathyroid hormone increases bone formation in adult rats by activation of bone lining cells. Endocrinology. 1995; 136: 3632 –3638.

33. Hauge EM, Qvesel D, Eriksen EF, Mosekilde L, Melsen F. Cancellous bone remodeling occurs in specialized compartments lined by cells expressing osteoblastic markers. J Bone Miner Res. 2001; 16: 1575 –1582.

34. Landis WJ. The strength of a calcified tissue depends in part on the molecular structure and organization of its constituent mineral crystals in their organic matrix. Bone. 1995; 16: 533 –544.

35. Gerstenfeld LC, Alkhiary YM, Krall EA. Three-dimensional reconstruction of fracture callus morphogenesis. Journal of Histochemistry & Cytochemistry. 2006; 54: 1215–28.

36. Cho TJ, Gerstenfeld LC, Einhorn TA. Differential temporal expression of members of the transforming growth factor beta superfamily during murine fracture healing. J Bone Min Res. 2002; 17: 513–20

37. Perren SM. Evolution of the internal fixation of long bone fractures. The scientific basis of biological internal fixation: choosing a new balance between stability and biology. J Bone Joint Surg Br. 2002; 84: 1093–110.

38. Gerstenfeld LC, Cullinane DM, Barnes GL. Fracture healing as a post-natal developmental process: molecular, spatial, and temporal aspects of its regulation. J Cell Biochem. 2003; 88: 873–84.

39. Kitaori T, Ito H, Schwarz EM. Stromal cell-derived factor 1/CXCR4 signaling is critical for the recruitment of mesenchymal stem cells to the fracture site during skeletal repair in a mouse model. Arthritis Rheum. 2009; 60: 813–23.

40. Yang X, Ricciardi BF, Hernandez-Soria A. Callus mineralization and maturation are delayed during fracture healing in interleukin-6 knockout mice. Bone. 2007; 41: 928–36.

41. Granero-Molto F, Weis JA, Miga MI. Regenerative effects of transplanted mesenchymal stem cells in fracture healing. Stem Cells. 2009; 27: 1887–98.

42. Bais MV, Wigner N, Young M. BMP2 is essential for post natal osteogenesis but not for recruitment of osteogenic stem cells. Bone. 2009; 45: 254–66.

43. Wan C, Gilbert SR, Wang Y. Activation of the hypoxia-inducible factor-1alpha pathway accelerates bone regeneration. Proceedings of the National Academy of Sciences of the United States of America. 2008; 105: 686-691.

44. Einhorn TA. The cell and molecular biology of fracture healing. Clinical Orthop Rel Res. 1998; 355: S7-21.

45. Tsuji K, Bandyopadhyay A, Harfe BD. BMP2 activity, although dispensable for bone formation, is required for the initiation of fracture healing. Nature Gen. 2006; 38: 1424-9.

46. Lehmann W, Edgar CM, Wang K. Tumor necrosis factor alpha (TNF-alpha) coordinately regulates the expression of specific matrix metalloproteinases (MMPS) and angiogenic factors during fracture healing. Bone. 2005; 36: 300–10.

47. Ai-Aql ZS, Alagl AS, Graves DT. Molecular mechanisms controlling bone formation during fracture healing and distraction osteogenesis. J Den Res. 2008; 87: 107-18.

48. Bassett CAL. Biophysical principles affecting bone structure. In: Bourne, GH., editor. Biochemistry and Physiology of bone. 2. Academic Press; New York: 1971. p.341-376.

49. Shapiro F. Cortical bone repair. The relationship of the lacunar-canalicular system and intercellular gap junctions to the repair process. J Bone Joint Surg Am. 1988; 70: 1067-81.

50. Kaderly RE. Primary bone healing. Seminars in Veterinary Medicine & Surgery (Small Animal). 1991; 6: 21-5.

51. Shapiro F. Cortical bone repair. The relationship of the lacunar-canalicular system and intercellular gap junctions to the repair process. J Bone Joint Surg Am. Volume. 1988; 70:1067-81.

52. Lienemann PS, Lutolf MP, Ehrbar M. Biomimetic hydrogels for controlled biomolecule delivery to augment bone regeneration. Adv Drug Deliv Rev. 2012; 64: 1078-89.

53. Praemer A, Furner S, Rice DP. Musculoskeletal conditions in the United States. Rosemont (IL): American Academy of Orthopaedic Surgeons. Frequency of occurrence. 1999; p. 83-7.

54. Wiss DA, Stetson WB. Tibial nonunion: treatment alternatives. J Am Acad Orthop Surg. 1996; 4: 249-257.

55. Clement ND, Beauchamp NJ, Duckworth AD, McQueen MM, Court-Brown CM. The outcome of tibial diaphyseal fractures in the elderly. Bone Joint J. 2013; 95: 1255-62.

56. Porter JR, Ruckh TT, Popat KC. Bone tissue engineering – a review in bone biomimetics and drug delivery strategies. Biotechnol Prog. 2009; 25: 1539-60.

57. Silber JS, Anderson DG, Daffner SD, Brislin BT, Leland JM, Hilibrand AS, Vaccaro AR, Albert TJ. Donor site morbidity after anterior iliac crest bone harvest for single-level anterior cervical discectomy and fusion. Spine. 2003; 28: 134–139.

58. Heary RF, Schlenk RP, Sacchieri TA, Barone D, Brotea C. Persistent iliac crest donor site pain: independent outcome assessment. Neurosurgery. 2002; 50: 510–516.

59. Kretlow JD, Mikos AG. Review: mineralization of synthetic polymer scaffolds for bone tissue engineering. Tissue Eng. 2007; 13: 927–938.

60. Nakajima T, Iizuka H, Tsutsumi S, Kayakabe M, Takagishi K. Evaluation of posterolateral spinal fusion using mesenchymal stem cells: differences with or without osteogenic differentiation. Spine. 2007; 32: 2432–2436.

61. Arrington ED, Smith WJ, Chambers HG, Bucknell AL, Davino NA. Complications of iliac crest bone graft harvesting. Clin Orthop Relat Res. 1996; 329: 300–309.

62. Gitelis S, Saiz P. What's new in orthopedic surgery. J Am Coll Surg. 2002; 194: 788–791.

63. Banwart JC, Asher MA, Hassanein RS. Iliac crest bone graft harvest donor site morbidity. A statistical evaluation. Spine.1995; 20: 1055–1060.

64. Mankin HJ, Hornicek FJ, Raskin KA. Infection in massive bone allografts. Clin Orthop Relat Res. 2005; 432: 210–216.

65. Nishida J, Shimamura T. Methods of reconstruction for bone defect after tumor excision: a review of alternatives. Med Sci Monit. 2008;14:RA107–RA113.

66. Hou CH, Yang RS, Hou SM. Hospital-based allogenic bone bank—10-year experience. J Hosp Infect. 2005;59:41–45.

67. Yang YG, Sykes M. Xenotransplantation: current status and a perspective on the future. Nat Rev Immunol. 2007; 7: 519–531.

68. Yoo D, Giulivi A. Xenotransplantation and the potential risk of xenogeneic transmission of porcine viruses. Can J Vet Res. 2000; 64: 193–203.

69. Laurencin CT, El-Amin SF. Xenotransplantation in orthopedic surgery. J Am Acad Orthop Surg. 2008; 16: 4–8.

70. Aryaei A, Jayatissa AH, Jayasuriya AC. Nano and Micro Mechanical Properties of Cross-Linked Chitosan Samples. Journal of the Mechanical Behavior of Biomedical Materials. J Mech Behav Biomed Mater 2012; 5: 82-89.

71. Jayasuriya AC, Aryaei A, Jayatissa AH. Study of Mesenchymal Stem Cell Function on Zinc Oxide Nanoparticles. Mat Sci Eng C Mater Biol Appl. 2013; 33: 3688-96.

72. Aryaei A, Jayatissa AH, Jayasuriya AC. Mechanical and biological properties of chitosan-carbon nanotube nanocomposite films. J Biomed Mater Res A. 2013 [Epub ahead of print].

73. Aryaei A, Jayatissa AH, Jayasuriya AC. The effect of graphene substrate on osteoblast cell adhesion and proliferation. J Biomed Mater Res A. 2013 [Epub ahead of print].

74. Aryaei A, Liu J, Jayasuriya AC. Mechanical properties of calcium phosphate-chitosan composites. J Biomed Mater Res A. (In review).

75. Langer R, Vacanti JP. Tissue engineering. Science. 1993;260: 920–926.

76. Albrektsson T, Johansson C. Osteoinduction, osteoconduction and osseointegration. Eur Spine J. 2001; 10: S96– S101.

77. Mistry AS, Mikos AG. Tissue engineering strategies for bone regeneration. Adv Biochem Eng Biotechnol. 2005; 94: 1–22.

78. Jayasuriya AC, Shah C, Ebraheim NA, Jayatissa AH. Acceleration of biomimetic mineralization to apply in bone regeneration. Biomed Mat. 2008; 3: 015003.

79. Jayasuriya AC, Ebraheim NA. Evaluation of Bone Matrix and Demineralized Bone Matrix Incorporated PLGA Matrices for Bone Repair. J Mater Sci: Materials in Medicine. 2009; 20: 1637-1644.

80. Jayasuriya AC, Mauch KJ, Ebraheim NA. Fabrication and Characterization of Injectable Biomaterials for Biomedical Applications. Advan Mater Res. 2012; 383-390: 4065-4069.

81. Jayasuriya AC, Darr A. Controlled release behavior of cisplatin encapsulated poly(lactic-co-glycolic acid) nanoparticles. J Biomed Sci Engg. 2013; 6, 586-592.

82. Dreifke M, Ebraheim NA, Jayasuriya AC. Investigation of Potential Injectable Polymeric Biomaterials for Bone Regeneration. J Biomed Mater Res A 2013; 101: 2436-2447.

83. Jayakumar R, Menon D, Manzoor K, Nair SV, Tamura H. Biomedical applications of chitin and chitosan based nanomaterials—A short review. Carbohydr Polym. 2010; 82: 227-232.

84. Kim IY, Seo SJ, Moon HS, Yoo MK, Park IY, Kim BC, Cho CS. Chitosan and its derivatives for tissue engineering applications. Biotechnol. Adv. 2008; 26: 1-21.

85. Peter M, Ganesh NSN, Nair SV, Furuike T, Tamura H, Jayakumar R. Preparation and characterization of chitosan-gelatin/nanohydroxyapatite composite scaffolds for tissue engineering applications. Carbohydr Polym. 2010; 80: 687-694.

86. Cui J, Liang J, Wen Y, Sun X, Li T, Zhang G, Sun K, Xu X. In vitro and in vivo evaluation of chitosan/β-glycerol phosphate composite membrane for guided bone regeneration. J Biomed Mater Res A. 2013 [Epub ahead of print].

87. Bhat A, Wooten RM, Jayasuriya AC. Secretion of growth factors from macrophages when cultured with microparticles. J Biomed Mater Res A 2013; 101:3170-3180.

88. Di Martino A, Sittinger M, Risbud MV. Chitosan: A versatile biopolymer for orthopaedic tissue-engineering. Biomaterials. 2005; 26: 5983-5990.

89. Senel S, McClure SJ. Potential applications of chitosan in veterinary medicine. Adv Drug Deliv Rev. 2004; 56: 1467-1480.

90. Khor E, Lim LY. Implantable applications of chitin and chitosan. Biomaterials. 2003; 24: 2339-2349.

91. Bumgardner JD, Wiser R, Gerard PD, Bergin P, Chestnutt B, Marini M, Ramsey V, Elder SH, Gilbert JA. Chitosan: Potential use as a bioactive coating for othopaedic and craniofacial/dental implants. J Biomater Sci Polym Ed. 2003; 14: 429-438.

92. Kumar MNVR. A review of chitin and chitosan applications. React Funct Polym. 2000; 46: 1-27.

93. Jaworska M, Sakurai K, Gaudon P, Guibal E. Influence of chitosan characteristics on polymer properties: I: Crystallographic properties. Polym Int. 2003; 52: 198-205.

94. Freier T, Koh HS, Kazazian K, Shoichet MS. Controlling cell adhesion and degradation of chitosan films by N-acetylation. Biomaterials. 2005; 26: 5872-5872.

95. Harish Prashanth KK, Kittur FS, Tharanathan RN. Solid state structure of chitosan prepared under different N-deacetylating conditions. Carbohydr Polym. 2002; 50: 27-33.

96. Prasitsilp M, Jenwithisuk R, Kongsuwan K, Damrongchai N, Watts P. Cellular responses to chitosan in vitro: The importance of deacetylation. J Mater Sci Mater Med. 2000; 11: 773-778.

97. Hidaka Y, Ito M, Mori K, Yagasaki H, Kafrawy AH. Histopathological and immunohistochemical studied of membranes of deacetylated chitin derivatives implanted over rat calvaria. J Biomed Mater Res. 1999; 46: 418-423.

98. Cao WL, Jing DH, Li JM, Gong YD, Zhao NM, Zhang XF. Effects of the degree of deacetylation on the physicochemical properties and Schwann cell affinity of chitosan films. J Biomater Appl. 2005; 20: 157-177.

99. Hsu SH, Whu SW, Tsai CL, Wu YH, Chen HW, Hsieh KH. Chitosan as Scaffold Materials: Effects of Molecular Weight and Degree of Deacetylation. J Poly Res. 2004; 11: 141-147.

100. Lieberman JR, Daluiski A, Einhorn TA. The role of growth factors in the repair of bone. Biology and clinical applications. J Bone Joint Surg Am. 2002; 84: 1032–1044.

101. Wozney JM, Rosen V, Celeste AJ. Novel regulators of bone formation: molecular clones and activities. Science. 1988; 242: 1528–1534.

102. Friedlaender GE, Perry CR, Cole JD. Osteogenic protein-1 (bone morphogenetic protein-7) in the treatment of tibial nonunions. J Bone Joint Surg Am. 2001; 83: 151-158.

103.   Reddi AH. Bone morphogenetic proteins: from basic science to clinical applications. J Bone Joint Surg Am. 2001; 83: S1-S6.

104.   Edgar CM, Chakravarthy V, Barnes G, Kakar S, Gerstenfeld LC, Einhorn TA. Autogenous regulation of a network of bone morphogenetic proteins (BMPs) mediates the osteogenic differentiation in murine marrow stromal cells. Bone. 2007; 40: 1389-1398.

105.   Andrades JA, Han B, Nimni ME, Ertl DC, Simpkins RJ, Arrabal MP, Becerra J. A modified rhTGF-β1 and rhBMP-2 are effective in initiating a chondro-osseous differentiation pathway in bone marrow cells cultured in vitro. Conn Tissue Res. 2003; 44: 188-197.

106.   Andrades JA, Santamaría JA, Nimni ME, Becerra J. Selection and amplification of a bone marrow cell population and its induction to the chondro-osteogenic lineage by rhOP-1: an in vitro and in vivo study. Int J Dev Biol. 2001; 45: 689-693.

107.   Cheng H, Jiang W, Phillips FM. Osteogenic activity of the fourteen types of human bone morphogenetic proteins (BMPs). J Bone Joint Surg Am. 2003; 85: 1544-52.

108.   Swolin D, Brantsing C, Matejka G, Ohlsson C. Cortisol decreases IGF-I mRNA levels in human osteoblast-like cells. J Endocrinol. 1996; 149: 397-403.

109.   Lind M. Growth factors, possible new clinical tools: a review. Acta Orthop Scand. 1996; 67: 407-417.

110.   Ohlsson C, Bengtsson BA, Isaksson OG, Andreassen TT, Slootweg MC. Growth hormone and bone. Endocr Rev. 1998; 19: 557-9.

111.   Cheng H, Jiang W, Phillips FM. Osteogenic activity of the fourteen types of human bone morphogenetic proteins (BMPs). J Bone Joint Surg Am. 2003; 85: 1544-52.

112.   Allori AC, Sailon AM, Warren SM. Biological basis of bone formation, remodeling, and repair-part II: extracellular matrix. Tissue Eng Part B Rev. 2008; 14: 275–283.

113.   Hacker U, Nybakken K, Perrimon N. Heparan sulphate proteoglycans: the sweet side of development. Nat Rev Mol Cell Biol. 2005; 6: 530–541.

114.   Macri L, Silverstein D, Clark RA. Growth factor binding to the pericellular matrix and its importance in tissue engineering. Adv Drug Deliv Rev. 2007; 59: 1366–1381.

115.   Gandhi NS, Mancera RL. Free energy calculations of glycosaminoglycan–protein interactions. Glycobiology. 2009; 19: 1103–1115.

116.   Hynes RO. The extracellular matrix: not just pretty fibrils. Science. 2009; 326: 1216–1219.

117.   Gautschi OP, Frey SP, Zellweger R. Bone morphogenetic proteins in clinical applications. ANZ J Surg. 2007; 77: 626–631.

118.   Luginbuehl V, Meinel L, Merkle HP, Gander B. Localized delivery of growth factors for bone repair. Eur J Pharm Biopharm. 2004; 58: 197–208.

119.   Molin D, Post MJ. Therapeutic angiogenesis in the heart: protect and serve. Curr Opin Pharmacol. 2007; 7: 158–163.

120.   Barnes GL, Kakar S, Vora S, Morgan EF, Gerstenfeld LC, Einhorn TA. Stimulation of fracture-healing with systemic intermittent parathyroid hormone

treatment. J Bone Joint Surg Am. 2008; 90: 120–127.

121.   Eppler SM, Combs DL, Henry TD, Lopez JJ, Ellis SG, Yi JH, Annex BH, McCluskey ER, Zioncheck TF. A target-mediated model to describe the pharmacokinetics and hemodynamic effects of recombinant human vascular endothelial growth factor in humans. Clin Pharmacol Ther. 2002; 72: 20–32.

122.   Lee K, Silva EA, Mooney DJ. Growth factor delivery-based tissue engineering: general approaches and a review of recent developments. J R Soc Interface. 2011; 8: 153–170

123.   Saik JE, Gould DJ, Watkins EM, Dickinson ME, West JL. Covalently immobilized platelet-derived growth factor-BB promotes angiogenesis in biomimetic poly(ethylene glycol) hydrogels. Acta Biomater. 2011; 7: 133–143.

124.   Carmeliet P. Mechanisms of angiogenesis and arteriogenesis. Nat Med. 2000; 6: 389–395.

125.   Lee RJ, Springer ML, Blanco-Bose WE, Shaw R, Ursell PC, Blau HM. VEGF gene delivery to myocardium: deleterious effects of unregulated expression. Circulation. 2000; 102: 898–901.

126.   Chen RR, Mooney DJ. Polymeric growth factor delivery strategies for tissue engineering. Pharm. Res. 2003; 20: 1103–1112.

127.   Ehrbar M, Djonov VG, Schnell C, Tschanz SA, Martiny-Baron G, Schenk U, Wood J, Burri PH, Hubbell JA, Zisch AH. Cell-demanded liberation of VEGF121 from fibrin implants induces local and controlled blood vessel growth. Circ Res. 2004; 94: 1124-32.

128.   Ehrbar M, Rizzi SC, Hlushchuk R, Djonov V, Zisch AH, Hubbell JA,

Weber FE, Lutolf MP. Enzymatic formation of modular cell-instructive fibrin analogs for tissue engineering. Biomaterials 2007; 28: 3856–3866.

129. Lanza RP, Langer RS, Vacanti J. Principles of tissue engineering. The Netherlands: Elsevier Academic. 2007

130. Mooney DJ, Kaufmann PM, Sano K, Mcnamara KM, Vacanti JP, Langer R. Transplantation of hepatocytes using porous, biodegradable sponges. Transplant Proc. 1994; 26: 3425–3426.

131. Hsu YY, Gresser JD, Trantolo DJ, Lyons CM, Gangadharam PR, Wise DL. Effect of polymer foam morphology and density on kinetics of *in vitro* controlled release of isoniazid from compressed foam matrices. J Biomed Mater Res. 1997; 35: 107–116.

132. Whang K, Thomas CH, Healy KE, Nuber G. A novel method to fabricate bioabsorbable scaffolds. Polymer. 1995; 36: 837–842.

133. Hua FJ, Kim GE, Lee JD, Son YK, Lee DS. Macroporous poly(L-lactide) scaffold. 1. Preparation of a macroporous scaffold by liquid–liquid phase separation of a PLLA–dioxane–water system. J Biomed Mater Res. 2002; 63: 161–167

134. Lo H, Ponticiello MS, Leong KW. Fabrication of controlled release biodegradable foams by phase separation. Tissue Eng. 1995; 1: 15–28.

135. Thomson RC, Yaszemski MJ, Powers JM, Mikos AG. Fabrication of biodegradable polymer scaffolds to engineer trabecular bone. J Biomater Sci Polym Ed. 1995; 7: 23–38.

136. Busby W, Cameron NR, Jahoda CA. Emulsion-derived foams

(PolyHIPEs) containing poly(epsilon-caprolactone) as matrixes for tissue engineering. Biomacromolecules. 2001; 2: 154–164.

137.   Bryant SJ, Anseth KS. The effects of scaffold thickness on tissue engineered cartilage in photocrosslinked poly(ethylene oxide) hydrogels. Biomaterials. 2001; 22: 619–626.

138.   Temenoff JS, Park H, Jabbari E, Conway DE, Sheffield TL, Ambrose CG, Mikos AG. Thermally cross-linked oligo(poly(ethylene glycol) fumarate) hydrogels support osteogenic differentiation of encapsulated marrow stromal cells *in vitro*. Biomacromolecules. 2004; 5: 5–10.

139.   Mooney DJ, Baldwin DF, Suh NP, Vacanti JP, Langer R. Novel approach to fabricate porous sponges of poly(D,L-lactic-co-glycolic acid) without the use of organic solvents. Biomaterials. 1996; 17: 1417–1422.

140.   Lee K, Silva EA, Mooney DJ. Growth factor delivery-based tissue engineering: general approaches and a review of recent developments. J R Soc Interface. 2011; 8: 153-170.

141.   Zhu XH, Wang CH, Tong YW. In vitro characterization of hepatocyte growth factor release from PHBV/PLGA microsphere scaffold. J Biomed Mater Res A. 2009; 89: 411–42.

142.   Berbari EF, Steckelberg JM, Osmon DR. Osteomyelitis. In: Mandell GL, Bennett JE, Dolin R, editors. Principles and practice of infectious diseases. 6th ed., New York: Churchill Livingstone; 2005. p. 1323–32.

143.   Lazzarini L, Mader JT, Calhoun JH. Osteomyelitis in long bones. J Bone Joint Surg. 2004; 86: 2305-2318.

144.   Lew DP, Waldvogel FA. Osteomyelitis. Lancet 2004; 364: 369-379.

145.   Wright JA, Nair SP. Interaction of staphylococci with bone. Inter J Med Micro. 2010; 300: 193-204.

146.   Khali H, William RJ, Stenbeck G, Henderson B, Meghji S, Nair SP. Invasion of bone cells by Staphylococcus epidermidis. Microbes Infect 2007; 9: 460-465.

147.   Zalavras CG, Christensen T, Rigopoulos N, Holtom P, Patzakis MJ. Infection following operative treatment of ankle fractures. Clin Orthop Relat Res. 2009; 467: 1715-1720.

148.   Vallianou N, Evangelopoulos A, Makri P, Zacharias G, Stefanitsi P, Karachalios A, Avgerinos PC. Vertebral osteomyelitis and native valve endocarditis due to Staphylococcus simulans: a case report. J Med Case Rep. 2008; 2: 183.

149.   Inman RD, Gallegos KV, Brause BD, Redecha PB, Christian CL. Clinical and microbial features of prosthetic and joint infection. Am J Med. 1984; 77: 47–53.

150.   Bandyk DF, Berni GA, Thiele BL, Towne JB. Aorto-femoral graft infections due to Staphylococcus epidermidis. Arch Surg 1984; 119: 102–8.

151.   Christensen GD, Simpson WA, Bisno AL, Beachey EH. Adherence of slime-producing strains of Staphylococcus epidermidis to smooth surfaces. Infect Immun. 1982; 37: 318–26.

152.   Christensen GD, Simpson WA, Bisno AL, Beachey EH. Experimental foreign body infections in mice challenged with slime-producing Staphylococcus epidermidis. Infect Immun. 1983; 40: 407–10.

153.   U.K.Health Protection Agency, 2008. Surgical Site Infection–National aggregated data on Surgical Site Infections for hospitals that have participated in Surgical Site Infection Surveillance Scheme (SSISS) between October 1997 and December 2005.

154.   Costerton JW, Cheng KJ, Geesey GG, Ladd TI, Nickel JC, Dasgupta M, Marrie TJ. Bacterial biofilms in nature and disease. Annu Rev Microbiol. 1987; 41: 435–464.

155.   Gristina AG, Oga M, Webb LX, Hobgood CD. Adherent bacterial colonization in the pathogenesis of osteomyelitis. Science 1985; 228: 990–993.

156.   Engelman AF, Van Dan GM, Van der Mei HC, Buscher HJ, Ploeg RJ. In vivo evaluation of bacterial infection involving morphologically different surgical meshes. Ann Surg. 2010; 251: 133–137.

157.   Gristina AG, Naylor P, Myrvik QN. Infections from biomaterials and implants: a race for the surface. Med Prog Technol, 1988; 14: 205–224.

158.   Engelsman AF, Krom BP, Busscher HJ, van Dam GM, Ploeg RJ, van der Mei HC. Antimicrobial effects of an NO-realising poly(ethylene vinylacetate) coating on soft-tissue implants in vitro in a murine model. Acta Biomater. 2009; 5: 1905–1910.

159.   Kong M, Chen XG, Xing K, Park HJ. Antimicrobial properties of chitosan and mode of action: A state of art review. Int J Food Micro. 2010; 144: 51-63.

160.   Zivanovic S, Basurto CC, Chi S, Davidson PM, Weiss J. Molecular weight of chitosan influences antimicrobial activity in oil-in-water emulsions. J Food Prot. 2004; 67: 952–959.

161.   Zivanovic S, Chi S, Draughon AF. Antimicrobial activity of essential oils incorporated in chitosan films. J Food Sci. 2005; 70: 45–51.

162.   Zivanovic S, Li JJ, Davidson PM, Kit K. Physical, mechanical and antimicrobial properties of chitosan/PEO blend films. Biomacromolecules. 2007; 8: 1505–1510.

163.   Jiang B, Li B. Polypeptide Nanocoatings for Preventing Dental and Orthopaedic Device-Associated Infection: pH-Induced Antibiotic Capture, Release, and Antibiotic Efficacy. J Biomed Mat Res Part B. 2007; 88: 332-338.

164.   Takemono K, Sunamoto J, Askasi M. Polymers and Medical Care. Mita, Tokyo; 1989; Chapter IV.

165.   Marzona L, Pavolini B. Play and players in bone fracture healing match. Clin Cases Miner Bone Metab. 2009; 6: 159–162.

166.   Lienau J, Schmidt-Bleek K, Peters A, Weber H, Bail HJ, Duda G, Perka C, Schell H. Insight into the molecular patho-physiology of delayed bone healing in a sheep model, Tissue Eng Part A. 2010; 16: 191–199.

167.   Qiu LY, Bae YH. Self-assembled polyethylenimine–graft-poly(e-caprolactone) micelles as potential dual carriers of genes and anticancer drugs. Biomaterials. 2007; 28: 4132–42.

168.   Lee JS, Bae JW, Joung YK, Lee SJ, Han DK, Park KD. Controlled dual release of basic fibroblast growth factor and indomethacin from heparin-conjugated polymeric micelle. Int J Pharm. 2008; 346: 57–63.

169.   Huang ZM, Yang AH. Encapsulation of pure drugs ento the central part of polycaprolactone ultrafine fibers. Acta Polymer Sin. 2006; 1: 48–52.

170.   Martins A, Duarte ARC, Faria S, Marques AP, Reis RL, Neves NM. Osteogenic induction of hBMSCs by electrospun scaffolds with dexamethasone release functionality. Biomaterials. 2010; 31: 5875–85.

171.   Duarte AR, Mano JF, Reis RL. Dexamethasone-loaded scaffolds prepared by supercritical-assisted phase inversion. Acta Biomater. 2009; 5: 2054–62.

172.   Schofer MD, Fuchs-Winkelmann S, Gräbedünkel C, Wack C, Dersch R, Rudisile M. Influence of poly(L-lactic acid) nanofibers and BMP-2-containing poly(L-lactic acid) nanofibers on growth and osteogenic differentiation of human mesenchymal stem cells. The Scientific World J. 2008; 8: 1269–79.

173.   Zhao YN, Chen B, Lin H, Sun WJ, Zhao WX, Zhang J, et al. The bone-derived collagen containing mineralized matrix for the loading of collagen-binding bone morphogenetic protein-2. J Biomed Mater Res A. 2009; 88: 725–34.

174.   Ryu SJ, Jung H, Oh JM, Lee JK, Choy JH. Layered double hydroxide as novel antibacterial drug delivery system. J Phy Chem Sol 2010;71:685-688.

175.   Cunha BA, Gossling HR, Pasternak HS, Nightingale CH, Quintiliani R. The penetration characteristics of cefazolin, cephalothin, and cephradine into bone in patients undergoing total hip replacement. J Bone Joint Surg Am. 1977; 59: 856-859.

176.   Cunha BA, Gossling HR, Pasternak HS, Nightingale CH, Quintiliani R. Penetration of cephalosporins into bone. Infection. 1984; 12: 80-84.

177.   Zeller V, Desplaces N. Antibiotherapy of bone and joint infections. Rev Rhum. 2006; 73: 129-135.

178.   Barberan J. Management of infections of osteoarticular prosthesis. Clin Microbiol Infect. 2006; 12: 93-101.

179.   Rayner C, Munckhof WJ. Antibiotics currently used in the treatment of infections caused by Staphylococcus aureus. Intern Med J. 2005; 36: 142-143.

180.   Jayasuriya AC, Bhat A. Optimization of scaled up chitosan microparticles, Biomed. Mat. 2009; 4: 5-12.

181.   Jayasuriya AC, Bhat A. Fabrication and Characterization of Novel Hybrid Organic/Inorganic Microparticles to apply in Bone Regeneration. J Biomed Mater Res A. 2010; 93:1280-1288.

182.   Bhat A, Dreifke M, Gomez C, Kandimalla Y, Ebraheim NA, Jayasuriya AC. Evaluation of cross-linked chitosan microparticles for bone regeneration. J Tissue Eng Regen Med. 2010; 4:532-542.

183.   Khor E, Lim LY. Implantable applications of chitin and chitosan. Biomaterials. 2003; 24: 2339–49.

184.   Jiang T, Kumbar SG, Nair LS, Laurencin CT. Biologically active chitosan systems for tissue engineering and regenerative medicine. Curr Top Med Chem. 2008; 8: 354–64.

185.   Jayasuriya AC, Kibbe S. Rapid biomineralization of chitosan microparticles to apply in bone regeneration. J Mater Sci Mater Med. 2010; 21:393-398.

186.   Jayasuriya AC, Mauch KJ. *In vitro* degradation behavior of chitosan based hybrid microparticles, J Biomed Sci Engg. 2011; 4: 383-390.

187.   Chia HH, Chung TS, Yang YY. Effect of preparation temperature on the characteristics and release profiles of PLGA microspheres containing protein fabricated by double-emulsion solvent extraction/evaporation method. J. Control. Release 2000; 69: 81-96.

188.   Crotts G, Park TG. Preparation of porous and nonporous biodegradable polymeric hollow microspheres. J. Control. Release 1995; 35: 91-105.

189.   Yamaguchi K, Anderson JM. In vivo biocompatibility studies of medisorb 65/35 D,L-lactide/glycolide copolymer microspheres. J. Control. Release 1993; 24: 81-93.

190.   Jiang T, Nukavarapu SP, Deng M, Jabbarzadeh E, Michelle DK, Doty SB, Abdel-Fattah WI, Laurencin CT. Chitosan-poly(lactide-co-glycolide) microsphere-based scaffolds for bone tissue engineering: In vitro degradation and in vivo bone regeneration studies. Acta Biomat. 2010; 6:3457-3470.

191.   Liburdi K, Straniero R, Benucci I, Maria A, Garzillo V, Esti M. Lysozyme immobilized on micro-sized magnetic particles: kinetic parameters at wine pH. Appl Biochem Biotech. 2012; 166: 1736-1746.

192.   Varum KM, Myhr MM, Hjerde RJN, Smidsrod O. In vitro degradation rates of partially N-acetylated chitosan in human serum. Carb Res. 1997; 299: 99-101.

193.   Erkan BT, Kadriye T, Joao MF, Reis RL. Enzymatic degradation behavior and cytocompatibility of silk fibroin-starch-chitosan conjugate membranes. Mat Sci Engg C. 2012; 32: 1314-1322.

194.   Shu XZ, Zhu KJ. The influence of multivalent phosphate structure on the properties of ionically cross-linked chitosan films for controlled drug release Eur J Pharm Biopharm. 2002; 54: 235–243.

195.   Tayalia P, Mooney DJ. Controlled growth factor delivery for tissue engineering. Adv Mat. 2009; 21: 3269-3285.

196.   Kanczler MJ, Barry J, Ginty P, Howdle SM, Shakesheff KM, Oreffo ROC. Supercritical carbon dioxide generated vascular endothelial growth factor encapsulated poly(DL-lactic acid) scaffolds induce angiogenesis in vitro. Biochem Biophy Res Comm. 2007; 352: 135-14.

197.   Drury JL, Mooney DJ. Hydrogels for tissue engineering: scaffold design variables and applications. Biomaterials. 2003; 24: 4337-51.

198.   Lee KY, Mooney DJ. Hydrogels for tissue engineering. Chem Rev. 2001; 101: 1869-79.

199.   Lee JE, Kim SE, Kwon IC, Ahn HJ, Cho H, Lee SH, Kim HJ, Seong SC, Lee MC. Effects of a chitosan scaffold containing TGF-β1 encapsulated chitosan microspheres on *in vitro* chondrocyte culture. Arti Organs. 2004; 28: 829-839.

200.   Chen FM, Zhao YM, Wu H, Deng ZH, Wang QT, Jin Y. Enhancement of periodontal tissue regeneration by locally controlled delivery of insulin-like growth factor-I from dextran-co-gelatin microspheres. J Cont Rel. 2006; 114: 209–22.

201.   Kim S, Kang Y, Krueger CA, Sen M, Holcomb JB, Chen D, Wenke JC, Yang Y. Sequential delivery of BMP-2 and IGF-1 using a chitosan gel with gelatin microspheres enhances early osteoblastic differentiation. Acta Biomater. 2012; 8: 1768-1777.

202.   Chen RR, Silva EA, Yuen WW, Brock AA, Fischbach C, Lin AS, Guldberg RE, Mooney DJ. Integrated approach to designing growth factor delivery systems. FASEB J. 2007; 21: 3896.

203.   Xian L, Wu X, Pang L, Lou M, Rosen CJ, Qiu T, Crane J, Frassica F, Zhang L, Rodriguez JP, Jia X, Yakar S, Xuan S, Efstratiadis A, Wan M, Cao X. Matrix IGF-1 maintains bone mass by activation of mTOR in mesenchymal stem cells. Nature Med. 2012; 18: 1095-1101.

204.   Jayasuriya AC, Shah C. Controlled Release of Insulin like Growth Factor-1 and Bone Marrow Stromal Cell Function of Bone-Like Mineral Layers Coated PLGA Scaffolds. J Tissue Eng Regen Med. 2008; 2: 43-49.

205.   Biondi M, Ungaro F, Quaglia F, Netti PA. Controlled drug delivery in tissue engineering. Adv. Drug Deliv. Rev 2008; 60: 229-42.

206.   Di Martino A, Sittinger M, Risbud MV. Chitosan: A versatile biopolymer for orthopaedic tissue-engineering. Biomaterials. 2005; 26: 5983-5990.

207.   Ma Z, Yeoh HH, Lim LE. Formulation pH modulates the interaction of insulin with chitosan microparticles. J Pharma Sci. 2002; 91: 1396-1404.

208.   Gupta KC, Kumar MNVR. Drug release behavior of beads and microgranules of chitosan. Biomaterials. 2000; 21: 1115-1119.

209.   Bradley JC, Simoni J, Bradley RH, McCartney DL, Brown SM. Time and temperature dependent stability of growth factor peptides in human autologous serum eye drops. Cornea. 2009; 28: 200-205.

210.   Berrier AL, Yamada KM. Cell-matrix adhesion. J Cell Physiol. 2007; 213: 565-73.

211.   Jayasuriya AC, Asaad M, Jayatissa AH, Ebraheim NA. Dissolution Behavior of Biomimetic Minerals on 3D PLGA Scaffold. Surface and Coatings Technology. 2006; 200: 6336-6339.

212.   Shin K, Jayasuriya AC, Kohn DH. Effect of Ionic Activity Products on the Structure and Composition of the Mineral formed on 3-D poly(lactic-co-glycolide) Scaffolds. J Biomed Mater Res A. 2007; 83:1076-1086.

213.   Cukierman E, Pankov R, Stevens DR, Yamada KM. Taking cell-matrix adhesion to the third dimension. Science. 2001; 294: 1708-12.

214.   Lu X, Leng Y. Quantitative analysis of osteoblast behavoiur on microgrooved hydroxyapatite and titanium substrata. J Biomed Mater Res A. 2003; 66: 677-87.

215.   Kieswetter K, Schwartz Z, Hummert TW, Cochran DL, Simpson J, Dean DD, Boyan BD. Surface roughness modulates the local production of growth

factors and cytokines by osteoblast like MG-63 cells. J Biomed Mater Res. 1996; 32: 55-63.

216.   Langer R, Tirrell DA. Designing materials for biology and medicine. Nature. 2004; 428: 487–492.

217.   Hollister SJ, Maddox RD, Taboas JM. Optimal design and fabrication of scaffolds to mimic tissue properties and satisfy biological constraints. Biomaterials. 2002; 23: 4095.

218.   Dalby MJ, McCloy D, Robertson M, Wilkinson CD, Oreffo RO. Osteoprogenitor response to defined topographies with nanoscale depths. Biomaterials. 2006; 27: 1306–1315.

219.   Baxter LC, Textor FM, Gwynn A, Richards RG. Fibroblasts and osteoblast adhesion and morphology on calcium phosphate surfaces. Eur Cell Mat. 2002; 4: 1-17.

220.   Jayasuriya AC, Bhat A. Mesenchymal stem cell function on hybrid organic/inorganic microparticles *in vitro.* J Tissue Eng Regen Med. 2010; 4: 340-348.

221.   Human BMP 7/OP1 induces the growth and differentiation of adipocytes and osteoblasts in bone marrow stromal cell cultures.

222.   Yilqor P, Tuzlakoglu K, Reis RL, Hasirci N, Hasirci V. Incorporation of a sequential BMP2/BMP7 delivery system into chitosan based scaffolds for bone tissue engineering, clinical applications of BMP-7/OP1 in fractures, nonunion and spinal fusion. Biomaterials. 2009; 30: 3551-3559.

223.   Dunn GA, Brown AF. Alignment of fibroblasts on grooved surfaces described by a simple geometric transformation. J Cell Sci. 1986; 83: 313–340.

224.   Stevens B, Yang Y, Mohandas A, Stucker B, Nguyen KT. A review of materials, fabrication methods, and strategies used to enhance bone regeneration in engineered bone tissues. J Biomed Mater Res B. 2008; 85: 573–582.

225.   Hayes JS, Khan IM, Archer CW, Richards RG. The role of surface microtopography in the modulation of osteoblast differentiation. Eur Cells Mat. 2010;20:98-108.

226.   Moutzouri AG, Athanassiou GM. Attachment, spreading and adhesion strength of human bone marrow cells on chitosan. Ann Biomed Eng. 2011; 39: 730-741.

227.   Di Martino A, Sittinger M, Risbud MV. Chitosan: A versatile polymer for orthopedic tissue engineering. Biomaterials. 2005; 26: 5983-5990.

228.   Long F. Building strong bones: molecular regulation of the osteoblast lineage. Nat Rev Mol Cell Biol. 2011;13: 27-38.

229.   Dudley HR, Spiro D. The fine structure of bone cells. J Biophys Biochem Cytol. 1961; 11: 627–649.

230.   Owen M. Cell population kinetics of an osteogenic tissue. I J Cell Biol. 1963; 19: 19–32.

231.   Burdick JA, Anseth KS. Photoencapsulation of osteoblasts in injectable RGD-modified PEG hydrogels for bone tissue engineering. Biomat. 2002; 23: 4315-4323.

232.   Chen TL, Shen WJ, Kraemer FB. Human BMP-7/OP-1 Induces the Growth and Differentiation of Adipocytes and Osteoblasts in Bone Marrow Stromal Cell Cultures. J Cell Biochem. 2001; 82: 187-199.

233.   Mendonça G, Mendonça DB, Aragão FJ, Cooper LF. Advancing dental implant surface technology – from micron- to nanotopography. Biomaterials. 2008;29: 3822–3835.

234.   Isa ZM, Schneider GB, Zaharias R, Seabold D, Stanford CM. Effects of fluoride modified titanium surfaces on osteoblast proliferation and gene expression. Int J Oral Maxillofac Implants. 2006; 21: 203–211.

235.   Guo J, Padilla RJ, Ambrose W, De Kok IJ, Cooper LF. Modification of TiO$_2$ grit blasted titanium implants by hydrofluoric acid treatment alters adherent osteoblast gene expression in vitro and in vivo. Biomaterials. 2007; 28: 5418–5425.

236.   Ducy P, Starbuck M, Priemel M, Shen J, Pinero G, Geoffroy V, Amling M, Karsenty G. A Cbfa1-dependent genetic pathway controls bone formation beyond embryonic development. Genes Dev 1999; 13: 1025–1036.

237.   Zhou X, Zhang Z, Feng JQ, Dusevich VM, Sinha K, Zhang H, Darnay BG, de Crombrugghe B. Multiple functions of Osterix are required for bone growth and homeostasis in postnatal mice. Proc Natl Acad Sci. 2010; 107: 12919–12924.

238.   Lee MH, Kim YJ, Yoon WJ, Kim JI, Kim BG, Hwang YS, Wozney JM, Chi XZ, Bae SC, Choi KY, Cho JY, Choi JY, Ryoo HM. Dlx5 specifically

regulates Runx2 type II expression by binding to homeodomain-response elements in the Runx2 distal promoter. J Biol Chem. 2005; 280: 35579–35587.

239.   Robledo RF, Rajan L, Li X, Lufkin T. The *Dlx5* and *Dlx6* homeobox genes are essential for craniofacial, axial, and appendicular skeletal development. Genes Dev. 2002; 16: 1089–1101.

240.   Viereck V, Siggelkow H, Tauber S, Raddatz D, Schutze N, Hufner M. Differential regulation of Cbfa1/Runx2 and osteocalcin gene expression by vitamin-D3, dexamethasone, and local growth factors in primary human osteoblasts. J Cell Biochem. 2002; 86: 348–356.

241.   Bessa PC, Casal M, Reis RL. Bone morphogenetic proteins in tissue engineering: the road from the laboratory to the clinic, part I (basic concepts). J Tissue Eng Regen Med. 2008; 2: 1-13.

242.   Payne RG, Yaszemski MJ, Yasko AW, Mikos AG. Development of an injectable, in situ crosslinkable, degradable polymeric carrier for osteogenic cell populations. Part 1. Encapsulation of marrow stromal osteoblasts in surface crosslinked gelatin microparticles. Biomat. 2002; 23: 4359-4371.

243.   Lian JB, Stein GS. The developmental stages of osteoblast growth and differentiation exhibit selective responses of genes to growth factors (TGFb1) and hormones (Vitamin D and Glucocorticoids). J Oral Implant. 1993; 19: 95–105.

244.   Kim K, Luu YK, Chang C, Fang D, Hsiao BS, Chu B, Hadjiargyrou M. Incorporation and controlled release of a hydrophilic antibiotic using poly (lactide-co-glycolide)-based electrospun nanofibrous scaffolds. J Control Rel. 2004; 98: 47–56.

245.   Liu W, Sun S, Cao Z, Zhang X, Yao K, Lu WW. An investigation on the physicochemical properties of chitosan/DNA polyelectrolyte complexes, Biomaterials. 2005; 26: 2705–2711.

246.   Jayasuriya AC, Bhat A. Optimization of scaled-up chitosan microparticles for bone regeneration. Biomed Mater 2009; 4:1-8.

247.   Loveymi BD, Jelvehgari M, Milani PZ, Valizadeh H. Design of vancomycin RS-100 nanoparticles in order to increase the intestinal permeability, Adv Pharma. 2012; 2: 43-56.

248.   Gupta M, Saini T. Preformulation parameters characterization to design, development and formulation of vancomycin hydrochloride tablets for psudomembranous colitis. Int J Pharm Res Dev. 2009; 1:1-7.

249.   Yin J, Noda Y, Yotsuyanagi T. Properties of poly(lactic-co-glycolic acid) nanospheres containing protease inhibitors: camostat mesilate and nafamostatmesilate, Int J Pharm. 2006; 314: 46–55.

250.   Feng K, Sun H, Bradley MA, Dupler EJ, Giannobile WV, Ma PX. Novel antibacterial nanofibrous PLLA scaffolds. J Control Rel. 2010; 146: 363-369.

251.   Gitelis S, Brebach GT. The treatment of chronic osteomyelitis with a biodegradable antibiotic impregnated implant. J Orthop Surg. 2002; 10: 53–60.

252.   Costerton JW, Lewandowski Z, Caldwell DE. Microbial biofilms. Annu Rev Microbiol. 1995; 49: 711–745.

253.   Matzke GR, Zhanel GG, Guay DR. Clinical pharmacokinetics of vancomycin. Clin Pharmacokinet. 1986; 11: 257-282.

254.   Roy ME, Peppers MP, Whiteside LA, Lazear RM. Vancomycin Concentration in Synovial Fluid: Direct Injection into the Knee vs. Intravenous Infusion. J Anthroplasty. 2013 [EPub ahead of print].

255.   Duewelhenke N, Krut O, Eysel P. Influence on mitochondria and cytotoxicity of different antibiotics administered in high concentrations on primary human osteoblasts and cell lines. Antimicrob Agents Chemother. 2007; 51: 54–63.

256.   Rathbone CR, Cross JD, Brown KV, Murray CK, Wenke JC. Effect of Various Concentrations of Antibiotics on Osteogenic Cell Viability and Activity. J Ortho Res. 2011; 29: 1070-1074.

257.   Li H, Ogle H, Jiang B. Cefazolin embedded biodegradable polypeptide nanofilms promising for infection prevention: A preliminary study on cell responses. J Orthop Res. 2010; 28: 992–999.

258.   Li H, Ogle H, Jiang B. Cefazolin embedded biodegradable polypeptide nanofilms promising for infection prevention: A preliminary study on cell responses. J Orthop Res. 2010; 28: 992–999.

259.   Salzmann GM, Naal FD, von Knoch F. Effects of cefuroxime on human osteoblasts in vitro. J Biomed Mater Res A. 2007; 82: 462–468.

260.   Li B, Brown KV, Wenke JC. Sustained release of vancomycin from polyurethane scaffolds inhibits infection of bone wounds in a rat femoral segmental defect model. J Control Rel. 2010; 145: 221–230.

261.   Rathbone CR, Cross JD, Brown KV, Murray CK, Wenke JC. Effect of Various Concentrations of Antibiotics on Osteogenic Cell Viability and Activity. J Ortho Res. 2011; 29: 1070-1074.

262.   Sayin B, Alis SC, Illa BLA, Marangoz SI, Hincal AL. Implantation of vancomycin microspheres in blend with human/rabbit bone grafts to infected bone defects. J Microencap. 2006; 23: 553-556.

263.   Chen X, Kidder LS, Lew WD. Osteogenic protein-1 induced bone formation in an infected segmental defect in the rat femur. J Orthop Res. 2002; 20: 142–150.

264.   Luttikhuizen DT, Harmsen MC, Van Luyn MJ. Cellular and molecular dynamics in the foreign body reaction. Tissue Eng. 2006;12:1955–70.

265.   Gretzer C, Emanuelsson L, Liljensten E, Thomsen P. The inflammatory cell influx and cytokines changes during transition from acute inflammation to fibrous repair around implanted materials. J Biomater Sci Polym Ed. 2006;17:669–87.

266.   Okamoto Y, Shibazaki K, Minami S. Evaluation of chitin and chitosan on open would healing in dogs. J Vet Med Sci. 1995; 57: 851-854.

267.   Ueno H, Yamada H, Tanaka I. Accelerating effects of chitosan for healing at early phase of experimental open wound in dogs. Biomaterials. 1999; 20: 1407-1414.

268.   Usami Y, Okamoto Y, Minami S. Chitin and chitosan induce migration of bovine polymorphonuclear cells. J Vet Med Sci. 1994; 56: 761-762.

269.   Chatelet C, Damour O, Domard A. Influence of the degree of acetylation on some biological properties of chitosan films. Biomaterials. 2001;22:261–8.

270.   Muzzarelli R, Baldassarre V, Conti F, Ferrara P, Biagini G, Gazzanelli G. Biological activity of chitosan: ultrastructural study. Biomaterials. 1988; 9: 247–52.

271.   Hidaka Y, Ito M, Mori K, Yagasaki H, Kafrawy AH. Histopathological and immunohistochemical studies of membranes of deacetylated chitin derivatives implanted over rat calvaria. J Biomed Mater Res A. 1999;46:418–23.

272.   Spin-Neto R, de Freitas RM, Pavone C, Cardoso MB, Campana-Filho SP, Marcantonio RA. Histological evaluation of chitosan-based biomaterials used for the correction of critical-size defects in rat's calvaria. J Biomed Mater Res A. 2009; 93: 107-14.

273.   Asikainen AJ, Hagstrom J, Sorsa T, Noponen J, Kellomaki M, Juuti H. Soft tissue reaction to bioactive glass 13–93 combined with chitosan. J Biomed Mater Res A. 2007; 83: 530–7.

274.   Chin H, Quinten Ruhe P, Mikos A.G. In vivo bone and soft tissue response to injectable, biodegradable oligo(poly(ethylene glycol) fumarate) hydrogels. Biomaterials. 2003; 24: 3201-3211.

275.   Shi S, Cheng X, Wang J, Zhang W, Peng L, Zhang Y. RhBMP-2 micropsheres-loaded chitosan/collagen scaffold enhances osseointegration: An experiment in dog. J Biomat Appl. 2009; 23: 331-348.

276.   Ohura K, Hamanishi C, Tanaka S, Matsuda N. Healing of segmental bone defects in rats induced by a b-TCP-MCPM cement combined with rhBMP-2. J Biomed Matr Res A. 1999; 44:168–175.

277.   Simmons CA, Alsberg E, Hsiong S. Dual growth factor delivery and controlled scaffold degradation enhance in vivo bone formation by transplanted bone marrow stromal cells. Bone. 2004; 35: 562–569.

278.   Oakes DA, Lee CC, Lieberman JR. An evaluation of human demineralized bone matrices in a rat femoral defect model. Clin Orthop Relat Res. 2003; 413: 281–290.

279.   Song E, Ouyang N, Horbelt M, Antus B, Wang M, Exton MS. Influence of alternatively and classically activated macrophages on fibrogenic activities of human fibroblasts. Cell Immunol. 2000;204:19–28.

280.   Henson PM. The immunologic release of constituents from neutrophil leukocytes. I. The role of antibody and complement on nonphagocytosable surfaces or phagocytosable particles. J Immunol. 1971;107:1535–46.

281.   Lowett G, Van der Perre G, Van Audekercke R, Haex B, Martel C, Murakami H, Lacheretz F, Barbier A. Tiludronate improves the strength of vertebral bones in the rat after long-term administration. J Bone Miner Res. 1997; 12: S472.

282.   Wronski T, Dann L, Horner S. Time course of vertebral osteopenia in overiectomized rats. Bone. 1989; 10: 295-301.

283.   Currey JD. The effect of porosity and mineral content on the Young's modulus of elasticity of compact bone. J Biomech. 1988; 21: 131–139.

284.   Zioupos P. Accumulation of in-vivo fatigue microdamage and its relation to biomechanical properties in ageing human cortical bone. J Microsc. 2001; 201: 270– 278.

285.   Wang X, Bank RA, TeKoppele JM, Agrawal CM. The role of collagen in determining bone mechanical properties. J Orthop Res. 2001; 19: 1021–1026.

286.   Wang X, Athanasiou KA, Agrawal CM. Contribution of collagen to bone mechanical properties. In: Proceedings of the 17th Southern Biomtedical Engineering Conference, San Antonio, TX; 1998; 112.

287.   Ottani V, Franchi M, De Pasquale V, Leonardi L, Morocutti M, Ruggeri A. Collagen fibril arrangement and size distribution in monkey oral mucosa. J Anat. 1998; 192; 321–328.

288.   Stamov DR, Müller A, Wegrowski Y, Brezillon S, Franz CM. Quantitative analysis of type I collagen fibril regulation by lumican and decorin using AFM. J Struct Biol. 2013; 183: 394-403.

289.   Viguet-Carrin S, Garnero P, Delmas PD. The role of collagen in bone strength. Osteoporos Int. 2006; 17: 319-336.

290.   Linenmayer TF. Collagen. In: Hay, E. (Ed.), Cell Biology of Extracellular Matrix, Vol. 2. Plenum Press, New York, London, pp. 1– 44, 1991.

291.   Tzaphlidou M, Berillis P. Collagen fibril diameter in relation to bone site. A quantitative ultrastructural study. Micron. 2005; 36: 703-705.

292.   Hootman JM, Helmick CG, Brady TJ. A Public Health Approach to Addressing Arthritis in Older Adults: The Most Common Cause of Disability. American Journal of Public Health. 2012; 102: 426-33.

293.   Helmick C, Felson D, Lawrence R, Gabriel S. Estimates of the prevalence of arthritis and other rheumatic conditions in the United States. Arthritis Rheum. 2008; 58: 15-25.

294.   Lee J, Song J, Hootman JM, Semanik PA, Chang RW, Sharma L, Van Horn L, Bathon JM, Eaton CB, Hochberg MC, Jackson R, Kwoh CK, Mysiw WJ, Nevitt M, Dunlop DD. Obesity and other modifiable factors for physical inactivity measured by accelerometer in adults with knee osteoarthritis: Data from the osteoarthritis initiative (OAI). Arthritis Care Res. 2013; 65: 53-61.

295.   Murphy L, Helmick CG. The impact of osteoarthritis in the United States: a population-health perspective: A population-based review of the fourth most common cause of hospitalization in U.S. adults. Orthop Nurs. 2012; 31: 85-91.

296.   Murphy L, Helmick CG. The impact of osteoarthritis in the United States: a population-health perspective: A population-based review of the fourth most common cause of hospitalization in U.S. adults. Orthop Nurs. 2012; 31: 85-91.

297.   Mantripragada VP, Jayasuriya AC. Injectable chitosan microparticles incorporating bone morphogenetic protein -7 for bone tissue regeneration: in vitro study. J Biomed Mater Res A. February 4, 2014 [Epub ahead of print].

298.   Mantripragada VP, Jayasuriya AC. IGF-1 Release Kinetics and Osteoblast function of Chitosan Microparticles Fabricated Using Environmentally Benign Conditions. J Biomed Mater Res A (In review) 2014.

299.   Mantripragada VP, Jayasuriya AC. Dual release of growth factor and antibiotics to determine their influence on effective bone regeneration: in vitro study. Inter J Pharm (Submitted) 2014.

300.   Mantripragada VP, Jayasuriya AC. Bone response to bone morphogenetic protein 7 incorporated chitosan microparticles- in vivo study. Biomaterials (Submitted) 2014.